Novel Uses of Alpha-Diimine Ligands and their Ru (II) Metal Complexes.

by

Oma V. Morgan

A dissertation submitted to the graduate Faculty
in Chemistry in partial fulfillment of the
requirements for the degree of Doctor of
Philosophy. The City of New York.

2001

This manuscript has been read and accepted for the Graduate

Faculty in Chemistry in satisfaction of the dissertation requirement

for the degree of Doctor of Philosophy.

Dec. 20, 2000
Date

A. D. Baker
Chairman of Examining Committee

Jan. 8, 2001
Date

Executive Officer

Dr. Lynn Francesconi
Supervisory Committee

The City University of New York

Abstract

Novel Uses of Alpha-Diimine Ligands and their Ru(II) Metal Complexes.

by

Oma V. Morgan

Adviser: Professor A.D. Baker.

The α-diimine ligands pyridino[3,2-f]quinoxalino[2,3-h]quinoline (bppz), 11,12-dimethylpyridino[3,2-f]quinoxalino[2,3-h]quinoline (mbppz), benzo[f]pyridino[3,2-h]quinoline (bzp), pyridino[3,2-f]quinoxalino[2,3-h]quinoline (ippz), 2-(2-pyridyl)-1,3-oxazoline (pyoxazo), 4,4-dimethyl-2-(2-pyridyl)-1,3-oxazoline (dmpyoxazo) and 2-(1,3-oxazolin-2-yl)-1,3-oxazoline (bisoxazo) and their Ru(II) polypyridine complexes have been prepared and characterized. The ground and excited state acid-base properties of the complexes $[Ru(bpy)_2bppz]^{2+}$ (pK_a 1.89, pK_a^* 2.62) (bpy = 2,2'-bipyridine) and its methylated derivative $[Ru(bpy)_2mbppz]^{2+}$ (pK_a 1.85, pK_a^* 3.18) have been measured.

A major focus of interest has been the interaction of mixed ligand complexes of the type $[Ru(bpy)_2L]^{2+}$ (L = bppz, mbppz, bzp, ippz, bisoxazo, pyoxazo, and dmpyoxzo) and also the tris complexes, $[RuL_3]^{2+}$ (L = bzp, pyoxazo, and dmpyoxazo) with calf thymus DNA (B-DNA). Spectroscopic methods have been utilized to investigate the binding to DNA. Among these were absorption, emission, circular dichroism (CD), fluorescence quenching, fluorescence titrations (salt effect on binding), and equilibrium dialysis. For the complexes containing bisoxazo, pyoxazo, and dmpyoxazo fluorescence techniques were precluded since these compounds do not luminesce in aqueous solution or in the presence of DNA. Optical isomers of the Ru(II) complexes (referred to as delta

and lambda) containing bppz, mbppz, bzp, and ippz which have been isolated. These enantiomers exhibit differential binding to

DNA, and therefore provide valuable information on the overall binding to calf thymus DNA (B-DNA).

Acknowledgements

I am grateful to a number of people whose efforts have made this work possible. First of all, I would like to express my appreciation to my research mentor, Dr. Arthur D. Baker, for his encouragement, support, guidance and unlimited patience in directing the work contained in this dissertation. Special thanks to Dr. Thomas C. Strekas for his guidance in the DNA studies. I am also thankful to Dr. Robert R. Engel for his encouragement and support.

Thanks to the department secretaries, Alice Brickman and Jeanne Deutsch and also to the technicians, Joe, Charlie, Jeanine, Bob and Randy for their help and support. Special thanks to Dianne Adeobowale and Vivian Mason who had to jump hoops sometimes to get me through my paper work and enrollment.

Finally, this work is dedicated to my husband and my entire family for their love and support.

Preface

Polypyridine complexes of ruthenium (II) have been the focus of considerable research effort.[1-3] Their stability and unique photophysical properties make them ideal candidates for photocatalysts, [3] for use in artificial photosynthesis, [4-5] as sensors, [6-10] as photoreactive materials, [11] for use in studies of electron transfer in proteins[12-14] and DNA, [15-17] and for a wide range of other purposes.

The interaction of these complexes with DNA [18-42] is of special interest. Among the primary modes of binding are intercalation, surface binding, and electrostatic binding. Intercalation is a common binding motif for d^6 and d^8 metal complexes containing planar polyaromatic diimine ligands. [19, 39,43-50] In this mode of binding the planar aromatic ligand can slip between the base pairs within the α- helix. In some instances these intercalated complexes have been shown to cleave DNA.[28, 38, 51-55] Powerful probes of the interactions with DNA include absorption and emission spectroscopies. Polypyridyl complexes of ruthenium (II) are intensely colored owing to a well characterized, localized metal-to-ligand charge transfer (MLCT) transition. [56,57] This transition is perturbed on binding to DNA. Therefore, by investigating the spectroscopic changes (absorption and fluorescence) of these complexes in aqueous solution and in the presence of DNA, powerful insights with DNA binding can be obtained.

Previous work in our group has centered on ruthenium (II) complexes containing cations of the type $[Ru(bpy)_2LL]^{2+}$ or $[Ru(phen)_2LL]^{2+}$ where bpy is 2,2'-bipyridine, phen is 1,10-phenanthroline, and LL is a diimine ligand. These types of metal complexes bind to double-stranded DNA in aqueous solution.[36] The strength of DNA binding is

affected by variations in geometry, [58] charge,[36] size, hydrophobicity, and and hydrogen bonding ability [59] of the ligands surrounding the metal.

The work of this dissertation is concerned with the preparation of modified bpy ligands and their racemic and chiral ruthenium (II) complexes, followed by an investigation of their spectroscopic properties in the presence and absence of DNA. Chapter I consist of background information on Ru(II) α-diimine complexes, and the photophysical properties of $[Ru(bpy)_3]^{2+}$, which is regarded as a prototype for all Ru(II) α-diimine complexes. Chapter II and III include the synthesis and characterization of the α-diimine ligands and their Ru(II) complexes. Chapter IV discusses the synthesis and characterization of RuL_3^{2+} complexes. The ground and excited state basicities of $\{Ru(bpy)_2bppz]^{2+}$ and $[Ru(bpy)_2mbppz]^{2+}$ in aqueous solution is discussed in chapter V. Chapter VI discusses the criteria Ru(II) complexes must possess to be useful probes of B-DNA as well as a discussion on the binding modes. Chapter VII and VIII examines the binding of $[Ru(bpy)_2L]^{2+}$ and $[RuL_3]^{2+}$complexes with B-DNA. Chapter IX contains the experimental section.

Table of Contents

List of Tables

Chapter II

Chapter III

Chapter IV

Chapter VII

Chapter VIII

List of Figures

Chapter I

Chapter II

Chapter III

Chapter VIII

List of Schemes

Chapter I

Photophysical Properties of $[Ru(bpy)_3]^{2+}$ and Other Ruthenium (II) Complexes.

Photophysical Properties of $[Ru(bpy)_3]^{2+}$

Introduction:

Tris(bipyridine) ruthenium (II) dication, $Ru(bpy)_3^{2+}$ has played a pivotal role in the development of inorganic photochemistry, and continues to play a role in this field. The importance of this compound is the result of its rich photophysics and photochemistry. A key finding that spurred much of this development was the initial observation of an orange triplet emission from the complex, which can be observed at ambient temperature. The discovery of such a feature in a stable metal complex has since led to considerable interest in explaining the nature of this observation. Also, a tremendous amount of work has been done involving the modification of the environment about the metal by means of substituting different α-diimine ligands for 2,2'-bipyridine in the cation. In this way it has been possible to fine-tune the lifetime, luminescence and excited state properties. In this type of work, the complex, $[Ru(bpy)_3]^{2+}$ is regarded as the prototype or "parent" complex, and the properties of other tris-α-diimines are compared to it. A novel application for the modified cations is possible when one or more α-diimine ligands can slide (intercalate) between the base pairs of DNA. Generally this requires the ligand to be planar. The intercalation can dramatically alter the physical properties of the complex especially in terms of shifting absorption and emission wavelengths, and altering the intensity and lifetime of luminescence. These changes can be used to probe the nature of the binding of the complexes to DNA and to measure

binding constants. This type of work was a major focus in this research. We will begin with a background summary of the relevant photophysical properties.

Electronic States

$[Ru(bpy)_3]^{2+}$ is a d^6 complex of ruthenium(II) in a strong ligand field (the maximum number of electrons are paired) with octahedral microsymmetry, D_3. The ground and low-lying excited states involve the t_{2g} (stabilized) and e_g (destabilized) levels originating from the 4*d* orbitals, and also the π-bonding and π*- antibonding orbitals of the aromatic system of the ligand. A simplified orbital diagram (Figure 1) can be used to explain the ground and excited state chemistry of $Ru(bpy)_3^{2+}$. This diagram shows the ground state ($^1A_1$) with a filled $(t_{2g})^6$ configuration in a strong ligand field. This means that ground state is a low-spin complex with all 6 d-electrons paired in the t_{2g} orbitals. The t_{2g} to e_g transition or metal-centered (MC) transition is a weak Laporte forbidden absorption (ε = 100 M^{-1} cm^{-1}) that leads to a short–lived excited state having the $t_{2g}^5e_g^1$ configuration. Such excited states resulting from d-d* transitions are usually the ones that give rise to photosubstitution reactions. Excitation of an electron from a t_{2g} orbital into a π*-antibonding orbital on the bipyridyl ligand results in an allowed d-π* (MLCT) transition (ε = 20,000 M^{-1} cm^{-1}). Such excited states resulting from MLCT transitions frequently give rise to electron transfer reactions. At even higher energies (UV region) lie the π-π* transitions that are localized on the bipyridyl ligands.

Absorption and Emission

In the absorption spectrum the π-π^* transitions in the UV region are observed at 185nm, 208nm, and 285nm. The d-d transitions are found at 238nm, 250nm, 323nm, and 345nm.[86-88] The intense absorption band at 452nm (ε = 14,450) is due to the MLCT transition where an electron is promoted from the metal centered t_{2g} orbital into a ligand centered π^* orbital. A long wavelength absorption tail (λ > 500nm, ε = 700 M^{-1} cm^{-1}) has been assigned to a spin forbidden MLCT transition that gives rise to the observed luminesence from the complex.[89, 90]

At ambient temperature, solutions of $Ru(bpy)_3^{2+}$ show an orange-yellow emission due to a broad featureless band centered around 600nm. At 77K in a glass matrix, however, the emission spectrum is well-resolved with a band origin at 579.9 nm. In a series of pioneering papers on the photophysical properties of $Ru(bpy)_3^{2+}$ it was established that the luminescence is of the spin-forbidden charge transfer type.[91-108] This intense emission occurs at lower energy than does the ligand centered $\pi^* \rightarrow \pi$ phosphoresence, hence there is a significant contribution to the excited state from an interaction between the metal *d* orbitals and the ligand π system. Such an interaction result in a large spin-orbit coupling, which cause significant mixing between the singlet and triplet states. As a consequence of this mixing between states, the emission can be described as occuring from a manifold of spin-orbit states rather than from a single spin-triplet state. The electronic states in this model will then be delocalized across the entire D_3 chelate system, with the excited state having C_2 symmetry.

Studies on the temperature dependence of the luminescence lifetime and quantum yield in the temperature range 2$\rightarrow$77K have shown that the emission originates from a set

of three closely spaced levels in equilibrium with ΔE = 10 and 61 cm^{-1} (Fig. 2). In the excited state an electron is transferred from a metal-centered to a ligand-centered orbital. This electron that is transferred to the ligand could be delocalized about all three bpy ligands such as in $Ru^{3+}(bpy^{-1/3})_3^{2+}$, or it could be localized at only one of the bpy ligands such as in $Ru^{3+}(LL)_2(LL^-)^{2+}$. For the delocalized model the promoted electron will reside in an a_2 orbital in D_3 symmetry. In this model the ligand-ligand overlap is disregarded, and the exchange interaction between the excited electron and the electrons remaining in the d^5 core cause the splitting among the energy levels.[109] By contrast, the localized description $Ru^{3+}(LL)_2(LL^-)^{2+}$ imposes a C_{2v} symmetry on the excited state. For this localized MLCT model four states are expected to lie at low energy, with three being closely spaced and a fourth being more widely separated at higher energy.[110] Molecular orbital calculations in the frame of trigonal C_{2v} symmetry are in agreement with the low temperature spectrum of $Ru(bpy)_3^{2+}$.[111] Other studies that provide evidence that the emitting state has the electron localized on a single ring include photoselection studies, [112,113] Raman spectroscopy,[114] and solvent effects on the absorption spectra.[115] Time-resolved Raman spectroscopy support the view that the localized excited state is present in solution for up to 1ns after the excitation pulse.[116] The model with the electron localized on one of the bpy rings also correlates with electrochemical experiments with $Ru(bpy)_3^{2+}$ where it has been found that the singly reduced species $Ru(bpy)_3^+$ is formed with the added electron localized on one of the bpy rings rather than delocalized across all three. [117]

The kinetic features of the excited state of $Ru(bpy)_3^{2+}$ and other metal complexes of this type can be demonstrated by a schematic Jablonski diagram (Fig.3). Direct

excitation to the triplet state is a forbidden process, but the triplet state can be populated by an allowed excitation to the singlet state, followed by a fast intersystem crossing to the triplet. The rate constant (k_{isc}) for this intersystem crossing is high, leading to a quantum yield for the phosphorescence of 0.042. With a triplet state lifetime of 0.062 microseconds at ambient temperature in aqueous solution and a relatively high quantum yield for its formation of 0.042, the excited state $Ru(bpy)_3^{2+*}$ can be formed in sufficient quantities in aqueous solution and it can participate in a wide range of bimolecular reactions with added substrates.

Ruthenium (II) diimine complexes

Polypyridine and related α-diimine complexes of ruthenium (II) have unique combinations of spectroscopic and electrochemical properties. Many are luminescent and have been used as photosensitizers, in energy conversion and as excited state electron transfer agents.[118] Other uses include probes of heterogenous binding dynamics[119] and macromolecular structures. [120,121] Complexes containing $Ru(II)L_3^{2+}$ cations (L = α-diimine) have proven particularly versatile in these applications owing to their strong visible absorption, stability, efficient emissions, and long-lived excited states. [118-122] In addition, the emitting-state energies and excited state redox properties of the complexes are often sensitive to variations in the metal, coordinating ligands, and local environment [118, 123-127] so that investigators can exact considerable control in fine-tuning properties to meet specific needs. For example, many of these sensitizers exhibit a variety of energetically accessible charge transfer (CT), ligand field (d-d), and intraligand excited

states that can have quite different excited-state characteristics. Understanding these allows the rational design of new, more useful sensitizers and probes.

Complexes containing $Ru(bpy)_3^{2+}$ and $Ru(phen)_3^{2+}$ cations are considered as the prototype complexes to which other Ru (II) complexes of α-diimines are compared. Changing the ligand surrounding the metal [106] from bpy to phen to other α-diimines is one of the most useful ways of modifying photophysical and photochemical properties. To this end, we have synthesized various types of modified bipyridines and related α-diimines in the hope of further elucidating the effects of these modifications on the excited state behaviour of Ru (II) complexes. Most emphasis has been put on synthesizing $Ru(bpy)_2L^{2+}$ type complexes, since in this case only one ligand is modified, which very often simplifies the spectral interpretation. However, in some cases the tris-complexes, RuL_3^{2+}, were also synthesized.

A major area of interest of Ru(II) α-diimine complexes that has evolved in the past two decades is the study of their ability to bind to double stranded DNA. Following the pioneering studies [21,128] of Barton et al, various co-workers including our group have shown [15, 18, 19, 20, 21, 29, 36, 38, 71,129-134] that a variety of six coordinate metal complexes in which the ligands are bidendate diimines with several fused aromatic rings bind enantioselectively with double stranded DNA's. The basis of this selectivity is usually assumed to be more favorable intercalative interaction of the one isomer within the major or minor groove of DNA via one of the metal bonded aromatic ligands. The intercalative nature of binding of specific complexes has been firmly established via studies [15,128,134] of the complex $Ru(phen)_2(dppz)^{2+}$ (dppz = dipyrido-[3,2-a:2',3'-c]phenazine). Both NMR studies and binding studies with T4-DNA have been interpreted in terms of a model

whereby the dppz ligand intercalates via access from the minor groove of the double stranded DNA. In this thesis the binding behavior of the Ru(II) α-diimines complexes that we synthesized will be discussed.

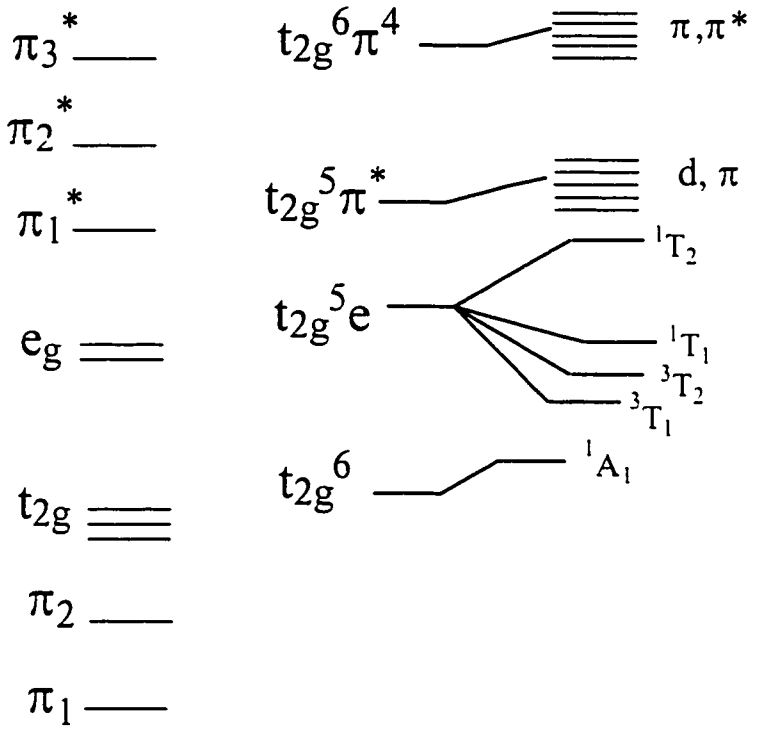

Figure 1. Simplified molecular orbital diagram of $Ru(bpy)_3^{2+}$

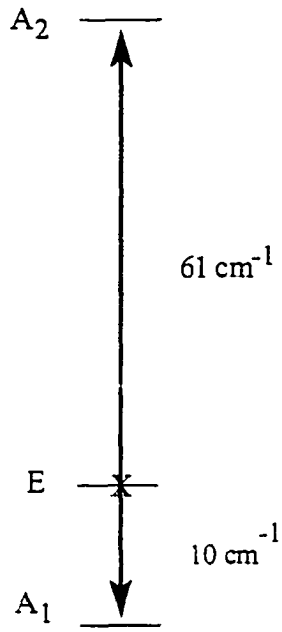

Fig. 2 Splitting of excited state manifold.

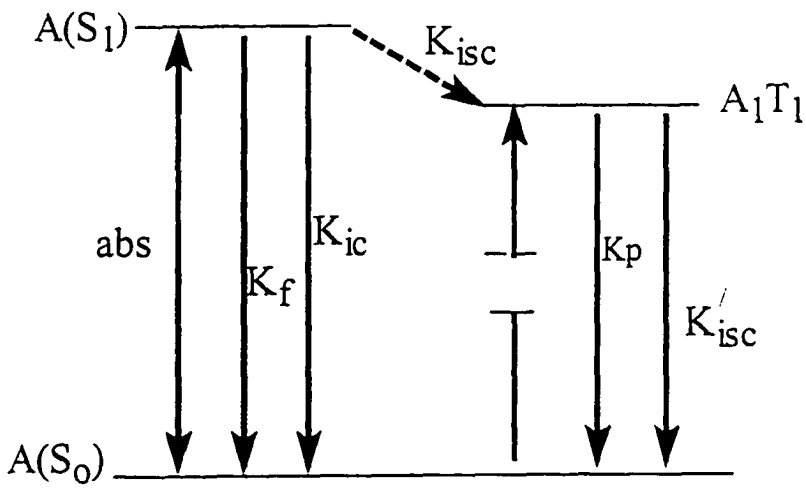

Fig. 3 Jablonski diagram for the ground and excited state process for $Ru(bpy)_3^{2+}$.

Chapter II

α-Diimine Ligands

Introduction

As noted earlier, the complexes $(Ru(bpy)_3)^{2+}$ and $Ru(phen)_3^{2+}$ are regarded as the parent systems against which the excited and ground state behavior of other Ru (II) α-diimine complexes are compared. There are significant changes in excited state behavior upon modification of the ligand surrounding the metal.[106] This has been exploited as the most useful way of modifying the photophysical and photochemical aspects of the system. In this spirit, we have synthesized various types of bpy's (bpy = 2,2'-bipyridine) to elucidate the effects of these modifications on the photophysical properties of Ru (II) complexes. Emphasis has been placed on synthesizing $Ru(bpy)_2L^{2+}$ and RuL_3^{2+} types of complexes. Figure 1 shows the ligands used in the synthesis of the Ru (II) complexes, which will be discussed in this dissertation (see experimental section for details). The complexes of the type $Ru(bpy)_2L^{2+}$ (L = ppz, bppz, mbppz, bzp, ippz) were emphasized since the optically pure enantiomers were prepared, thus allowing the gathering of more useful data on the binding to DNA. Complexes of the type RuL_3^{2+} (L = bzp, pyridyl oxazoline, dimethyl pyridyl oxazoline) were also studied to compare their effects on binding with DNA to that of the relevant $Ru(bpy)_2L^{2+}$ complexes.

The Ru bis-bipyridine complexes of ppz, [36, 71] bppz, and mbppz (Figure 1) make up a series of complexes which show the effect of ligand modification (aromatic ring in bppz, dimethylated aromatic ring in mbppz) on one ligand of the complex. These complexes are especially useful in examining the effects of ligand size on binding to DNA.

The Ru (II) complexes of ppz, ippz and bzp make up another series of complexes which show the how subtle changes on one ligand of the complex affects its binding to DNA. Yet another comparison can be made with Ru bis-bipyridine isomers of bzp and the tris Ru (II) complex of bzp.

The Ru (II) complexes of bis-oxazoline, pyridyl-oxazoline, and methylpyridyl-oxazoline make up another series. These ligands are neither aromatic nor planar and it is interesting to see how these small molecules bind to DNA. The tris Ru (II) complexes of pyridyl-oxazoline, and methyl pyridyl oxazoline can be further compared to the related bis complexes.

Results

Synthesis and Characterization.

Pyridino[3,2-f]quinoxalino[2,3-h]quinoline (bppz, benzophenanthroline pyrazine) was prepared from 1,2-phenylenediamine and 4,7-phenanthroline-5,6-dione (see fig.2). Similar in structure to the ligand bppz, 11,12-dimethylpyridino[3,2-f]quinoxalino[2,3-h]quinoline (mbppz, methyl benzophenanthroline pyrazine) was prepared from 4,5-dimethyl-1,2-phenylene diamine and 4,7-phenanthroline-5,6-dione (see fig.2). The ligands bppz and mbppz were characterized by NMR and mass spectrometry (see experimental section for details). The ultraviolet (UV) spectrum for the ligand bppz and mbppz are given in figure 2 – 3 and their related absorption bands are represented in table 1.

The ligands benzo[f]pyridino[3,2-h]quinoline (bzp), pyrazino[2,3-f]pyridino[3,2-h]quinoline (ippz), 2-(1,3-oxazolin-2-yl)-1-3-oxazoline (bis-oxazoline), 2-(2-pyridyl)-

1,3-oxazoline (pyridyl oxazoline), and 4,4-dimethyl-2-(2-pyridyl)-1,3-oxazoline (dimethyl pyridyl oxazoline) were prepared from existing methods (see fig.2).[135-136] NMR was used to confirm the structures of the above ligands (see experimental for details). Figures 4–7 shows the ultraviolet (UV) spectra of the above ligands in water. Their associated absorption bands are represented in Table 1.

Conclusion

The preparation of the ligands bppz, mbppz, bzp, ippz, bis-oxazoline, pyridyl-oxazoline and dimethyl pyridyl-oxazoline has been presented. The structure of all the ligands have been confirmed by NMR, and also by mass spectrometry in some cases (see experimental).

Table I. Absorption bands of α-diimine ligands in water.

α-Diimine Ligand	**π – π* Transitions (nm)**
bppz	380, 364, 308, 296, 268
mbppz	390, 378, 272
bzp	320, 278 (shoulder), 260, 224
bis-oxazoline	212, 202 (shoulder)
pyridyl-oxazoline	272, 222, 194
dimethyl pyridyl-oxaxoline	268, 222, 194

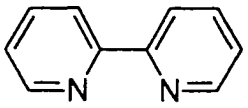

2,2'-bipyridine
(bpy

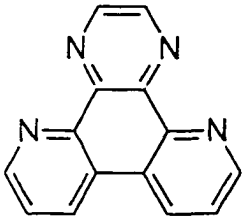

yrazino[2,3-f][4,7]phenanthroline
(ppz, "phenanthrolino pyrazine"

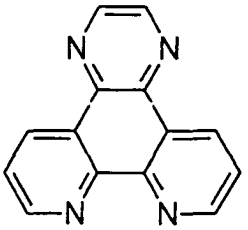

yridino[3,2-f]quinoxalino[2,3-h]quinoline
(ippz, "isophenanthrolino pyrazine"

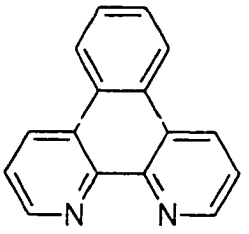

enzo[f]pyridino[3,2-h]quinolin
(bzp, "benzophenanthroline"

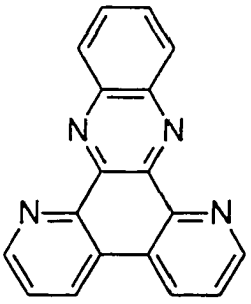

yridino[3,2-f]quinoxalino[2,3-h]quinoline
(bppz, "benzophenanthrolino pyrazine") ne

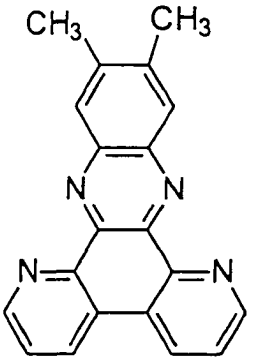

11,12-dimethylpyridino[3,2-f]quinoxalino[2,3-h]quinoline
(mbppz, "methyl benzophenanthrolino pyrazine") ne

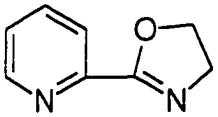

2-(2-pyridyl)-1,3-oxazoline
(pyridyl-oxazoline, pyoxazo

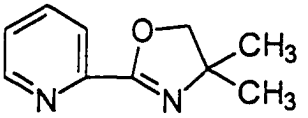

,4-dimethyl-2-(2-pyridyl)-1,3-oxazoline
(dimethyl pyridyl-oxazoline, dmpyoxazo

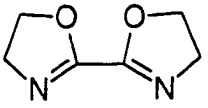

2-(1,3-oxazolin-2-yl)-1,3-oxazol
(bis-oxazoline, bisoxazo

Figure 1. α-Diimine Ligands.

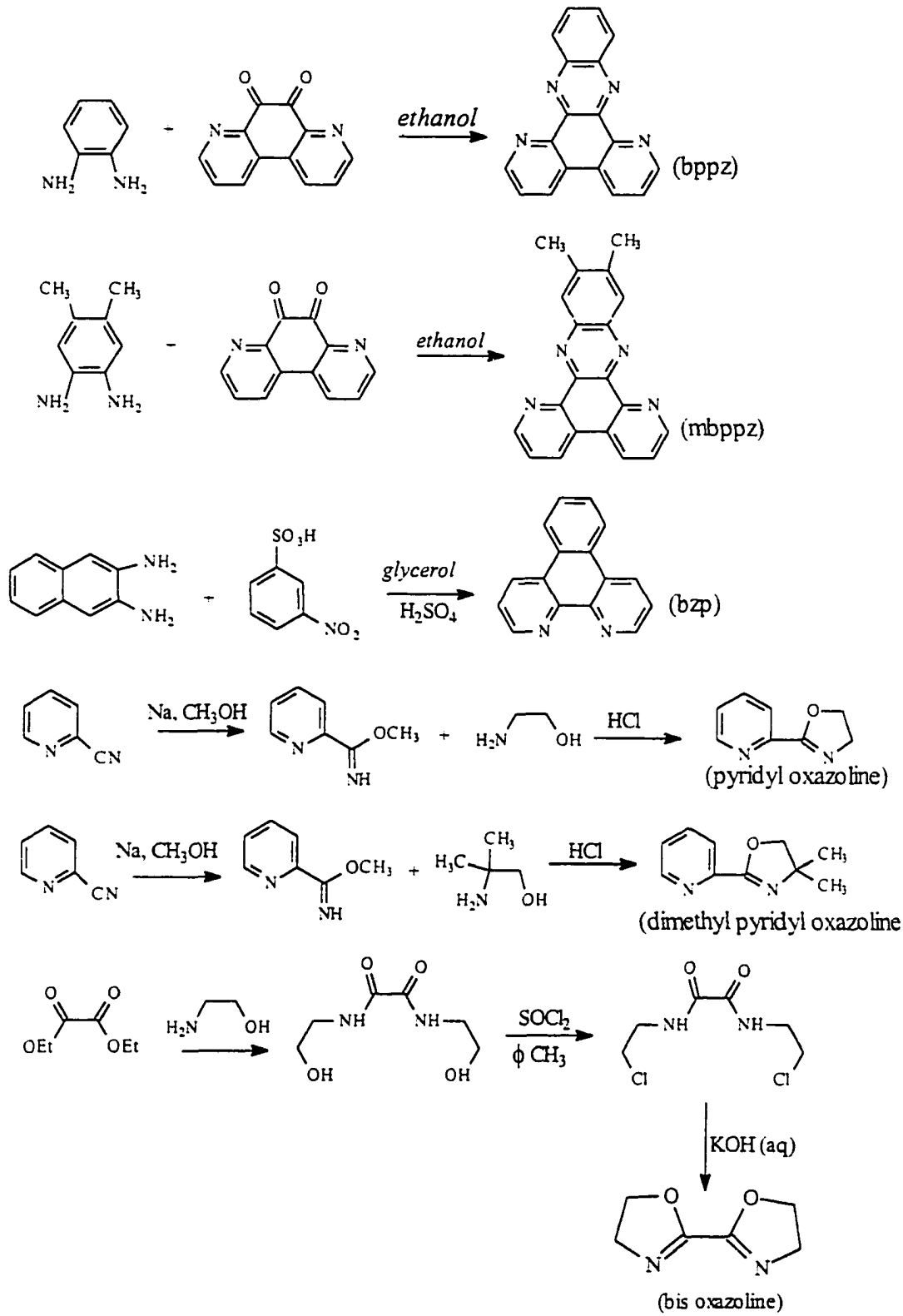

Scheme 1. Preparation of α-Diimine Ligands

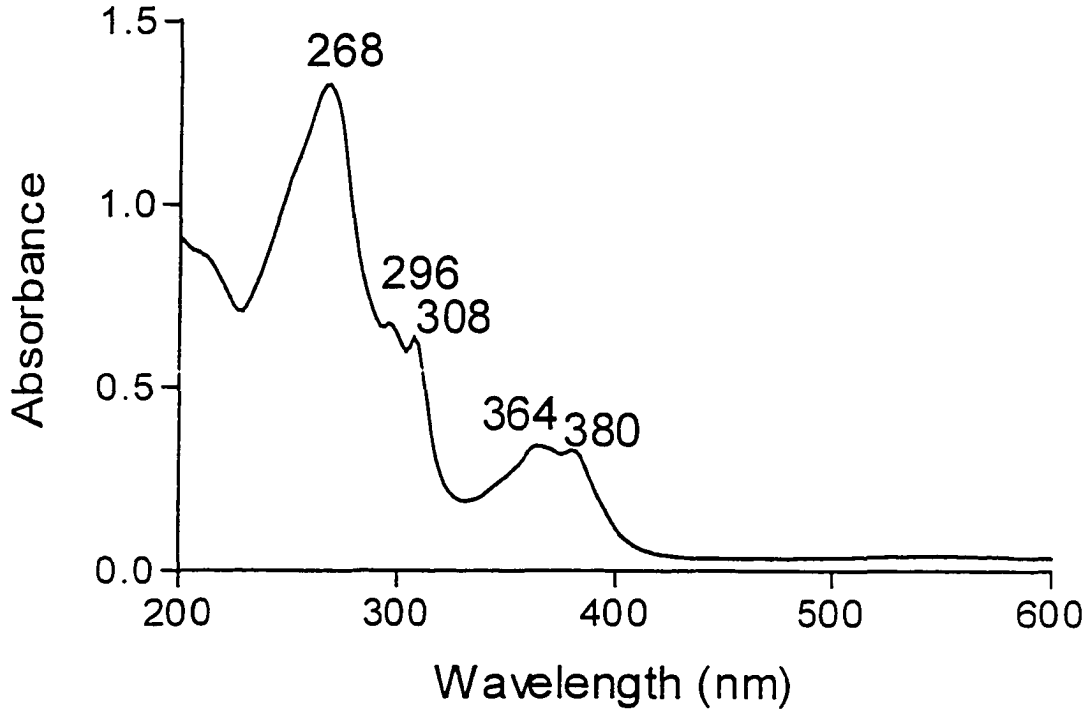

Fig.2. Absorbance spectrum of Bppz in water.

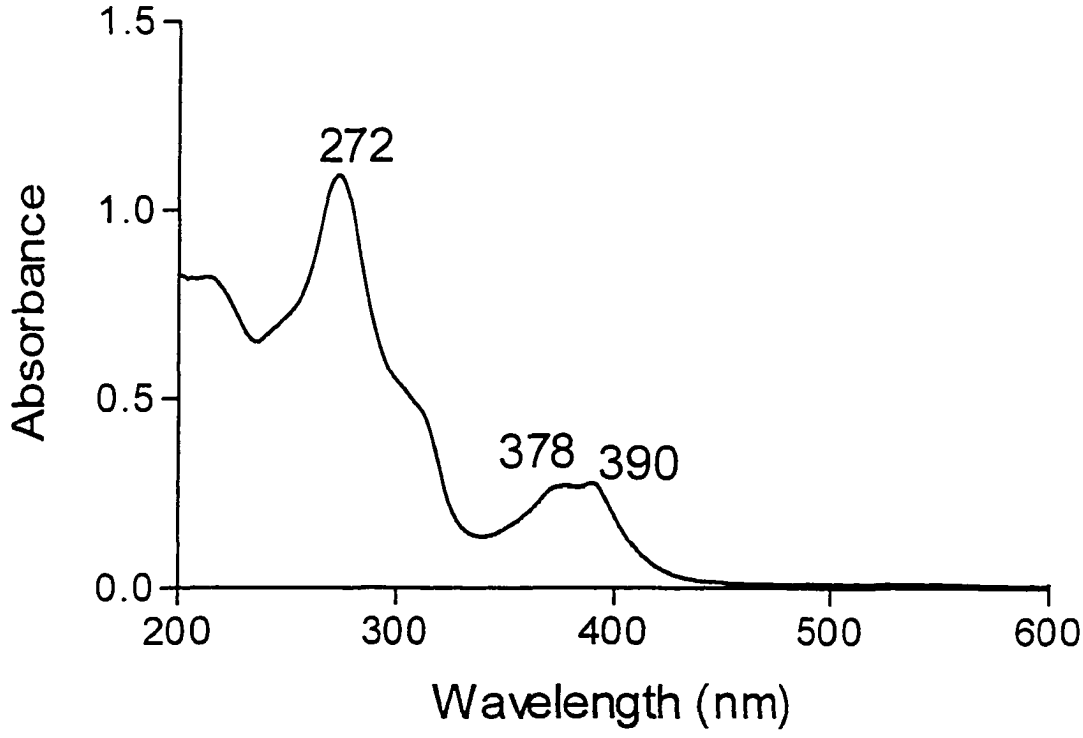

Fig.3. Absorbance spectrum of mbppz in water.

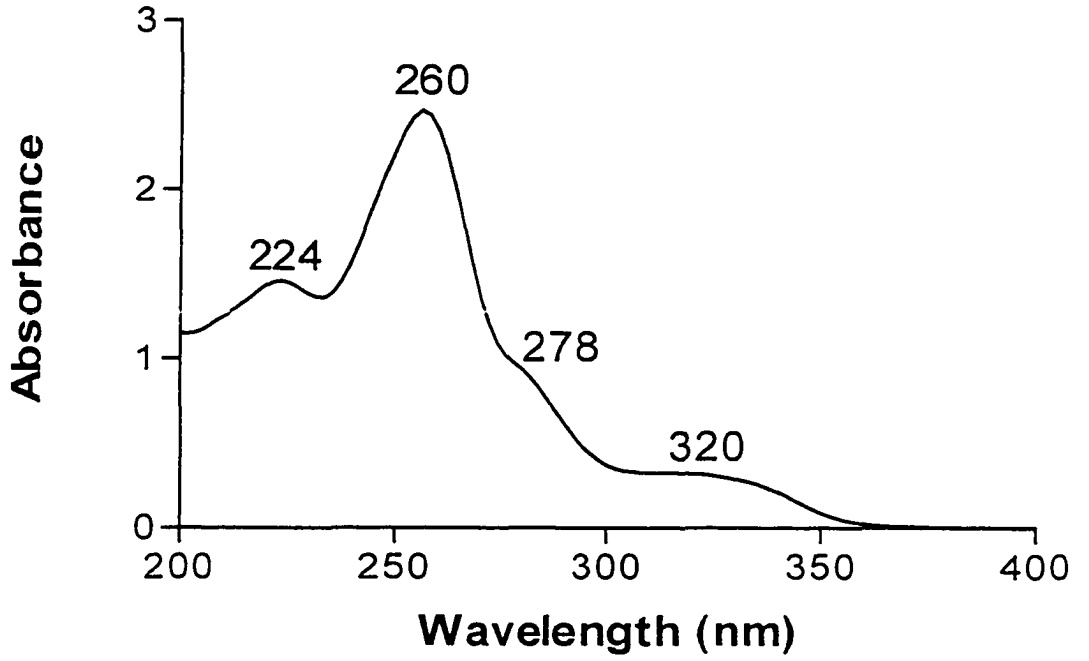

Fig.4. Absorbance spectrum of bzp in water.

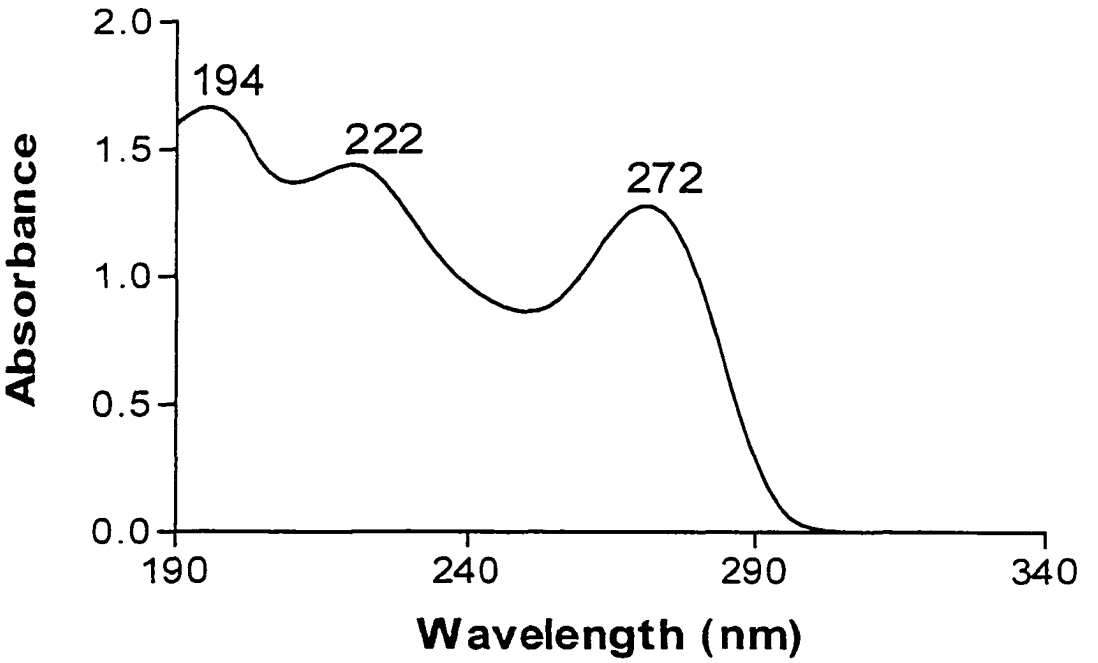

Fig.5. Absorbance spectrum of pyridyl-oxazoline in water.

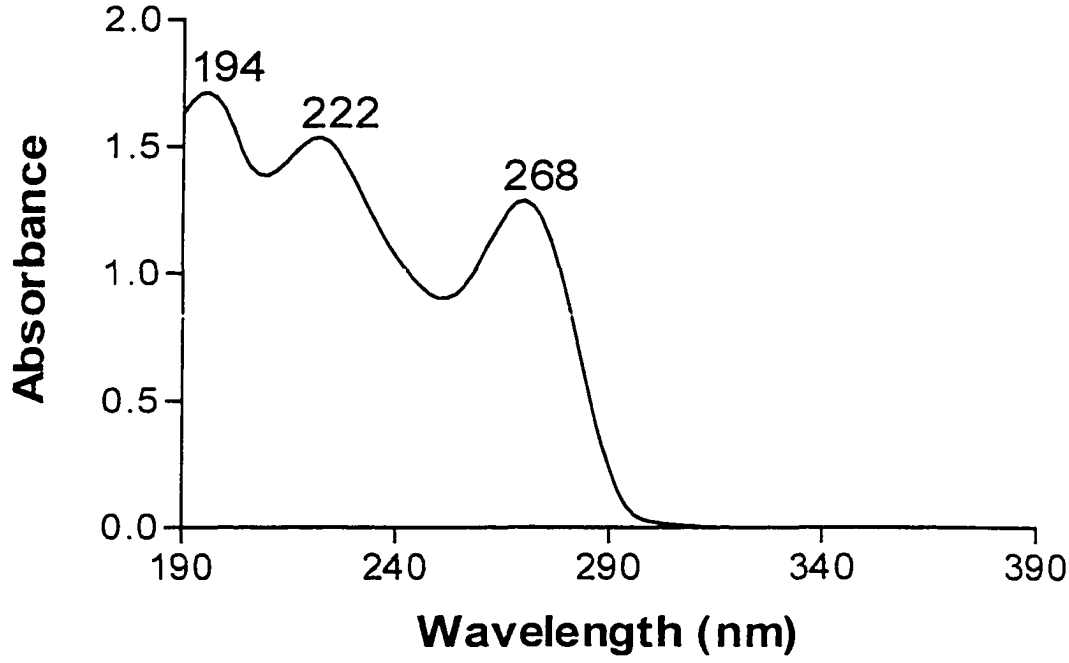

Fig.6. Absorbance spectrum of dimethyl pyridyl-oxazoline.

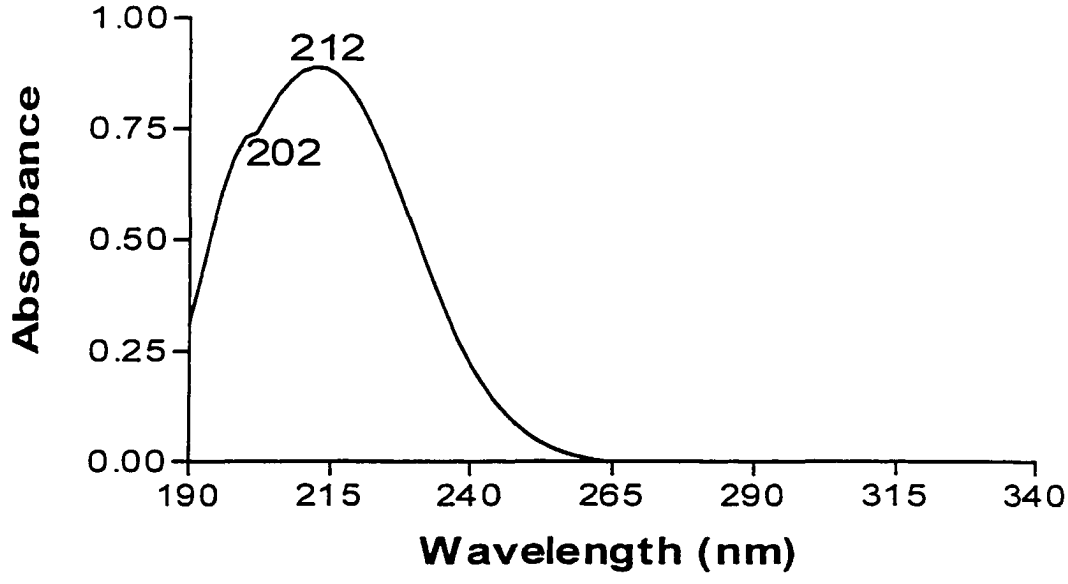

Fig.7. Absorbance spectrum of bis-oxazoline in water.

Chapter III.
New $Ru(bpy)_2L^{2+}$ Complexes.

Synthesis

Racemic bis-bipyridine complexes of $[Ru(bpy)_2L)]^{2+}$ (L = ppz, bppz, mbppz, ippz, bzp, bis-oxazoline (bisoxazo), pyridyl-oxazoline (pyoxazo), dimethyl pyridyl-oxazoline (dmpyoxazo) was prepared by refluxing one equivalent of Ru $(bpy)_2Cl_2$ with an excess of the ligand in 50% ethanol. The optical isomers were prepared by refluxing one equivalent of Δ / Λ-$[Ru(bpy)_2 (py)_2]^{2+}$ (resolution in experimental section) with an excess of the ligand in ethylene glycol.

Characterization

3.1 Racemic, and Δ/Λ $Ru(bpy)_2bppz^{2+}$

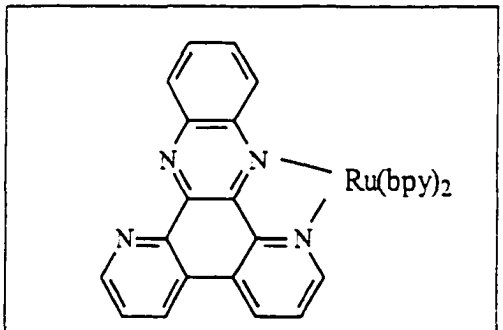

(Racemic, and Δ / Λ isomers)

NMR

The 400MHz ^1H NMR spectrum measured in DMSO-d_6 exhibited a complex series of signals in the range of δ 6.55058 – 9.55461.This series of signals were identical for all three complexes (racemic and optical isomers). The 400MHz ^{13}C NMR spectrum

measured in DMSO-d_6 were also identical for all three complexes. The frequencies of the resonances are summarized in Table I. Shown in the table are the expected 38 resonances, 20 for the carbons on the coordinated bipyridines, and 18 on the coordinated bppz ligand.

HRFAB

Complex		Calculated MW	Found
Λ-$[Ru(bpy)_2bppz]^{2+}$	$-2PF_6$	696.1324	696.1316
	$-PF_6$	841.1060	841.1
Δ-$[Ru(bpy)_2bppz]^{2+}$	$-2PF_6$	696.1324	696.1343
	-PF6	841.1060	841.0
$[Ru(bpy)_2bppz]^{2+}$	$-2PF_6$	696.1324	696.1327
	$-PF_6$	841.1060	841.0

Absorption Spectra.

All three complex ions exhibited identical absorption spectra, Fig.1, and identical molar absorbtivities in water. The molar absorptivity determined in water was as follows: $\varepsilon_{546} = 10400$.

Circular Dichroism

The chirality of the optical isomers was determined by circular dichroism as shown in Fig.8. The delta (Δ) isomer exhibited an ellipticity of -116, $\Delta\epsilon_{292} = -116\ M^{-1}cm^{-1}$. The lambda ($\Lambda$) isomer exhibited an ellipticity of +116, $\Delta\epsilon_{292} = +116\ M^{-1}cm^{-1}$.

Emission Spectra.

The luminescence spectra of all three complexes are identical in fluid solution at room temperature. These complexes on excitation at 540 nm, luminesce in water at 820nm, but in acetonitrile solution an enhancement of emission intensity was observed accompanied by a blue shift in emission maximum to 806nm. The emission spectra for $[Ru(bpy)_2bppz]^{2+}$ is represented in Figure12, and the emission data is represented in Table 14.

3.2 Racemic and Δ/Λ $Ru(bpy)_2mbppz^{2+}$

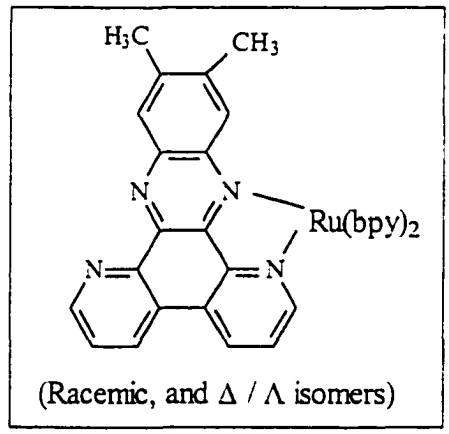

(Racemic, and Δ / Λ isomers)

NMR

The 400MHz ^1H NMR spectrum measured in DMSO-d_6 exhibited a complex series of signals in the range of 7.05-9.48. This series of signals were identical for all three complexes (racemic and optical isomers). The 400MHz ^{13}C NMR spectrum measured in DMSO-d_6 were also identical for all three complexes. The frequencies of the resonances are summarized in Table 2. Shown in the table are the expected 40 resonances, 20 for the carbons on the coordinated bipyridines, and 20 on the coordinated mbppz ligand.

HRFAB

Complex		Calculated MW	Found
Λ-$[Ru(bpy)_2mbppz]^{2+}$	$-2PF_6$	724.1637	724.1637
	$-PF_6$	869.091718	869.1
Δ-$[Ru(bpy)_2mbppz]^{2+}$	$-2PF_6$	724.1637	724.1624
	$-PF_6$	869.0917	869.0
$[Ru(bpy)_2mbppz]^{2-}$	$-2PF_6$	724.1637	724.1640
	$-PF_6$	869.0917	869.0

Absorption Spectra.

All three complex ions exhibited identical absorption spectra, Figure 2, and identical molar absorbtivities in water. The molar absorptivity determined in water was as follows: $\varepsilon_{534} = 10100$.

Circular Dichroism

The chirality of the optical isomers was determined by circular dichroism as shown in Figure 9. The delta (Δ) isomer exhibited an ellipticity of -105, $\Delta\epsilon_{292} = -105\ M^{-1}cm^{-1}$. The lambda ($\Lambda$) isomer exhibited an ellipticity of $+103$, $\Delta\epsilon_{292} = +103\ M^{-1}cm^{-1}$.

Emission Spectra.

All three complexes exhibited identical luminescence spectra in fluid solution at room temperature. These complexes on excitation at 540nm luminesce in water at

802nm, whereas in acetonitrile an enhancement in emission was observed accompanied by a blue shift in emission maximum to 780nm. The emission spectrum for $[Ru(bpy)_2mbppz]$ is represented in Figures 13, and the emission data is summarized in Table 14.

3.3 Racemic, Δ/Λ $Ru(bpy)_2bzp^{2+}$

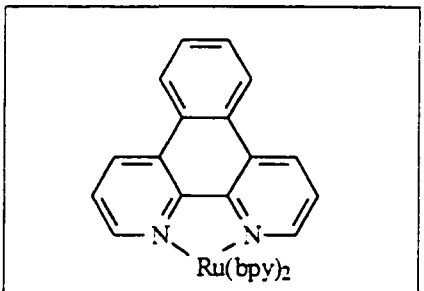

(Racemic, and Δ / Λ isomers)

NMR

The 400MHz 1H NMR spectrum measured in DMSO-d_6 exhibited a complex series of signals in the range of δ 6.71-9.52. This series of signals were identical for all three complexes (racemic and optical isomers). The 400MHz ^{13}C NMR spectrum measured in DMSO-d_6 were also identical for all three complexes. The frequencies of the resonances are summarized in Table 3. Shown in the table are the expected 18 signals, 10 for the carbons on the coordinated bipyridines, and 8 on the coordinated benzo-1,10-phenanthroline ligand.

HRFAB

Complex		Calculated MW	Found
Λ-$[Ru(bpy)_2bzp]^{2+}$	$-2BF_4$	644.1262	644.1252
	$-BF_4$	730.9308	731.0
Δ-$[Ru(bpy)_2bzp]^{2+}$	$-2PF_6$	644.1262	644.1261
	$-PF_6$	789.0542	789.0
$[Ru(bpy)_2bzp]^{2-}$	$-2PF_6$	644.1262	644.1273
	$-PF_6$	789.0542	789.0

Absorption Spectra

All three complex ions exhibited identical absorption spectra, Fig.3, and identical molar absorbtivities in water. The molar absorbtivity determined in water was as follows: $\varepsilon_{452} = 18000$.

Circular Dichroism

The chirality of the optical isomers was determined by circular dichroism as shown in Fig.10. The delta (Δ) isomer exhibited an ellipticity of –199.7, $\Delta\epsilon_{292} = -199.7$ $M^{-1}cm^{-1}$. The lambda (Λ) isomer exhibited an ellipticity of +182.5, $\Delta\epsilon_{292} = +182.5$ $M^{-1}cm^{-1}$.

Emission Spectra

In water all three complexes on excitation at 450nm exhibit identical luminescence spectra at 605nm. However, in acetonitrile an enhancement of the emission maximum accompanied by a blue shift in the emission maximum to 604nm was observed. The emission spectrum of $[Ru(bpy)_2bzp]^{2+}$ is represented in Figure 14, and the emission data is summarized in Table 14.

3.4 Racemic, and Δ/Λ $Ru(bpy)_2(ippz)^{2+}$

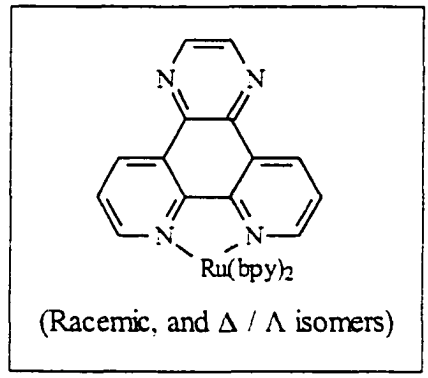

(Racemic, and Δ / Λ isomers)

NMR

The 400MHz ^1H NMR spectrum measured in DMSO-d_6 exhibited a complex series of signals in the range of δ7.36-9.57. This series of signals were identical for all three complexes (racemic and optical isomers). The 400MHz ^{13}C NMR spectrum measured in DMSO-d_6 were also identical for all three complexes. The frequencies of the resonances are summarized in Table 4. Shown in the table are the expected 34 resonances, 20 for the carbons on the coordinated bipyridines, and 14 on the coordinated ippz ligand.

HRFAB

Complex		Calculated MW	Found
Λ-$[Ru(bpy)_2ippz]^{2+}$	$-2BF_4$	646.1167	646.1179
	$-BF_4$	732.9213	733.0
Δ-$[Ru(bpy)_2ippz]^{2+}$	$-2BF_4$	646.1167	646.1174
	$-BF_4$	732.9213	733.0
$[Ru(bpy)_2ippz]^{2+}$	$-2PF_6$	646.1167	646.1165
	$-PF_6$	791.0447	791.0

Absorption Spectra.

All three complex ions exhibited identical absorption spectra, Fig.4, and identical molar absorbtivities in water. The molar absorbtivity determined in water was as follows: $\varepsilon_{450} = 16000$.

Circular Dichroism.

The chirality of the optical isomers was determined by circular dichroism. The delta (Δ) isomer exhibited an ellipticity of –186.5, $\Delta\epsilon_{292} = -186.5\ M^{-1}cm^{-1}$. The lambda (Λ) isomer exhibited an ellipticity of +158.2, $\Delta\epsilon_{292} = +158.2\ M^{-1}cm^{-1}$. The circular dichroism spectra of each optical isomer are shown in Fig.11.

Emission Spectra.

In water all three complexes exhibit identical luminescence spectra on excitation at 450nm at 612nm in water. However, in acetonitrile a small enhancement and blue shift of the emission maximum to 608nm was observed. The emission spectrum for $[Ru(bpy)_2ippz]^{2-}$ is presented in Fig.15, and the corresponding emission data in Table 14.

3.5 $Ru(bpy)_2L^{2+}$ (L = bis-oxazoline (bisoxazo), pyridyl-oxazoline (pyoxazo), dimethyl pyridyl-oxazoline (dmpyoxazo))

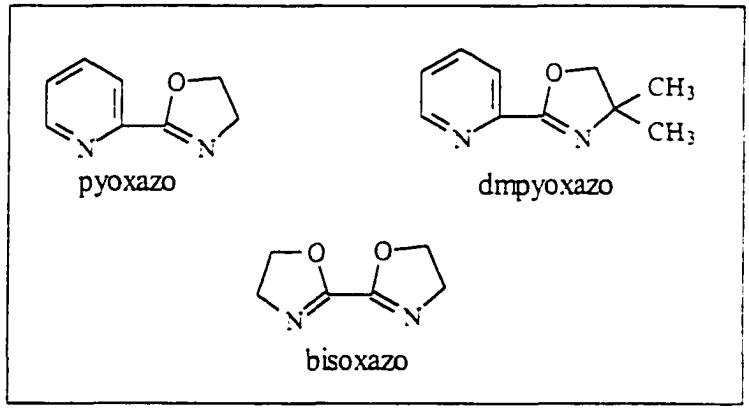

NMR

The 400 MHz ^1H spectrum for $[Ru(bpy)_2(pyoxazo)]^{2+}$ measured in DMSO-d_6 exhibited a complex series of signals in the range of δ 4.82-5.10 and δ 7.47-8.84. The 400MHz ^{13}C NMR spectrum measured in DMSO-d_6 exhibited 28 signals in accordance with the number of unique carbon atoms in the proposed structure. Twenty of the resonances are for the carbons on the coordinated bipyridines, and the remaining 8 resonances are on the coordinated pyridy-oxazoline ligand. The frequencies of the resonances are summarized in Table 5.

The ^{1}H NMR spectrum for $[Ru(bpy)_2(dmpyoxazo)]^{2+}$ measured in DMSO-d_6 exhibited a series of signals in the range of δ 4.37-4.56 and δ 7.22-8.76. The ^{13}C NMR spectrum measured in DMSO-d_6 exhibited 30 signals in accordance with the number of unique carbon atoms in the proposed structure. Twenty of the resonances are for the carbons on the coordinated bipyridines, and the remaining 10 resonances are on the coordinated dimethylpyridyl- oxazoline ligand. The frequencies of the resonances are summarized in Table 6.

The ^{1}H NMR spectrum for $[Ru(bpy)_2(bisoxazo)]^{2+}$ measured in DMSO-d_6 exhibited a series of signals in the range of δ 2.51-3.43 and δ 7.17-10.11. The ^{13}C NMR spectrum measured in DMSO-d_6 exhibited 13 signals in accordance with the number of unique carbon atoms in the proposed structure. Ten of the resonances are for the carbons on the coordinated bipyridines, and the remaining 3 resonances are on the coordinated bis- oxazoline ligand. The frequencies of the resonances are summarized in Table 7.

HRFAB

Ru(II) Complex		**Calculated MW**	**MW Found**
Pyridyl-oxazoline	$-2PF_6$	562.1055	562.1040
	$-PF_6$	707.0335	707.0
dimethylpyridyl-oxazoline	$-2PF_6$	590.1368	590.1386
	$-PF_6$	735.064818	735.0

Absorption Spectra.

The absorption spectrum for each metal complex are shown in Fig. 5 to 7. Their molar absorbtivities in aqueous solution are as follows:

Complex	Molar Absorptivity
$[Ru(bpy)_2(bisoxazo)]^{2+}$	$\varepsilon_{446} = 15500$
$[Ru(bpy)_2(pyoxazo)]^{2+}$	$\varepsilon_{456} = 10200$
$[Ru(bpy)_2(dmpyoxazo)]^{2+}$	$\varepsilon_{454} = 20400$

3.6 Two complete stereochemical sets of dinuclear ruthenium complexes.

Ligands such as ppz have two α-diimine sites and they can serve as bridging ligands in binuclear complexes such as $[(bpy)_2RuLRu(bpy)_2]^{4+}$. They could also be used to prepare multinuclear complexes. Because the local stereochemistry around each Ru atom is chiral, binuclear and multinuclear complexes should exist in various diasteomeric forms. With the chiral complex $[Ru(bpy)_2ppz]^{2+}$ (see earlier) we decided to explore this novel feature.[138]

By way of background, the preparation of ionic dendrimers incorporating multiple transition metal sites has been a topic of interest of late.[139] Numerous multinuclear Ru(II) complexes bearing bidentate bridging ligands at each metal site as well as multidentate bridging ligands have been prepared; in most instances these syntheses have generated mixtures of the possible stereoisomers.[140-152] Stereoisomeric mixtures of the present dinuclear ruthenium (II) complexes have been reported.[140, 141]

The preparation of stereochemically pure enantiomers of the dinuclear ruthenium (II) complexes generated from the $Ru(II)(phen)_2$ (phen = phenanthroline) building block has already been reported using the bridging ligands 2,5-bis(2-pyridyl)pyrazine and 2,2'-bipyrimidine.[153] More recently, MacDonnell and Bodgie[154] have reported the preparation of the complete set of stereoisomers ($\Delta\Delta$,$\Delta\Lambda$,$\Lambda\Lambda$) based on a pair of $Ru(II)(phen)_2$ building blocks with the bridging ligand tetrapyrido[3,2-a:',3'-c:3",2"-h:2",3"-j]phenazine (tpphz), and Tzalis and Tor [155] have prepared 'string-like' multiruthenium species in diastereoisomerically pure form. In the spirit of this effort we have prepared two complete sets of stereoisomers using as the bridging ligands 2,3-bis(2-pyridyl)pyrazine (dpp) and 4', 7'-phenanthroline-5',6':5,6-pyrazine (ppz) with $Ru^{II}(bpy)_2$ (bpy = 2,2'-bipyridine) as the metal building block. These stereochemically pure species are proposed as entry points for the generation of stereochemically pure multiruthenium complexes.

Results and Discussion

Separate reactions of each of the enantiomeric $[Ru(bpy)_2(py)_2]^{2+}$ (Δ1, Λ1) salts of equimolar amounts in ethylene glycol/water with each of the bridging ligands dpp and ppz provided the anticipated sets of enantiomers, Δ-$[Ru(bpy)_2dpp]^{2+}$ Δ2 and Λ-$[Ru(bpy)_2dpp]^{2+}$ Λ2 and Δ-$[Ru(bpy)_2ppz]^{2+}$ Δ3 and Λ-$[Ru(bpy)_2ppz]^{2+}$ Λ3.

Subsequent reaction of each of the optically pure materials Δ2, Λ2, Δ3 and Λ3 with each of Δ1 and Λ1 provided the enantiomeric sets of dinuclear complexes $\Delta\Delta$ -$[(bpy)_2Ru(dpp)Ru(bpy)_2]^{2+}$ $\Delta\Delta$4 and $\Lambda\Lambda$ -$[(bpy)_2Ru(dpp)Ru(bpy)_2]^{2+}$$\Lambda\Lambda$4 related to dpp and $\Delta\Delta$ -$[(bpy)_2Ru(ppz)Ru(bpy)_2]^{2+}$$\Delta\Delta$5 and $\Lambda\Lambda$ -$[(bpy)_2Ru(ppz)Ru(bpy)_2]^{2+}$$\Lambda\Lambda$5 related

to ppz. Reaction of Δ2 and Δ3 with each of Λ1 provided the meso species ΔΛ -$[(bpy)_2Ru(dpp)Ru(bpy)_2]^{2+}$ΔΛ4 related to dpp and ΔΛ -$[(bpy)_2Ru(ppz)Ru(bpy)_2]^{2+}$ ΔΛ5 related to ppz.

NMR

The 400MHz ^1H and ^{13}C spectrum for all the complexes were measured in DMSO-d_6. The ^1H spectra for Δ2 and Λ2 were identical. The spectrum exhibited a complex series of signals in the range of δ 7.1-8.9. The ^{13}C spectrum exhibited 34 signals in accord with the number of unique carbon atoms in the proposed structure, eight of which were indicated by distortionless enhancement of polarisation transfer (DEPT) measurement to be devoid of attached hydrogens. The frequencies of the resonances are summarized in Table 8.

Identical ^1H spectrum for Δ3 and Λ3 were measured which exhibited a complex series of signals in the range δ 7.2-9.8. The ^{13}C spectrum exhibited 34 signals in accord with the unique carbon atoms in the proposed structure, ten of which were indicated by DEPT measurement to be devoid of attached hydrogen atoms. The frequencies of the resonances are summarized in Table 9.

For ΔΔ4 and ΛΛ4 the ^1H and ^{13}C spectra were also identical. The ^1H spectrum exhibited a complex series of signals in the range δ 7.1-9.1. The ^{13}C spectrum exhibited 54 signals in accord with the number of unique carbon atoms in the proposed structure, twelve of which were indicated by DEPT measurement to be devoid of attached hydrogen atoms. Table 10 summarizes the frequencies of the ^{13}C resonances.

The ^{1}H spectrum for the complex $\Delta\Lambda 4$ exhibited a complex series of signals in the range δ 7.1-9.4. The ^{13}C spectrum exhibited 27 signals in accord with the number of unique carbon atoms in the proposed structure, six of which were indicated by DEPT measurement to be devoid of hydrogen atoms. Table 11 summarizes the frequencies of the ^{13}C resonances.

For $\Delta\Delta 5$ and $\Lambda\Lambda 5$ the ^{1}H and ^{13}C spectra were also identical. The ^{1}H spectrum exhibited a complex series of signals in the range δ 7.2-9.8. Although the structures of $\Delta\Delta 5$ and $\Lambda\Lambda 5$ contain 54 unique carbon atoms, its ^{13}C spectrum exhibited only 29 completely resolved unique signals. We could not improve the resolution to obtain fully separated signals for each unique carbon atom; it appears that in numerous instances the signals of several carbon atoms are clustered in a relatively broad unresolved band. The frequencies of the resonances are summarized in Table 12.

The ^{1}H spectrum of $\Delta\Lambda 5$ exhibited a complex series of signals in the range δ 7.2-9.8. The ^{13}C spectrum exhibited only 27 signals, in accord with the number of unique carbon atoms in the proposed structure, seven of which were indicated by DEPT measurement to be devoid of attached hydrogen atoms. The frequencies of the ^{13}C resonances are summarized in Table 13.

UV/VIS and CD Spectra

Measurements of UV/VIS and CD spectra were virtually identical but oppositely sensed (in the case of CD) for each enantiomeric pair. Thus, indicating that for each salt prepared these reactions proceed stereoselectively with retention of the absolute configuration. The meso compounds exhibited UV/VIS spectra corresponding to the

respective enantiomeric forms, and were inactive in the CD spectrum. Table 15 summarizes the CD data for the stereoisomers in aqueous solution.

Conclusion

Preparations of the racemic and chiral $Ru(bpy)_2L^{2+}$ (L = ppz, bppz, mbppz, ippz, bzp,dpp) have been reported. For the oxazolines, the chiral $Ru(bpy)_2L^{2+}$ (L= bis-oxazoline, pyridyl-oxazoline, dimethylpyridyl-oxazoline) complexes did not form from the reaction of these ligands with Δ/Λ-$[Ru(bpy)_2(py)_2]^{2+}$. Therefore, only the racemic Ru(II) polypyridyl complexes were synthesized. In addition, we have prepared two complete sets of binuclear complexes ($\Delta\Delta4$, $\Lambda\Lambda4$, $\Delta\Lambda4$, $\Delta\Delta5$, $\Lambda\Lambda5$, and $\Delta\Lambda5$) such as $[(bpy)_2RuLRu(bpy)_2]^{4+}$ (L = ppz, dpp). The structures of the complexes have been confirmed by NMR and mass spectrometry. All of the $[Ru(bpy)_2L]^{2+}$ complexes studied with the exception of the oxazolines emitted in aqueous solution and comparison of their enantiomers with the racemic complex demonstrated how chirality affects its emission in polar solvents such as acetonitrile.

Table I. ^{13}C NMR Resonances for $Ru(bpy)_2bppz^{2+}$ Complexes

Resonance	Shift	Resonance	Shift
1	123.700	20	138.327
2	124.214	21	138.732
3	124.701	22	138.880
4	124.701	23	143.715
5	124.771	24	144.104
6	125.351	25	144.316
7	125.901	26	145.108
8	127.563	27	147.118
9	127.732	28	148.835
10	127.797	29	150.970
11	128.319	30	150.970
12	128.388	31	151.638
13	130.734	32	151.830
14	131.692	33	152.035
15	132.645	34	153.636
16	132.667	35	156.062
17	132.876	36	156.118
18	133.068	37	156.323
19	138.163	38	156.525

Spectrum measured relative to TMS.

Table 2. ^{13}C NMR Resonances of $Ru(bpy)_2mbppz^{2+}$ (relative to TMS)

Resonance	Shift	Resonance	Shift
1	19.50	21	139.129
2	20.296	22	139.309
3	123.339	23	143.040
4	124.736	24	143.581
5	125.157	25	143.726
6	125.157	26	144.259
7	125.258	27	145.927
8	125.258	28	145.428
9	125.934	29	146.305
10	127.684	30	149.260
11	128.260	31	151.486
12	128.426	32	151.793
13	128.765	33	152.187
14	128.886	34	152.187
15	129.873	35	152.617
16	130.526	36	154.255
17	133.002	37	156.479
18	133.390	38	156.557
19	138.533	39	156.913
20	138.743	40	157.273

Table 3. ^{13}C NMR Resonances of $Ru(bpy)_2bzp^{2+}$

Resonance	Shift	Resonance	Shift
1	126.891	10	134.932
2	126.973	11	140.343
3	127.488	12	140.484
4	129.405	13	149.752
5	130.285	14	153.880
6	130.407	15	153.880
7	130.407	16	154.095
8	132.317	17	159.006
9	132.706	18	159.245

Spectrum measured relative to TMS.

Table 4. ^{13}C NMR Resonances for $Ru(bpy)_2(ippz)^{2+}$.

Resonance	Shift	Resonance	Shift
1	119.15	18	135.990
2	120.313	19	136.359
3	122.802	20	136.359
4	122.802	21	136.495
5	122.920	22	137.880
6	122.920	23	145.135
7	123.297	24	147.368
8	124.428	25	147.368
9	125.856	26	147.898
10	125.897	27	148.211
11	126.151	28	149.717
12	126.151	29	149.862
13	126.343	30	150.327
14	127.587	31	151.844
15	127.954	32	154.901
16	127.954	33	155.225
17	131.447	34	155.225

Spectrum measured relative to TMS.

Table 5. ^{13}C NMR Resonances for $Ru(bpy)_2(pyoxazo)^{2+}$

Resonance	Shift	Resonance	Shift
1	51.261	15	137.467
2	72.599	16	137.584
3	123.834	17	138.077
4	123.897	18	145.286
5	124.031	19	151.236
6	124.270	20	151.530
7	125.327	21	151.742
8	126.433	22	152.689
9	127.016	23	152.742
10	127.544	24	156.467
11	127.704	25	156.506
12	128.044	26	156.978
13	129.791	27	157.059
14	137.438	28	167.558

Spectrum measured relative to TMS.

Table 6. ^{13}C NMR Resonances $Ru(bpy)_2(dmpyoxazo)^{2+}$

Resonance	Shift	Resonance	Shift
1	25.200	16	137.776
2	26.180	17	137.776
3	69.229	18	137.853
4	81.867	19	138.059
5	123.915	20	145.818
6	124.118	21	150.944
7	124.218	22	152.098
8	124.218	23	152.163
9	126.986	24	152.652
10	127.226	25	152.958
11	127.672	26	156.408
12	127.765	27	157.711
13	127.970	28	157.097
14	137.717	29	157.181
15	137.727	30	165.984

Spectrum measured relative to TMS.

Table 7. ^{13}C NMR Resonances $[Ru(bpy)_2(bisoxazo)]^{2+}$.

Resonance	Shift	Resonance	Shift
1	124.2	8	138.4
2	124.5	9	138.9
3	125.7	10	152.0
4	126.7	11	153.4
5	127.5	12	156.9
6	128.1	13	157.8
7	128.1		

Spectrum measured relative to TMS.

Table 8. ^{13}C and DEPT NMR Resonances for Δ and Λ-$[Ru(bpy)_2dpp]^{2+}$ (Δ2, Λ2)

Resonance	^{13}C	Resonance	^{13}C	DEPT
1	125.59	18	150.69	
2	125.62	19	151.93	
3	125.79	20	152.17	
4	126.73	21	152.22	
5	128.70	22	152.24	
6	128.74	23	152.27	
7	128.82	24	152.28	
8	128.96	25	152.30	
9	128.97	26	152.81	
10	129.04	27		155.19
11	129.06	28		156.16
12	137.67	29		156.64
13	139.35	30		157.00
14	139.51	31		157.25
15	139.54	32		157.26
16	145.86	33		157.36
17	146.22	34		157.45

Spectra measured relative to TMS.

Table 9. ^{13}C and DEPT NMR Resonances forΔ and Λ-$[Ru(bpy)_2ppz]^{2+}$ (Δ3, Λ3)

Resonance	^{13}C	DEPT	Resonance	^{13}C	DEPT
1	124.08		18	138.10	
2	124.12		19		144.16
3	124.22		20		144.26
4	125.12		21		144.76
5	125.26		22	146.41	
6	125.47		23		147.05
7	127.02		24	148.30	
8	127.45		25	150.82	
9	127.53		26	151.16	
10	127.65		27	151.82	
11	127.70		28	151.92	
12	128.44		29	151.98	
13	132.56		30		155.81
14	132.90		31		155.97
15	137.91		32		155.99
16	138.01		33		156.40
17	138.06		34		156.42

Spectra measured relative to TMS.

Table 10. ^{13}C and DEPT NMR Resonances for ΔΔ and ΛΛ-$[(bpy)_2Ru(dpp)Ru(bpy)_2]^{4+}$ (ΔΔ4, ΛΛ4)

Resonance	^{13}C	Resonance	^{13}C	Resonance	^{13}C	DEPT
1	129.11	19	133.75	37	155.47	
2	129.15	20	133.78	38	155.65	
3	129.20	21	133.82	39	155.68	
4	129.22	22	133.84	40	156.04	
5	129.23	23	137.83	41	156.53	
6	129.25	24	141.91	42	156.69	
7	129.32	25	141.94	43		158.27
8	129.36	26	141.97	44		159.37
9	129.42	27	142.92	45		159.71
10	131.95	28	142.99	46		160.17
11	131.98	29	143.10	47		160.21
12	132.55	30	143.12	48		160.22
13	132.61	31	143.20	49		160.42
14	132.65	32	143.27	50		160.54
15	132.81	33	143.37	51		160.64
16	133.21	34	149.35	52		160.68
17	133.25	35	149.80	53		160.81
18	133.62	36	151.47	54		160.83

Spectra measured relative to TMS.

Table 11. ^{13}C and DEPT NMR Resonances of ΔΛ-$[(bpy)_2Ru(dpp)Ru(bpy)_2]^{4+}$ (ΔΛ4)

Resonance	^{13}C	Resonance	^{13}C	DEPT
1	125.57	15	151.75	
2	128.89	16	151.92	
3	128.96	17	152.12	
4	129.50	18	152.96	
5	130.06	19	153.29	
6	130.43	20	154.57	
7	132.38	21	155.58	
8	132.51	22		156.52
9	138.25	23		156.54
10	138.44	24		156.72
11	139.48	25		157.01
12	139.61	26		157.04
13	139.67	27		157.13
14	147.54			

Spectra measured relative to TMS.

Table 12.. ^{13}C and DEPT NMR Resonances for ΔΔ and ΛΛ-$[(bpy)_2Ru(ppz)Ru(bpy)_2]^{4+}$ (ΔΔ5, ΛΛ5)

Resonance	^{13}C	DEPT	Resonance	^{13}C	DEPT
1	126.93		16	141.03	
2	126.98		17	141.13	
3	127.06		18	141.30	
4	127.20		19		149.14
5	127.25		20		149.68
6	127.93		21	152.13	
7	130.18		22	153.58	
8	130.39		23	154.22	
9	130.45		24	154.60	
10	130.70		25	155.14	
11	130.85		26	156.41	
12	130.88		27	158.56	
13	131.21		28	158.72	
14	136.32		29	159.24	
15	136.36				

Spectra measured relative to TMS.

Table 13. ^{13}C and DEPT NMR Resonances for $\Delta\Lambda$-$[(bpy)_2Ru(ppz)Ru(bpy)_2]^{2+}$ ($\Delta\Lambda$5)

Resonance	^{13}C	DEPT	Resonance	^{13}C	DEPT
1	125.41		15		148.36
2	125.60		16	150.73	
3	125.68		17	151.97	
4	128.90		18	152.50	
5	128.94		19	153.41	
6	129.19		20	154.07	
7	129.39		21	154.79	
8	129.68		22		156.93
9	130.24		23		157.19
10	139.52		24		157.33
11	139.67		25		157.73
12	139.69		26		157.78
13	139.82				
14	147.69				

Spectra measured relative to TMS.

Table 14. Luminescence Data

Complex	λ_{max} (nm)	Conditions
$[Ru(bpy)_2bppz]^{2+}$	820	H_2O, 25°C
	808	CH_3CN, 25°C
$[Ru(bpy)_2mbppz]^{2+}$	802	H_2O, 25°C
	780	CH_3CN, 25°C
$[Ru(bpy)_2bzp]^{2+}$	605	H_2O, 25°C
	604	CH_3CN, 25°C
$[Ru(bpy)_2ippz]^{2+}$	612	H_2O, 25°C
	608	CH_3CN, 25°C

Table 15. The CD data for the stereoisomers in 4.6 (aqueous solution)

Compound	λ/nm	$\Delta\epsilon$ / $M^{-1}cm^{-1}$
Δ1	295	-154
Λ1	295	+156
Δ2	284	-112
Λ2	284	+135
Δ3	289	-123
Λ3	289	+127
ΔΔ4	288	-183
ΛΛ4	288	+177
ΔΛ4	Inactive	
ΔΔ5	288	-113
ΛΛ5	288	+112
ΔΛ5	Inactive	

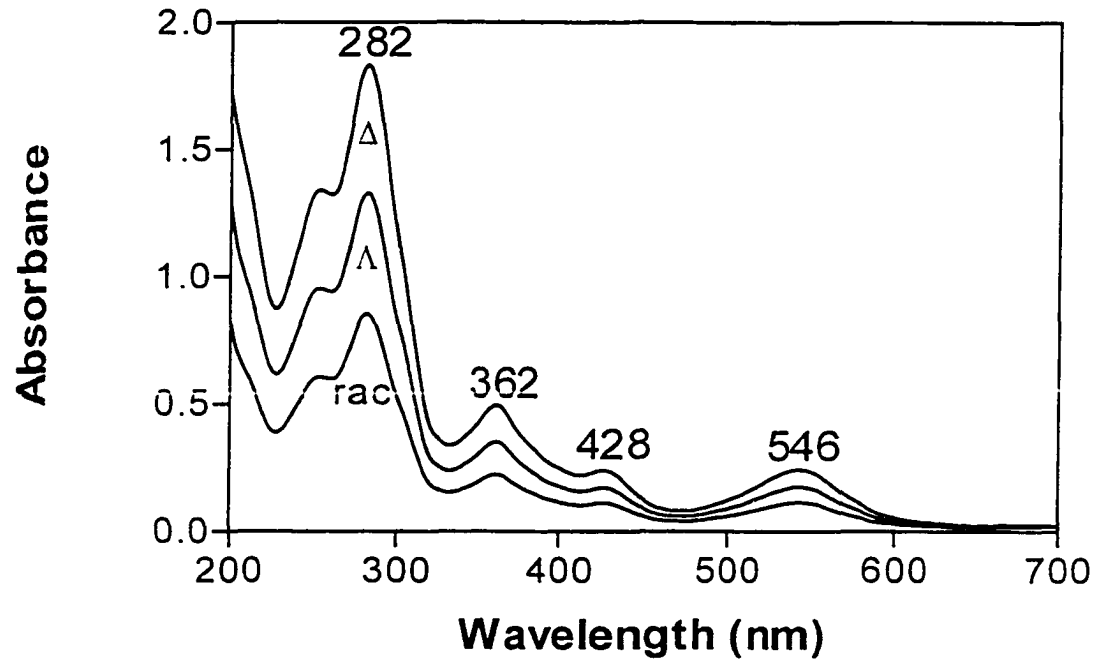

Fig.1. Absorption spectra of Δ-$[Ru(bpy)_2(bppz)]^{2+}$, Λ-$[Ru(bpy)_2(bppz)]^{2+}$, and racemic-$[Ru(bpy)_2(bppz)]^{2+}$ (rac) in aqueous solution.

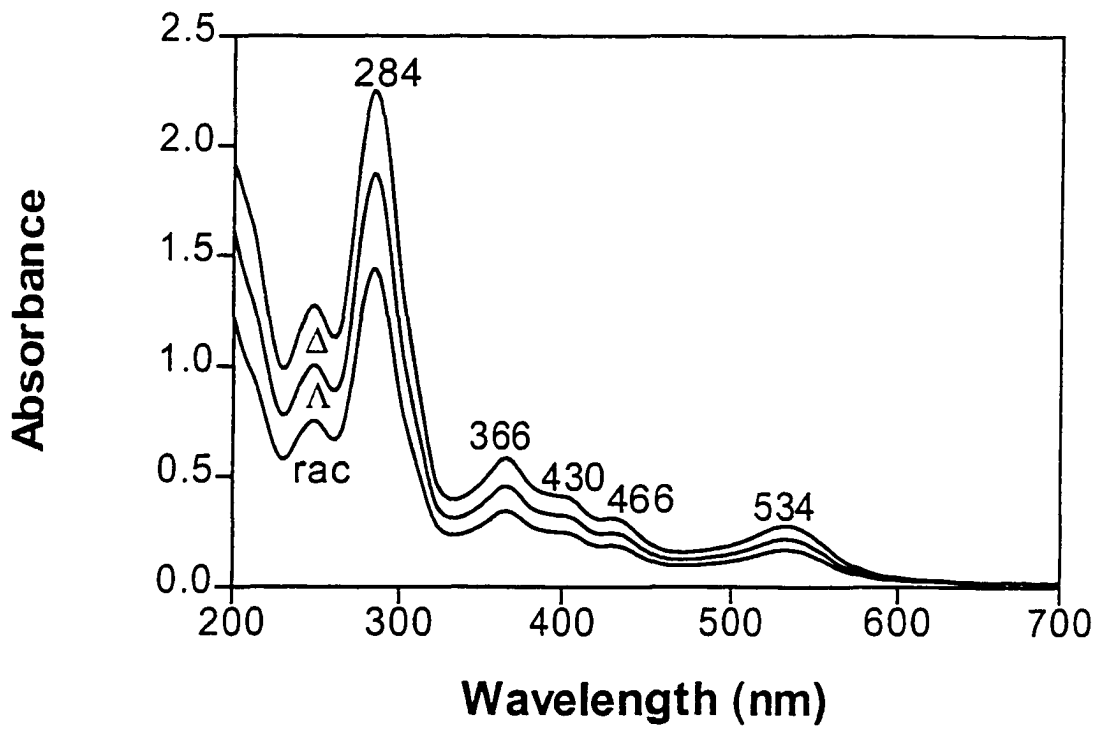

Fig.2 Absorption spectra of Δ-$[Ru(bpy)_2(mbppz)]^{2+}$, Λ-$[Ru(bpy)_2(mbppz)]^{2+}$, and -$[Ru(bpy)_2(mbppz)]^{2+}$ (rac) in aqueous solution.

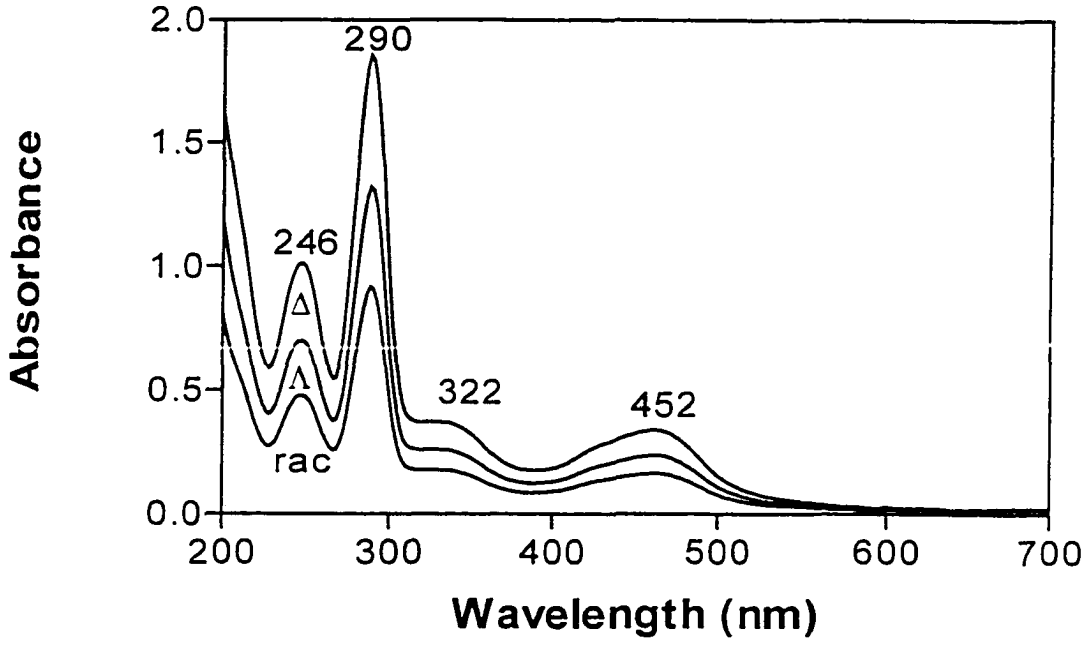

Fig.3 Absorbance spectra of Δ-$[Ru(bpy)_2(bzp)]^{2+}$, Λ-$[Ru(bpy)_2(bzp)]^{2+}$, and $[Ru(bpy)_2(bzp)]^{2+}$ (rac) in aqueous solution.

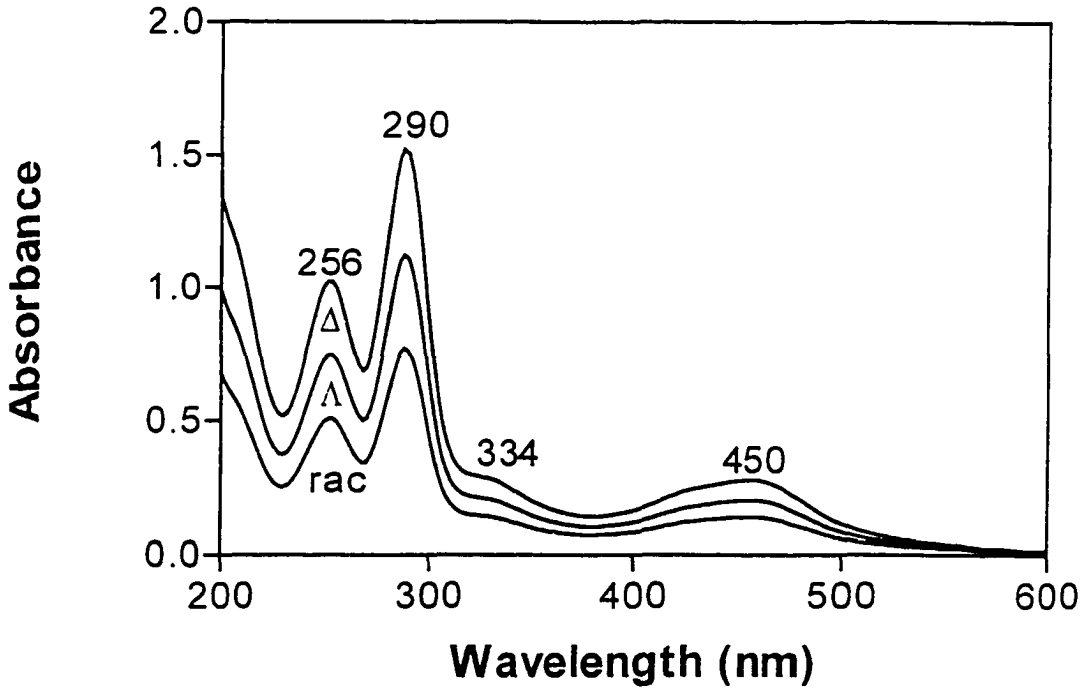

Fig.4. Absorbance Spectra of Δ-$[Ru(bpy)_2(ippz)]^{2+}$ (a), Λ-$[Ru(bpy)_2(ippz)]^{2+}$ (b), and $[Ru(bpy)_2(ippz)]^{2+}$ (c) in aqueous solution.

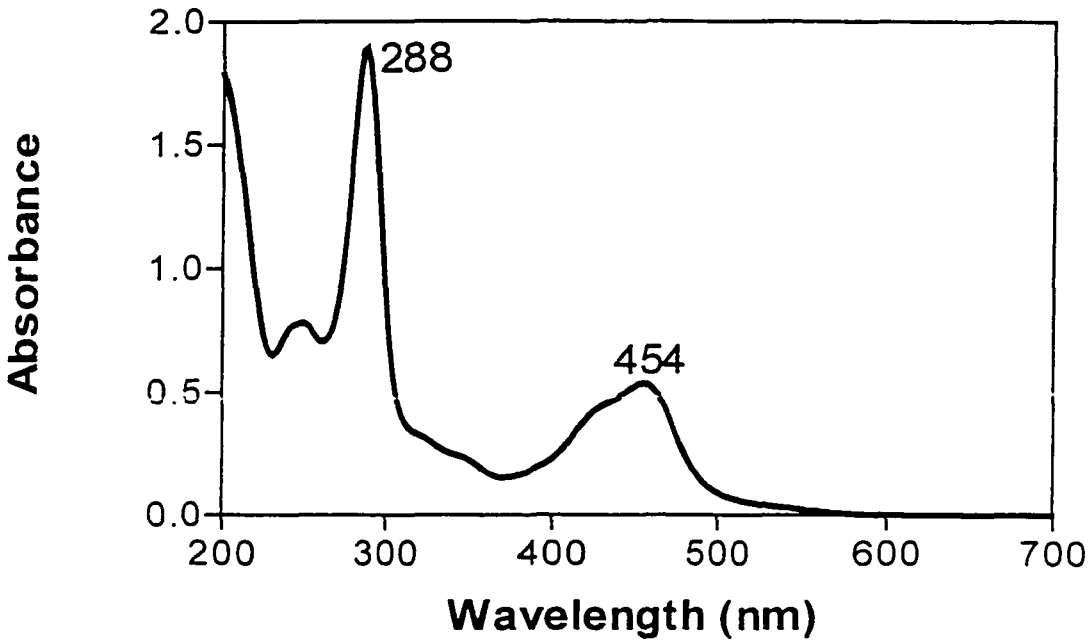

Fig. 5 Absorbance Spectrum of $[Ru(bpy)_2(dmpyoxazo)^{2+}$ in aqueous solution.

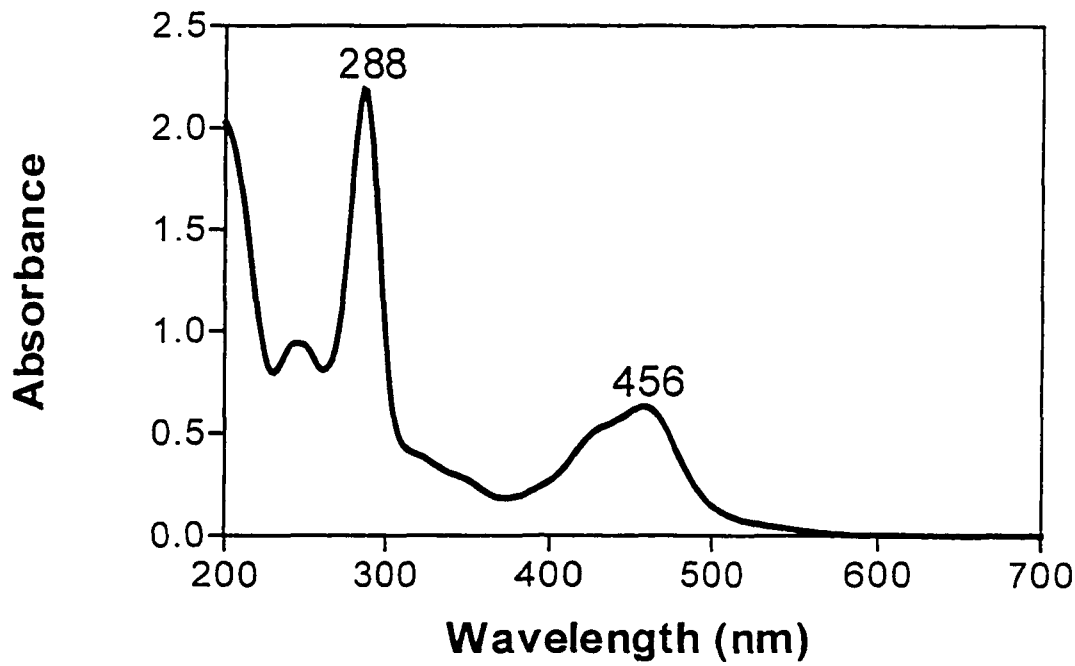

Fig.6 Absorbance Spectrum of $[Ru(bpy)_2(pyoxazo)]^{2+}$ in aqueous solution.

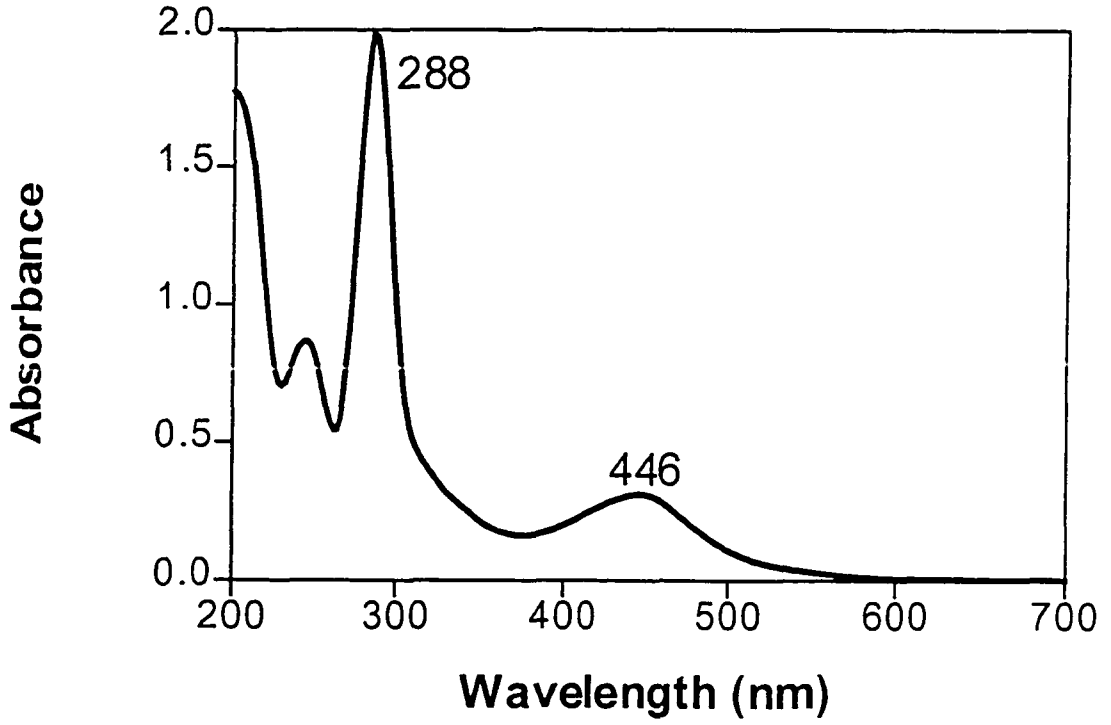

Fig.7 Absorbance Spectrum of $[Ru(bpy)_2(bisoxazo)]^{2+}$ in aqueous solution.

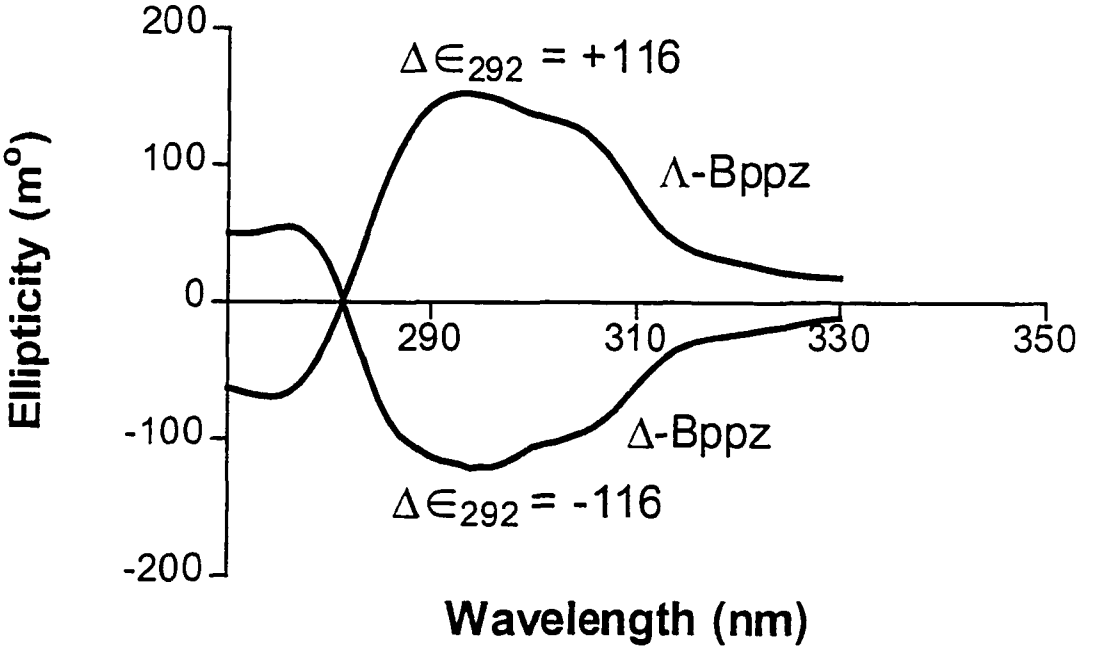

Fig.8. Circular Dichroism spectra of Δ and Λ-$[Ru(bpy)_2bppz]^{2+}$ in water.

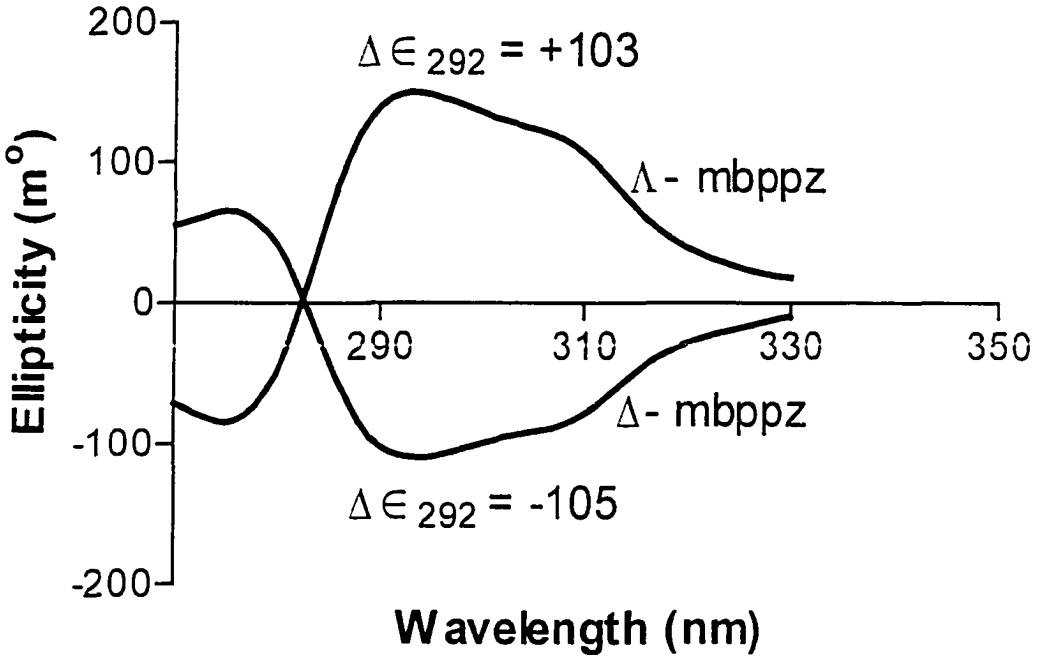

Fig.9 Circular Dichroism spectra of Δ and Λ- $[Ru(bpy)_2mbppz]^{2+}$ in water.

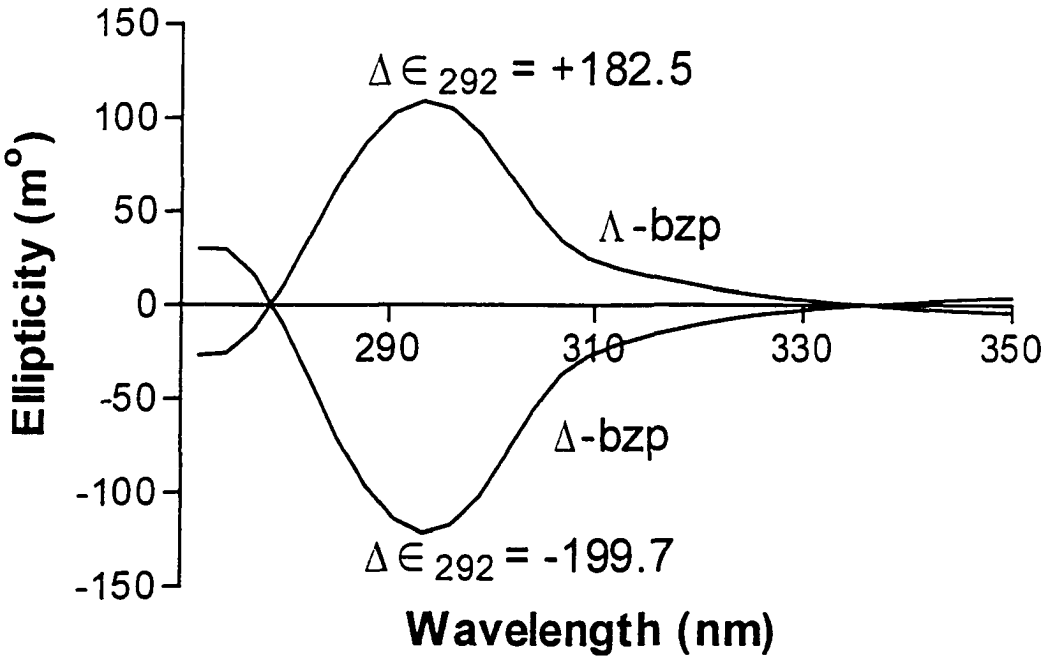

Fig.10 Circular Dichroism spectra of Δ and Λ-$[Ru(bpy)_2bzp]^{2+}$ in water.

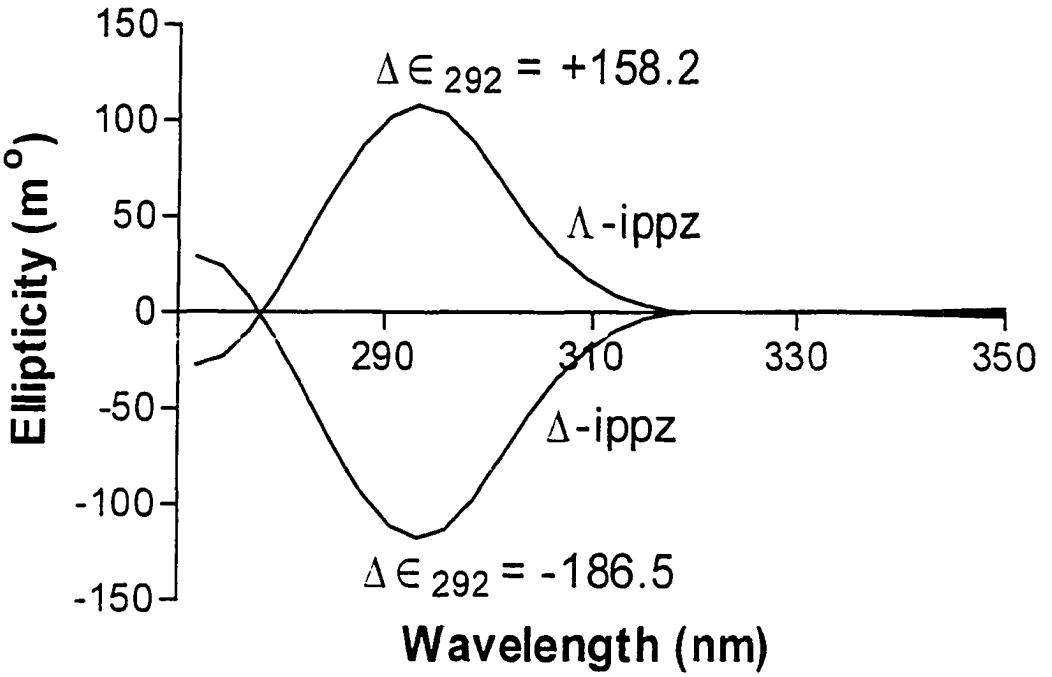

Fig.11. Circular Dichroism Spectra of Δ and Λ-$[Ru(bpy)_2ippz]^{2+}$ in water.

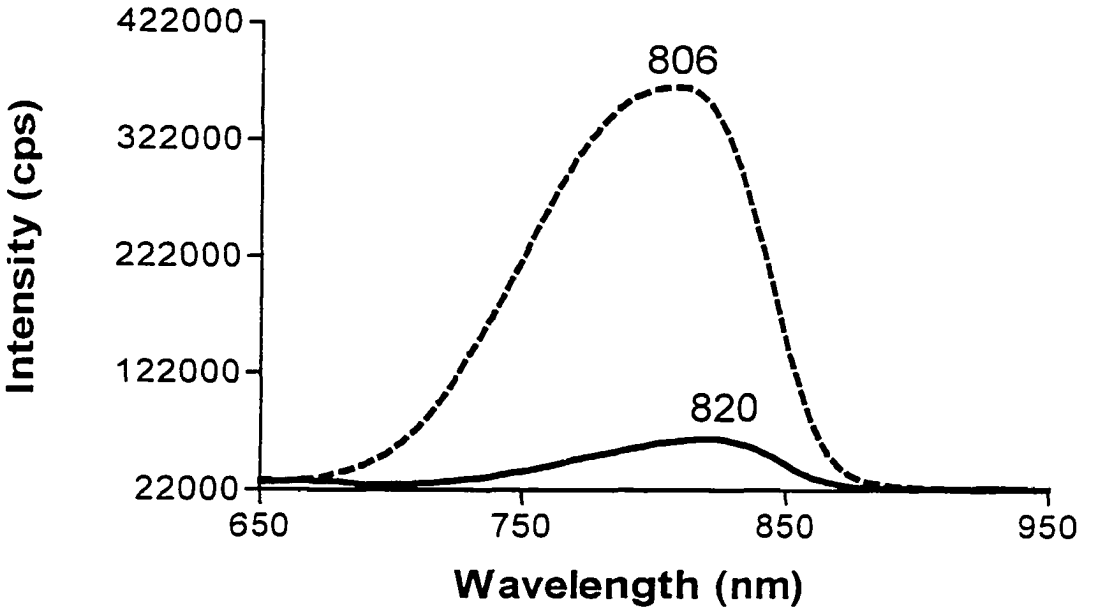

Fig.12. Emission Spectra of $[Ru(bpy)_2bppz]^{2+}$ in water (___) and in acetonitrile (---) at 25°C.

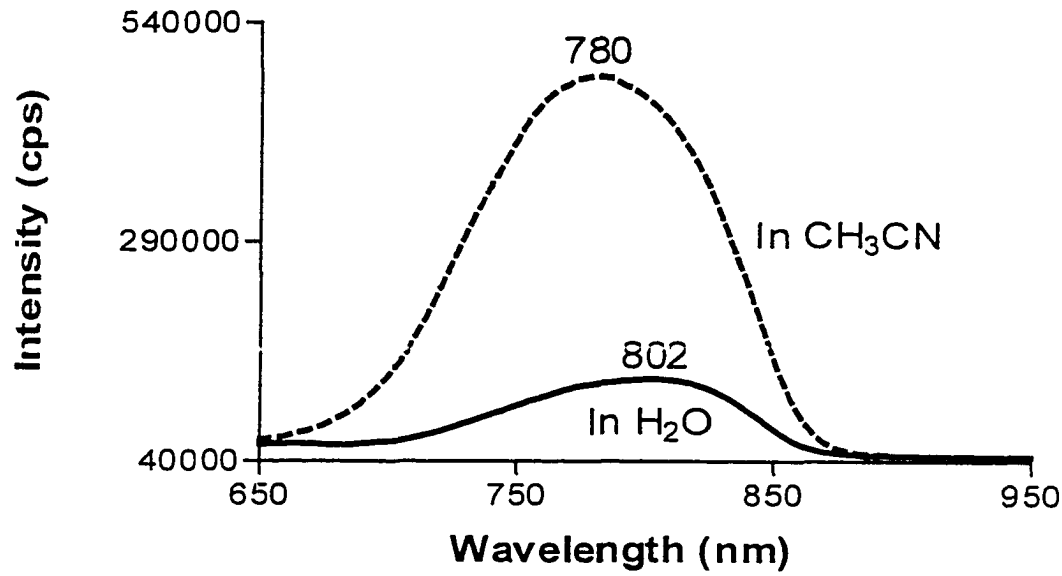

Fig.13. Emission Spectra of $[Ru(bpy)_2mbppz]^{2+}$ in water (___) and in acetonitrile (---) at 25°C.

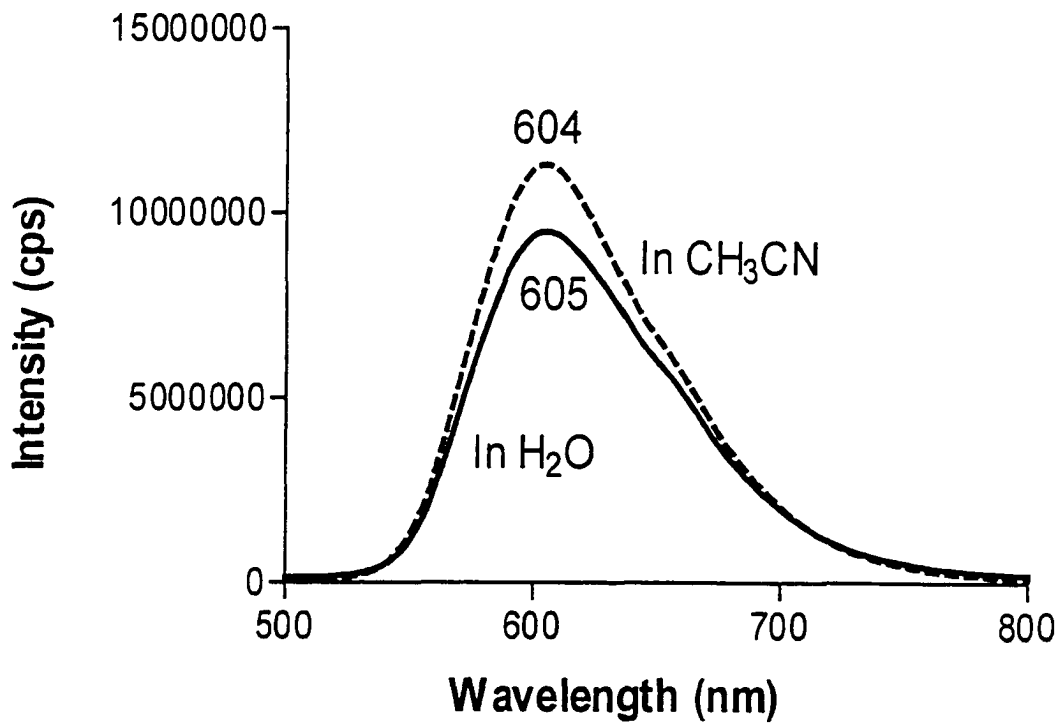

Fig.14. Emission Spectra of $[Ru(bpy)_2bzp]^{2+}$ in water (___) and in acetonitrile (---) at 25°C.

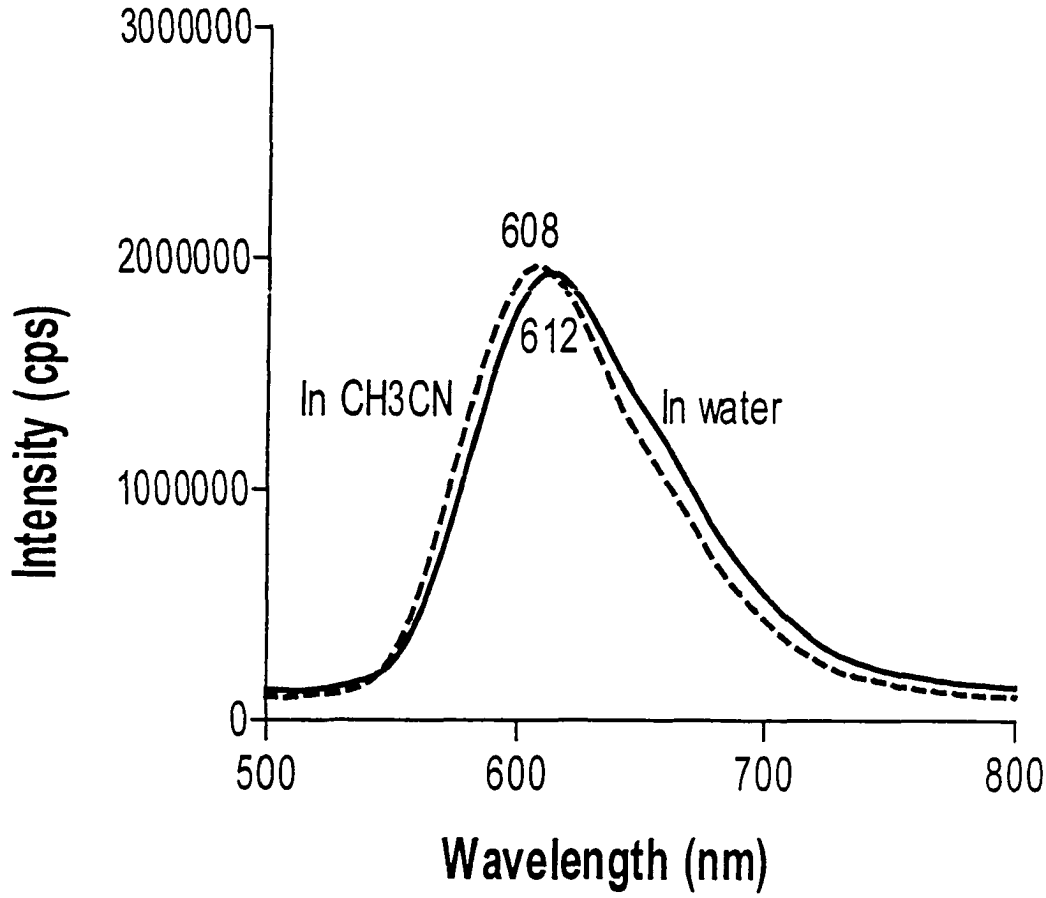

Fig.15. Emission Spectra of $[Ru(bpy)_2ippz]^{2+}$ in water (___) and in acetonitrile (---) at 25°C.

Chapter IV.
New RuL_3^{2+} Complexes.

Synthesis

The tris Ru(II) polypyridyl complexes, RuL_3^{2+} (L = bppz, pyridyl-oxazoline (pyoxazo), dimethyl pyridyl-oxazoline (dmpyoxazo)) were prepared by refluxing one equivalent of $Ru(DMSO)_4Cl_2$ with three equivalents of the respective ligand in 50% ethanol.

Characterization

4.1 $[Ru(bzp)_3]^{2+}$

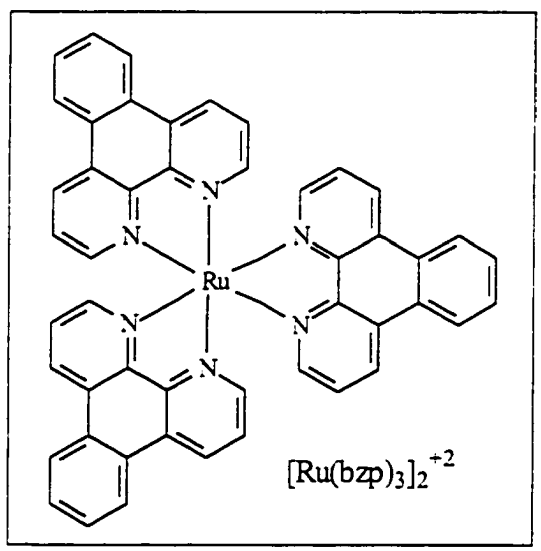

NMR

The 400MHz 1H NMR spectrum measured in DMSO-d_6 exhibited 5 signals in accordance with the structure which are as follows: δ 7.85 (dd, 2H), δ 8.07 (dd, 2H), δ 8.14 (d, 2H), δ 9.10 (dd, 2H), and δ 9.51 (d, 2H). The 400MHz ^{13}C NMR spectrum measured in DMSO-d_6 exhibited 8 signals. Since, the tris complex is symmetrical, D_3, the

resonances observed were in accordance with the 8 unique carbons in the structure. The frequencies of the resonances are summarized in Table 1.

HRFAB

Complex		Calculated MW	MW Found
$[Ru(bzp)_3]^{2+}$	$-2BF_4$	792.1575	792.1569
	$-BF_4$	878.9621	879.0

Absorption Specta.

The absorption spectrum is shown in Fig.1. The absorption bands are seen to be red shifted from that of the bis-complexes based on the ligand bzp. The molar absorptivity measured in water was identical to that of the bis-complexes (ε_{452} = 18000).

Emission Spectra.

The $[Ru(bzp)_3]^{2+}$ complex is luminescent in fluid solution at room temperature. This complex on excitation at 450nm luminescence strongly at 596nm in water, but an enhancement in emission intensity and a shift in emission maximum to 594nm was observed in acetonitrile at 25°C. The emission spectra are represented in Figure 4.

4.2 $[Ru(pyoxazo)_3]^{2+}$

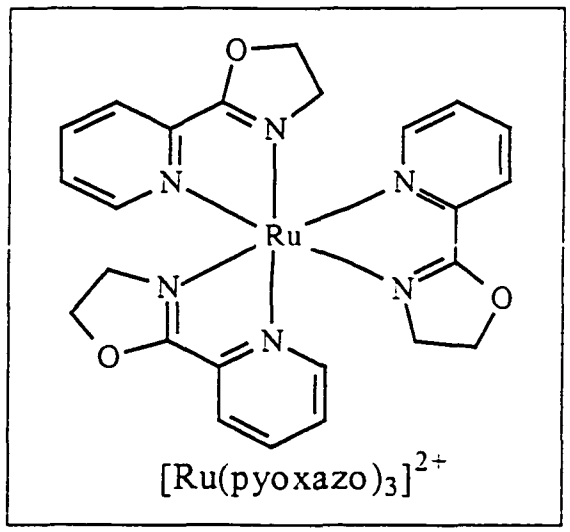

$[Ru(pyoxazo)_3]^{2+}$

NMR

The 400MHz ^1H NMR spectrum for the tris pyridyl-oxazoline complex, measured in DMSO-d_6, shows a complex series of signals ranging from δ 3.71-8.64. The 400MHz ^{13}C NMR spectrum, also measured in DMSO-d_6, exhibits 24 signals. For the tris pyridyl oxazoline complex there are two isomers possible which are the *fac* (facial, three similar ligands arranged in an all-*cis* fashion in an octahedron) and *mer* (meridional, three similar ligands but one pair arranged in a *trans* fashion) as shown in Figure 5. The *fac* isomer has a three-fold axis whereas the *mer* isomer lacks a center of symmetry. Additionally, in the *mer* isomer the ligands are diasterotopic so there will be a unique signal for each carbon atom because they are all in a different environment. Apparently, only the *mer* isomer forms because 24 ^{13}C NMR signals observed (An additional eight signals would have been expected if any *fac* isomer formed). The frequencies of the resonances are summarized in Table 2.

HRFAB

Tris Ru(II) Complex		**Calculated MW**	**MW Found**
Pyoxazo	$-2PF_6$	546.0953	546.0954
	$-PF_6$	691.0233	691.0

Absorption Spectra.

Figure 3 shows the absorption spectrum measured in water. The molar absorptivity measured in water is 1.22×10^4 ($\varepsilon_{466} = 1.22 \times 10^4$).

4.3 $[Ru(dmpyoxazo)_3]^{2+}$

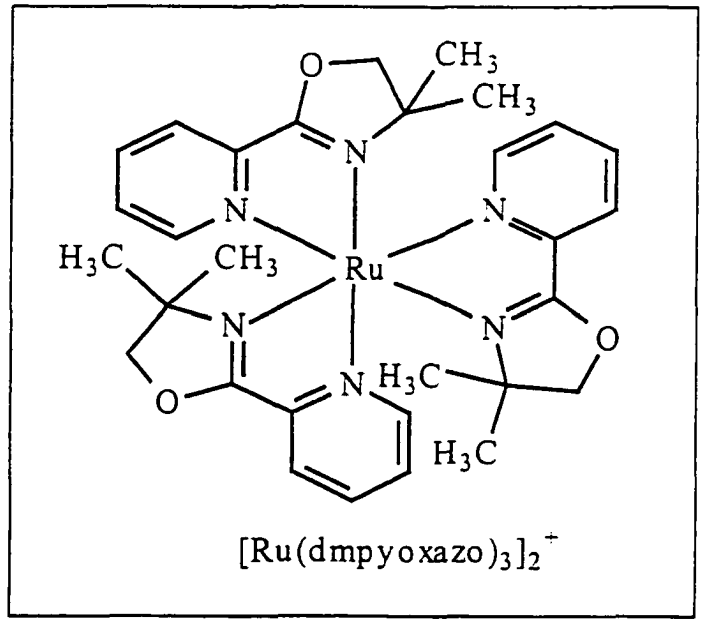

$[Ru(dmpyoxazo)_3]_2^+$

NMR

The 400MHz ^1H NMR spectrum for tris dimethyl pyridyl-oxazoline complex measured in DMSO-d_6 exhibited a complex series of signals from δ 4.36- 8.80. The

400MHz ^{13}C NMR spectrum measured in DMSO-d_6 exhibited 30 signals. The ^{13}C signals observed for the tris complex are due to formation of the *mer* isomer (*fac* isomer not formed) in which the ligands are diasterotopic (see Figure 5). Each carbon atom is therefore in a different environment, so 30 signals are observed (Additional peaks would be present if the *fac* isomer formed). The frequencies of the resonances are listed in Table 3.

HRFAB

Tris Ru(II) Complex		**Calculated MW**	**MW Found**
Dmpyoxazo	$-2PF_6$	630.1892	630.1890
	$-PF_6$	775.1172	775.0

Absorption Spectra.

Figure 4 shows the absorption spectrum of $[Ru(bpy)_2(dmpyoxazo)]^{2+}$ in water. The molar absorptivity measured in water is 1.05×10^4 ($\varepsilon_{456} = 1.05 \times 10^4$).

Table 1. ^{13}C NMR Resonance for $[Ru(bzp)_3]^{2+}$.

Resonance	Shift
1	125.837
2	127.647
3	128.786
4	130.593
5	131.015
6	133.256
7	148.277
8	152.761

Spectrum measured relative to TMS.

Table 2. ^{13}C Resonances for $[Ru(pyoxazo)_3]^{2+}$.

Resonance	Shift	Resonance	Shift
1	70.7	13	136.2
2	71.3	14	136.4
3	71.5	15	144.8
4	77.5	16	144.8
5	77.8	17	144.9
6	78.1	18	152.4
7	124.5	19	152.6
8	124.6	20	153.7
9	125.0	21	153.8
10	127.8	22	165.7
11	128.0	23	166.4
12	128.3	24	166.6

Spectrum measured relative to TMS.

Table 3. ^{13}C Resonances for $[Ru(dmpyoxazo)_3]^{2+}$.

Resonance	Shift	Resonance	Shift
1	70.4	16	138.9
2	70.6	17	139.2
3	70.7	18	139.4
4	70.8	19	139.4
5	82.6	20	147.4
6	82.7	21	148.0
7	83.0	22	148.4
8	125.5	23	150.2
9	127.1	24	154.9
10	127.8	25	155.7
11	128.0	26	157.4
12	130.2	27	166.8
13	130.5	28	166.8
14	131.2	29	167.8
15	131.3	30	168.0

Spectrum measured relative to TMS.

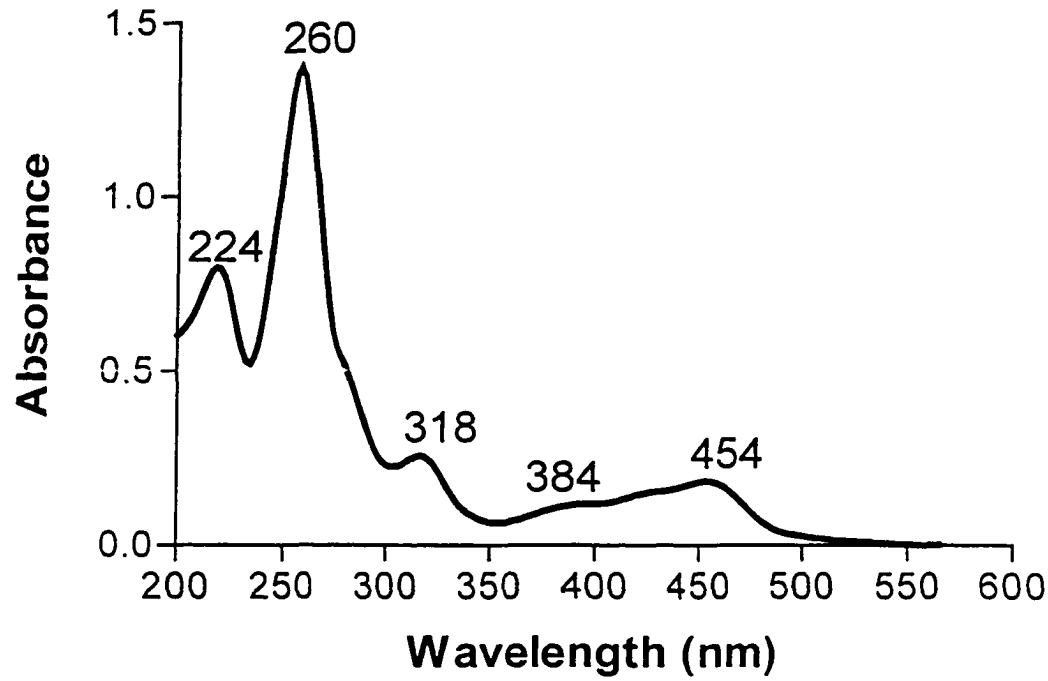

Fig.1. Absorbance spectrum of $[Ru(bzp)_3]^{2+}$ in aqueous solution.

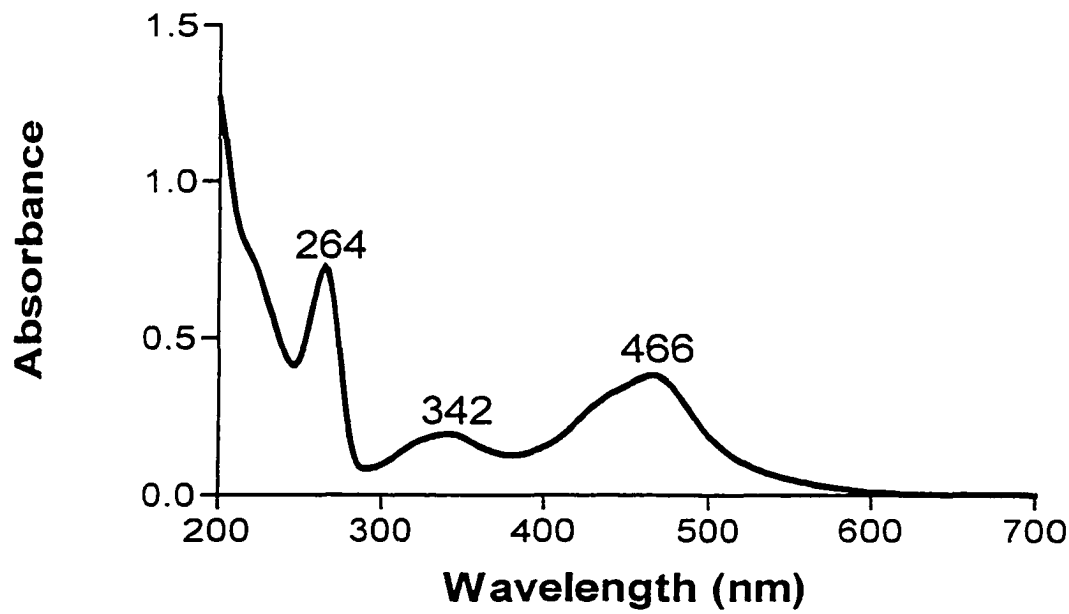

Fig.2. Absorption spectrum of $[Ru(pyoxazo)_3]^{2+}$ in aqueous solution.

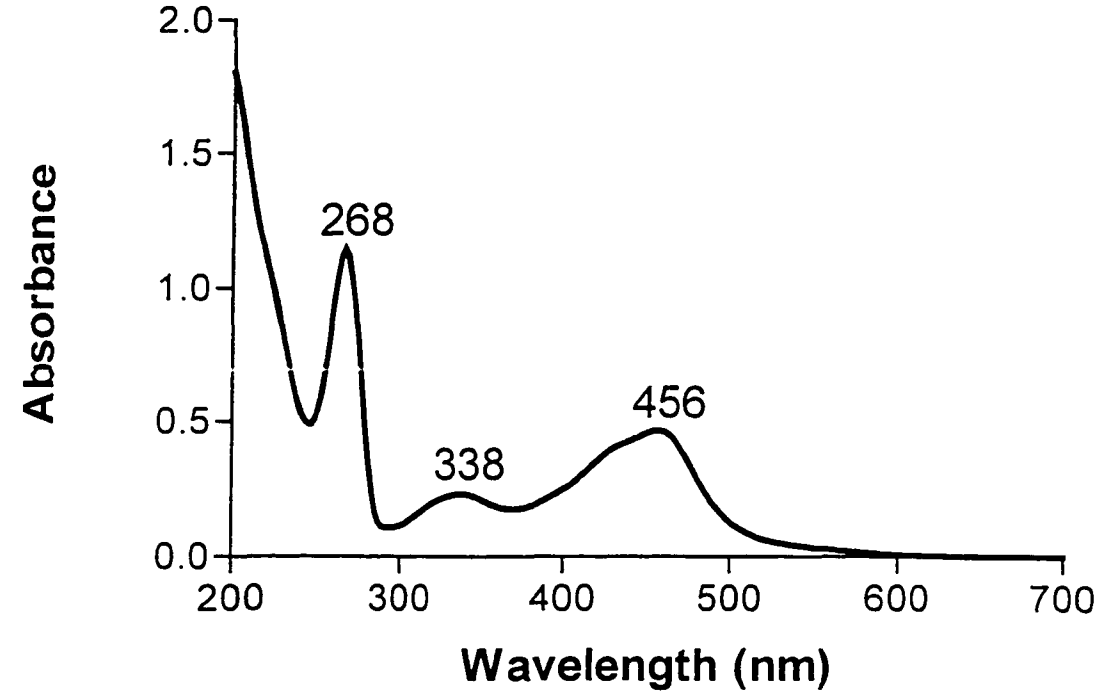

Fig.3. Absorption spectrum of $[Ru(dmpyoxazo)_3]^{2+}$ in aqueous solution.

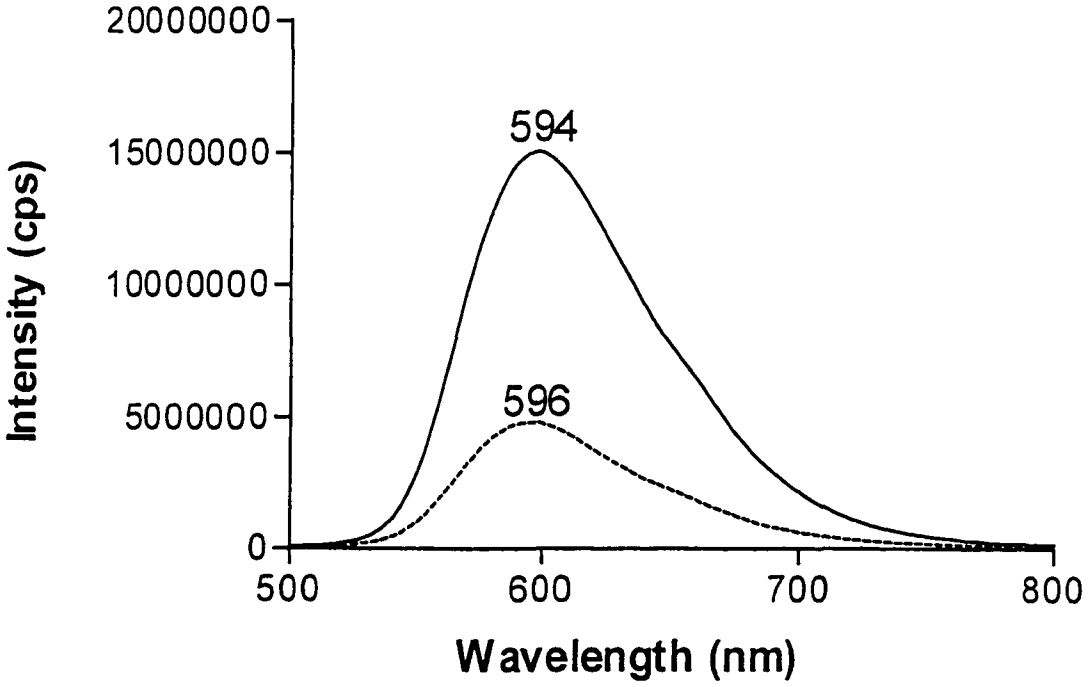

Fig.4. Emission spectra of $[Ru(bzp)_3]^{2+}$ in water (----) and acetonitrile (___) at 25°C.

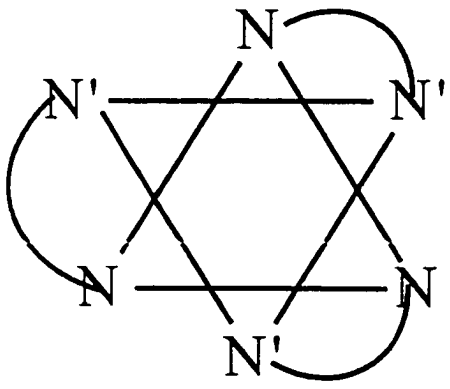

fac

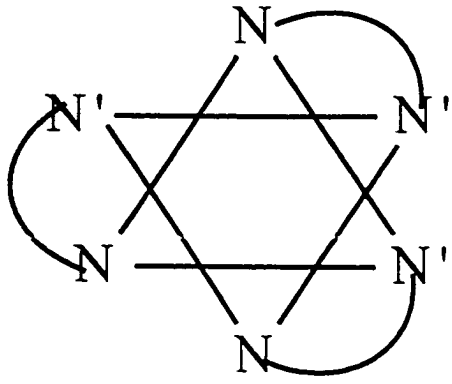

mer

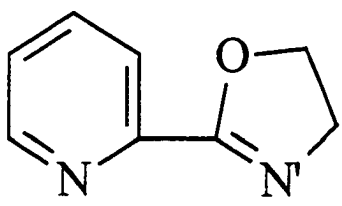

Pyoxazo

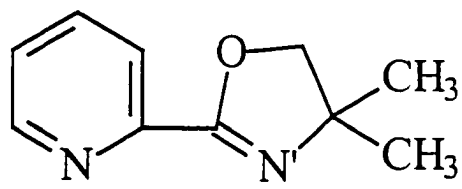

Dmpyoxazo

α- Diimine Ligands

Figure 5. Stereoisomers of $[Ru(pyoxazo)_3]^{2+}$ and $[Ru(dmpyoxazo)_3]^{2+}$

Chapter V
Ground and Excited State pK_a's of $[Ru(bpy)_2bppz]^{2+}$ and $[Ru(bpy)_2mbppz]^{2+}$

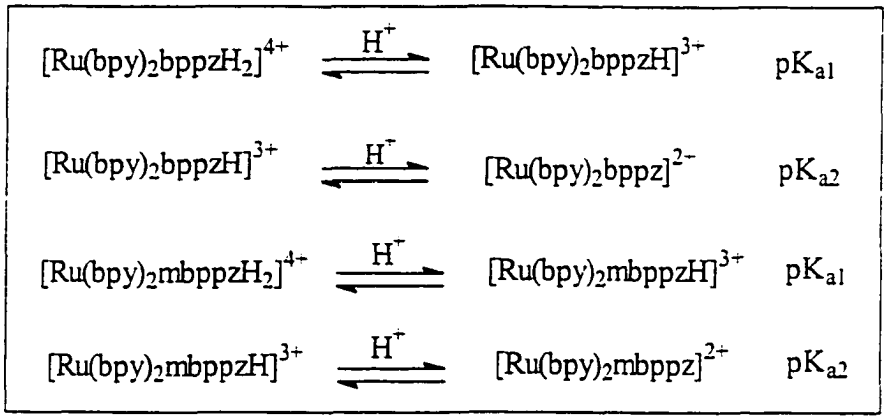

Scheme 1. Protonation of $[Ru(bpy)_2bppz]^{2+}$ and $[Ru(bpy)_2mbppz]^{2+}$

Introduction.

During the past 20 years there has been great activity studying the ground and excited state chemistry of $Ru(bpy)_3^{2+}$ (bpy = 2,2'-bipyridine). One particular area of interest involves the mechanism of quenching of excited states of complexes such as $Ru(bpy)_3^{2+}$ by various ions and molecules and the implications of the results for electron transfer to or from the excited state. In cases where one of the ligands has one or more protonable sites, the quenching may be observed as a function of pH. Several such systems have been studied and the ground and excited state pK_a's have been determined for Ru(II) complexes, including those of $[Ru(bpz)_3]^{2+}$ (where bpz = 2,2'-bipyrazine),[156] $[Ru(bpy)_2bpz]^{2+}$, [157] $[Ru(bpy)_2dpp]^{2+}$ (where dpp = 2,3-bis(2-pyridyl)pyrazine), [158] and $[Ru(bpy)_2ppz]^{2+}$ (where ppz = [4,7]phenanthrolino[5,6-b]pyrazine). [158]

The complexes $[Ru(bpy)_2bppz]^{2+}$ and $[Ru(bpy)_2mbppz]^{2+}$ possess two basic sites located on the non-coordinating pyridine and pyrazine of the chelated bppz and mbppz complexes. Each of these basic sites is associated with an acidity constant (pK_a), whose

value can be determined by spectrophotometric titrations (details in experimental). Therefore, this chapter is concerned with the study of the acid-base behavior of $[Ru(bpy)_2bppz]^{2+}$ and $[Ru(bpy)_2mbppz]^{2+}$ in both the ground and excited state.

Results and Discussion

Ground State pK_a of $[Ru(bpy)_2bppz]^{2+}$

Visible absorption spectra of $[Ru(bpy)_2bppz]^{2+}$ from pH 4.02 to 1.21 are shown in Fig.1. The absorption shifts noticeably to the red as the acidity of the solution is increased, with an isobestic point at 557nm. As pH decreases the band at 564nm increases in intensity and the band at 545nm decreases. The largest changes in the spectrum, the band at 564nm, occur between pH 2.49 and pH 1.21. Absorption spectra in this narrow region of pH are shown in Fig.2. The ground state pK_a value of 1.89 was determined from a titration curve (Fig.3) obtained by plotting the absorbance at 564nm vs pH of the solution.

Ground State pK_a of $[Ru(bpy)_2mbppz]^{2+}$

The visible absorption spectra of $[Ru(bpy)_2mbppz]^{2+}$ from pH 5.64 to 1.09 are shown in Fig.4. Analogous to $[Ru(bpy)_2bppz]^{2+}$ the absorption shifts to the red as the acidity of the solution is increased, with an isobestic point at 549nm. Furthermore, as pH decreases the band at 554nm increases in intensity. The largest changes in the spectrum, the band at 554nm, occur between pH 2.73 and pH 1.09. Absorption spectra in this narrow region of pH are shown in Fig.5. The ground state pK_a value of 1.85 was

determined from a titration curve (Fig.6) obtained by plotting the absorbance at 554nm vs pH of the solution.

Excited State pk_a of $[Ru(bpy)_2bppz]^{2+}$

At pH 5.38 and above, the complex shows an emission maximum at 812nm. As the pH of the solution is decreased the emission intensity decreases and shifts to the red (maximum shift of 8nm). Figure 7 shows the shift and decrease in the intensity of the luminescence as a function of pH, and the corresponding titration curve is shown in Fig.8. The latter permits an excited state pK_a to be calculated as 2.62.

Excited State pK_a of $[Ru(bpy)_2mbppz]^{2+}$

Above pH 4.02, the complex shows an emission maximum at 808nm. Similar to $[Ru(bpy)_2bppz]^{2+}$, as the pH of the solution is decreased the emission intensity decreases and shifts to the red (maximum shift of 12nm). Figure 9 shows the shift and decrease in the intensity of the luminescence as a function of pH, and the corresponding titration curve is shown in Fig.10. An excited state pK_a of 3.18 was calculated from the titration curve.

Conclusion.

For both complexes $[Ru(bpy)_2bppz]^{2+}$ and $[Ru(bpy)_2mbppz]^{2+}$ the excited state pK_a was higher than that of the ground state. This suggests that the complexes are stronger bases in the excited state than in the ground state. Although each complex contains two basic sites, only a single pKa and pKa* were determined. Either the spectroscopic changes due to addition of the second proton are small, or the pK_a values

were not within the range of acidity used in our experiments. It is likely, based on results for similar complexes [158] obtained by our laboratory, that the first pKa and pKa* would be much less than unity. Also, for the complexes studied we believe that the pyridine nitrogen is protonated and not the pyrazine nitrogen. Protonation of the pyrazine nitrogen will put another positive charge on the pyrazine ring, which is less likely to occur.

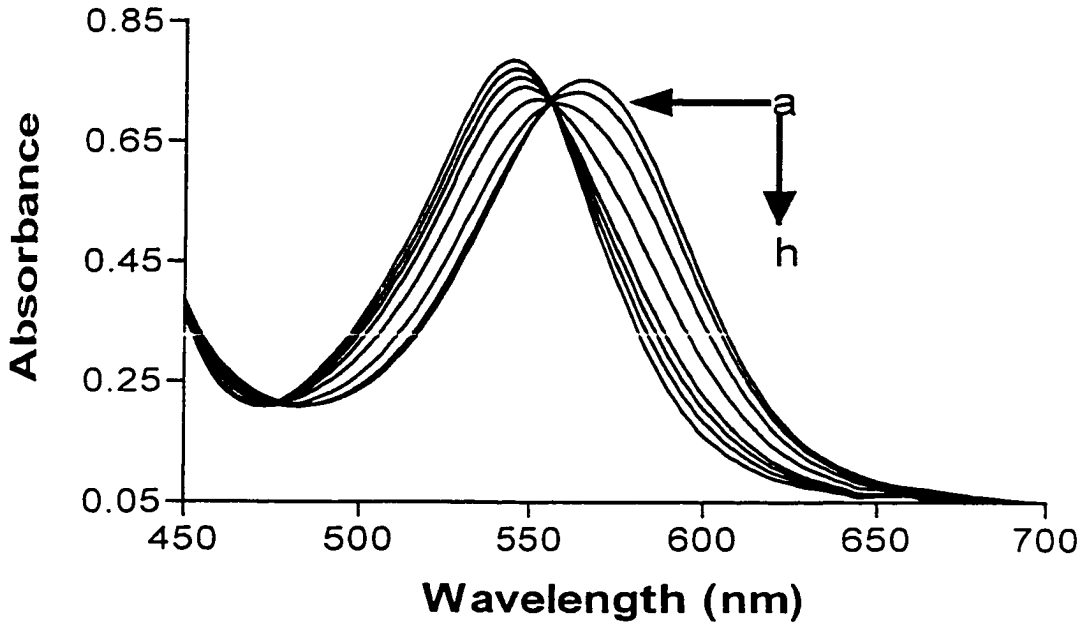

Fig.1. Absorption Spectra of $[Ru(bpy)_2bppz]^{2+}$ at pH (a) 1.21, (b) 1.41, (c) 1.75, (d) 2.13, (e) 2.49, (f) 2.70, (g) 3.02, and (h) 4.02.

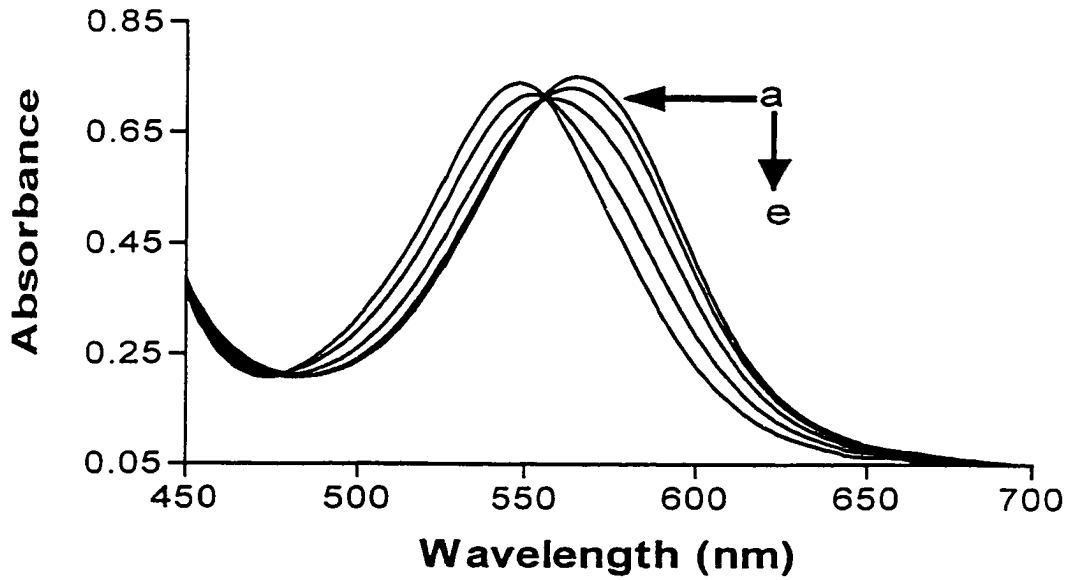

Fig.2. Absorption Spectra of $[Ru(bpy)_2bppz]^{2+}$ at pH (a) 1.21, (b) 1.41, (c) 1.75, (d) 2.13, (e) 2.49.

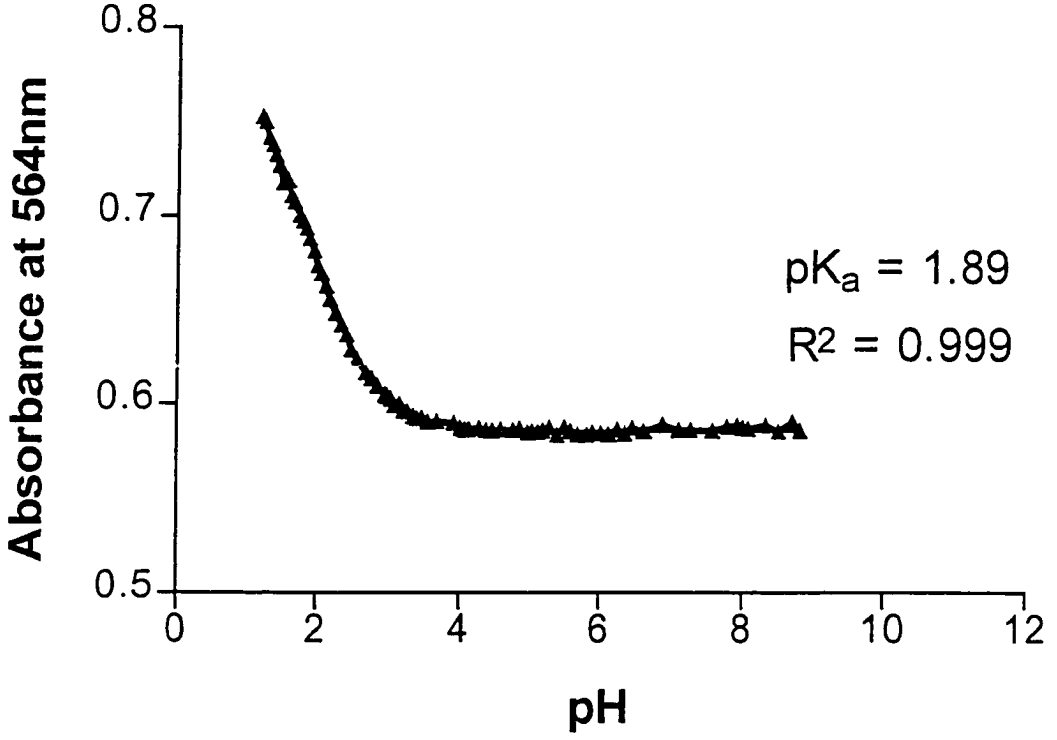

Fig.3. Titration Curve for $[Ru(bpy)_2bppz]^{2+}$.

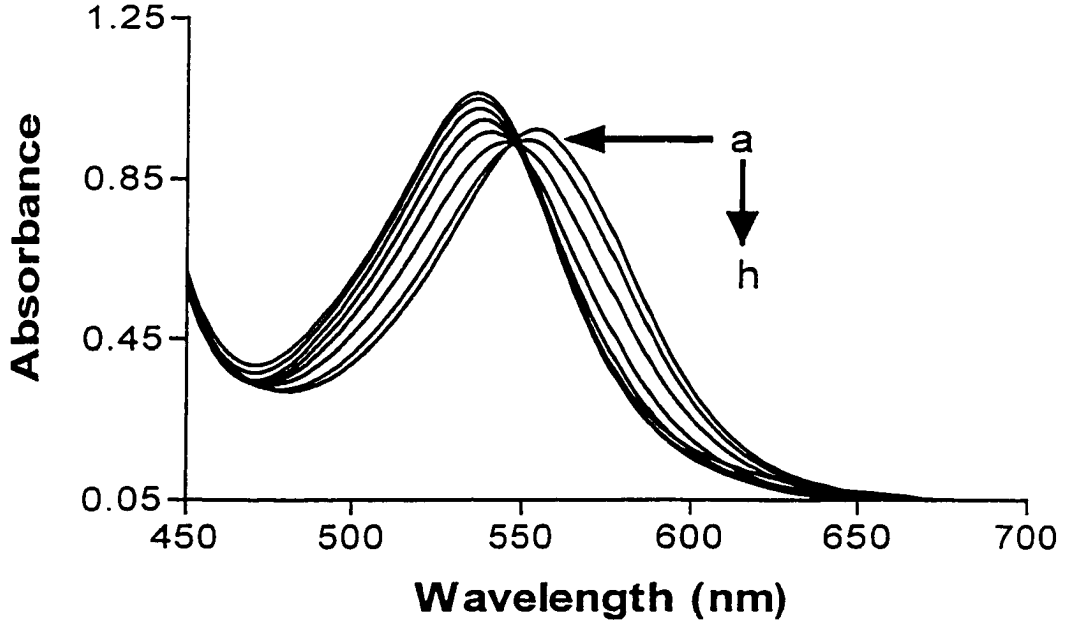

Fig.4. Absorption Spectra of $[Ru(bpy)_2mbppz]^{2+}$ at pH (a) 1.09, (b) 1.46, (c) 1.92, (d) 2.35, (e) 2.73, (f) 3.42, (g) 4.41, and (h) 5.64.

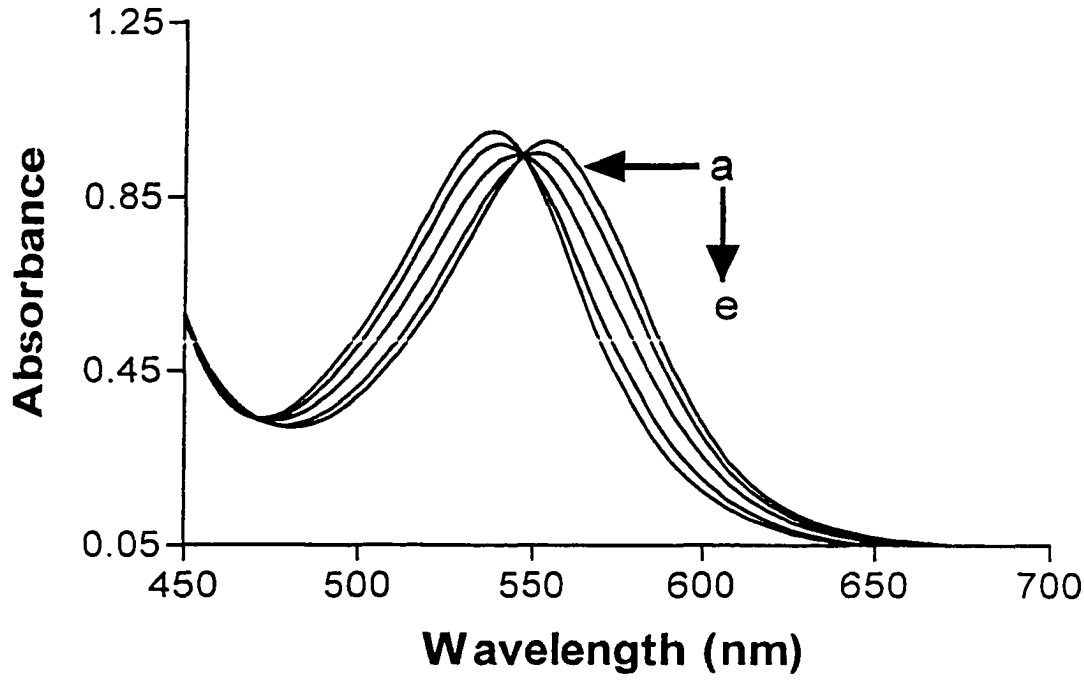

Fig.5. Absorption Spectra of $[Ru(bpy)_2mbppz]2+$ at pH (a) 1.09, (b) 1.46, (c) 1.92, (d) 2.35, and (e) 2.73.

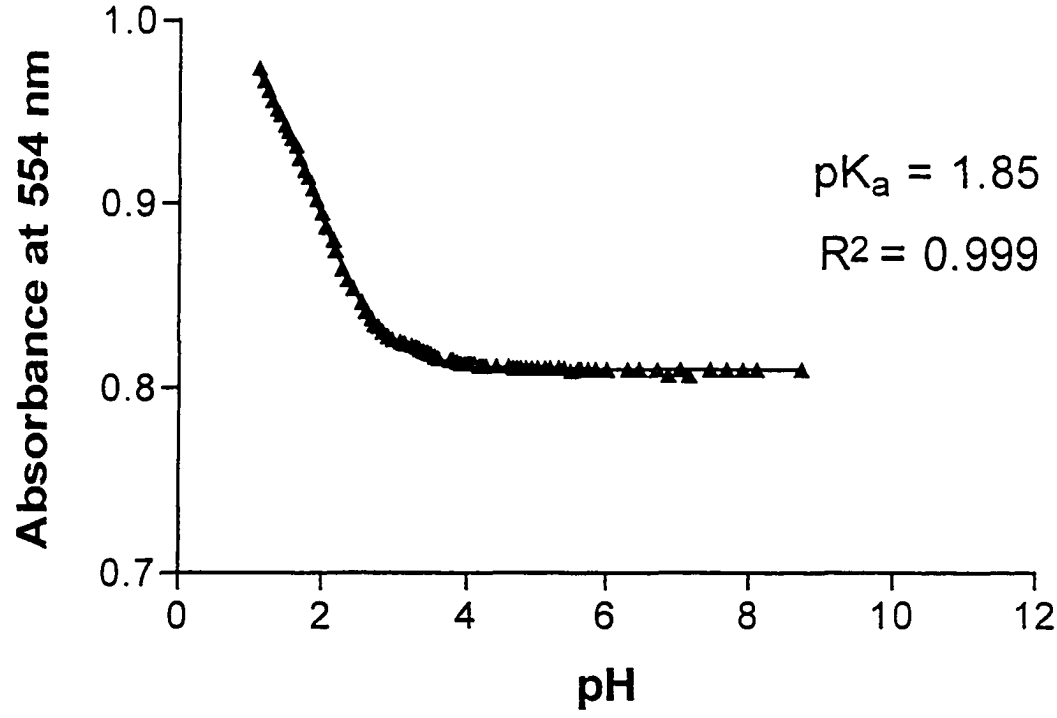

Fig.6. Titration Curve for $[Ru(bpy)_2mbppz]^{2+}$.

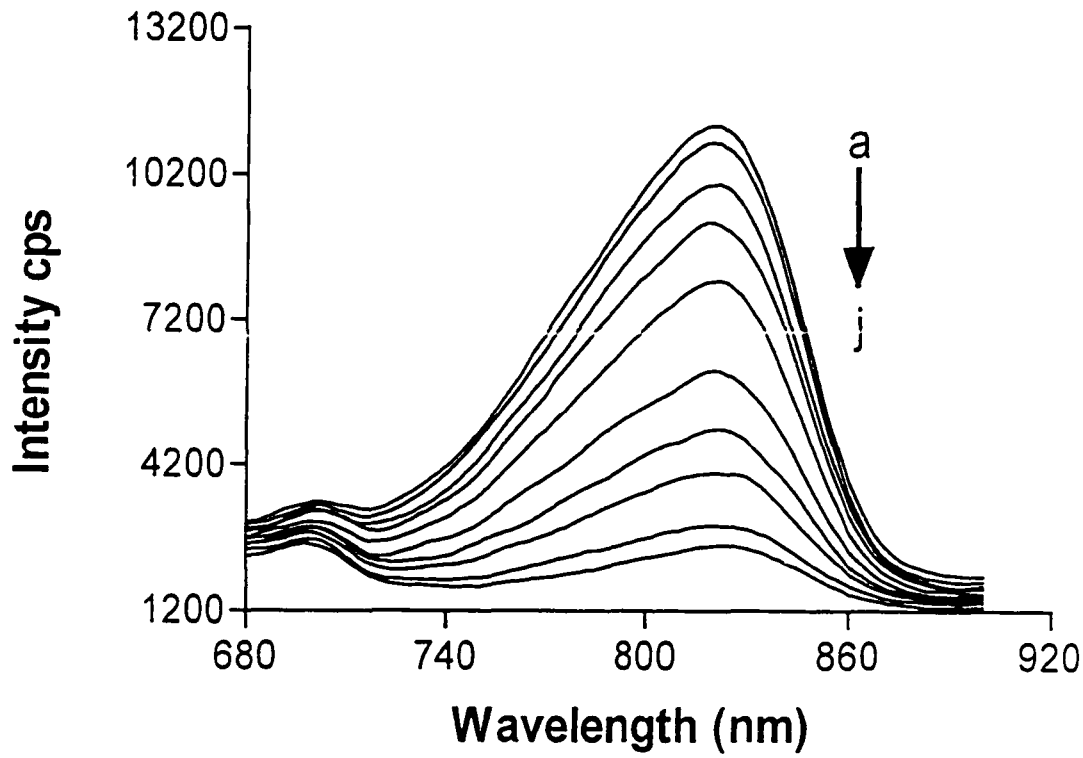

Fig.7. Emission Spectra of [Ru(bpy)$_2$bppz]2+ at pH (a) 5.38, (b) 4.03, (c) 3.47, (d) 3.21, (e) 2.93, (f) 2.62, (g) 2.42, (h) 2.26, (i) 2.02, and (j) 1.88

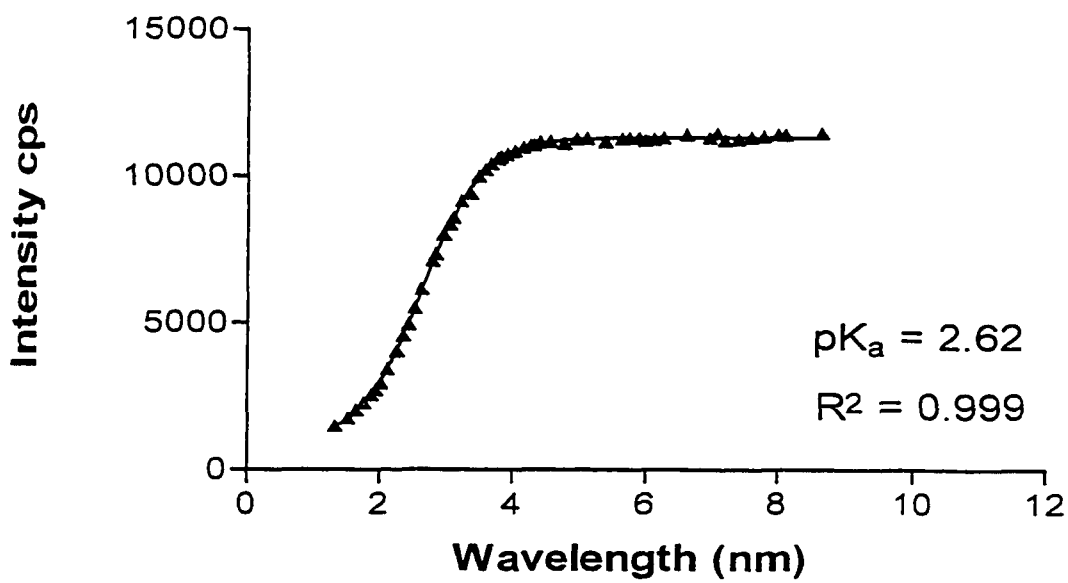

Fig.8. Titration Curve for [Ru(bpy)$_2$bppz]$^{2+}$.

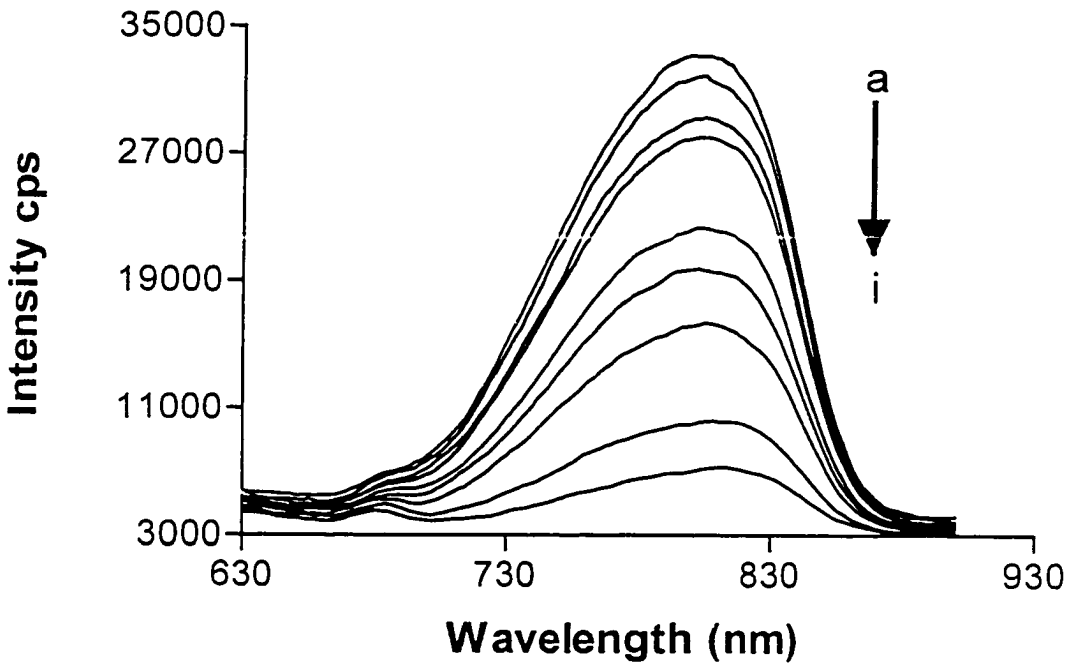

Fig.9. Emission Spectra of $[Ru(bpy)_2mbppz]^{2+}$ at pH (a) 5.24, (b) 4.71, (c) 4.02, (d) 3.81, (e) 3.40, (f) 3.27, (g) 3.03, (h) 2.68, and (i) 2.43.

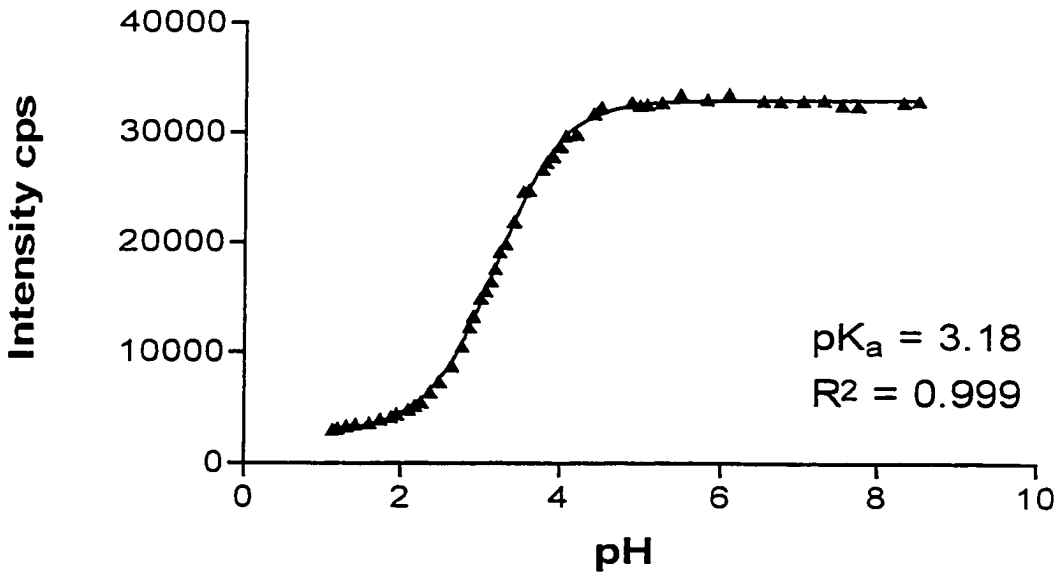

Fig.10. Titration Curve for $[Ru(bpy)_2mbppz]^{2+}$.

Chapter VI
DNA-Drug Interactions

Introduction

The specific non-covalent interaction of small organic molecules with duplex DNA is the molecular basis of many antitumor, antiviral and antibiotic drugs. Other compounds that also interact with DNA include carcinogens, mutagens and complex ions. These varied molecules contain extended heterocyclic aromatic chromophores, and most if not all posses planar portions of the molecule, which interact with the nucleic acid double helix.[159]

Nucleic Acid (B-DNA) Structure

The structure of DNA as depicted by the classical Watson and Crick model is in the B-conformation. B-DNA is a right-handed double helix composed of two strands; each strand consists of an alternating sequence of sugar and phosphate which forms the backbone of the structure. The deoxyribose sugars (5 carbon sugars) are bonded to the phosphates via phosphodiester linkages at the 5' position of one sugar and the 3' position of another sugar. The sugar is substituted at the C1' position and a nitrogenous base is covalently bonded there, aligned perpendicular to the helical axis. This repeating unit (sugar-phosphate-nitrogenous base) is referred to as a nucleotide (Fig. 1).

The right handed helix has 10 base pairs per complete turn with the two polynucleotide chains antiparallel to each other and linked by Watson-Crick adenine-thymine (A-T) and guanine-cytosine (G-C) base pairs. The adenine-thymine (A-T) base pair is held together by two hydrogen bonds and the guanine-cytosine (G-C) pair by three

hydrogen bonds (Fig. 2). This makes stretches of DNA containing many GC base pairs somewhat more stable than those containing AT pairs. The paired bases are almost exactly perpendicular to the helix axis and they are stacked perpendicular to the axis itself (on top of each other). Consequently, the base pair separation is the same as the helical rise, i.e. 0.34nm.

An important consequence of the Watson-Crick base pairing arrangement is that the two-deoxyribose sugars linked to an individual base pair are on the same side of it. So, when successive base pairs are stacked on each other in the helix, the gap between these sugars forms continuous indentations in the surface that wind along, parallel to the sugar phosphodiester chains. These indentations are termed grooves. The symmetry of the base pairs results in two parallel types of groove referred to as the major and minor grooves (Fig. 3), whose dimensions (especially their depth) are related to the distances of the base pairs from the axis of the helix and their orientation with respect to the axis. Since the strand backbones are closer together on one side of the helix than on the other, the major groove occurs where the backbones are far apart, and the minor groove occurs where they are close together. Therefore, the grooves twist around the molecule on opposite sides.

Other features of the double helix include the negative charge and hydrophilic nature of the outer region of the macromolecule. This is due to the presence of the phosphate moieties along the backbone of the DNA double helix. Furthermore, the inner region of the macromolecule is mainly hydrophobic due to the presence of the aromatic heterocyclic base pairs in this location.

Types of Non-covalent Binding to B-DNA

Several major research efforts have focused on the study of molecular probes and their interaction with DNA. Some probes have been found to recognize certain conformations of DNA and can prove useful in the development of site specific reagents or drug delivery systems. Therefore, an understanding of how molecular probes interact with DNA is crucial in examining their effectiveness towards these applications. In general, substances that bind to DNA are generically known as "drugs" even if no therapeutic uses have been found. Examples of some molecular probes of DNA are given in Fig. 4. Non-covalent binding of these probes to DNA are believed to occur as follows:

1. Electrostatic

Electrostatic binding occurs when a positively charged drug (cation) is attracted to the negatively charged phosphate backbone of DNA. This type of interaction exists with all positively charged molecular probes, e.g. ethidium bromide. One can also have bridging electrostatic interactions. This type of interaction is thought to occur with polycations, where a phosphate on one strand of DNA can bind one portion of the probe, and a phosphate either on the same strand or the opposing strand binds to another portion of the probe, forming a bridge.[36]

Intercalation

In 1961 Lerman [67] published his fundamental studies on the binding of proflavine to DNA in which he proposed the intercalation model. However, intercalation is by no means limited to proflavine. It is observed in many more or less planar molecules with

conjugated $\pi-$ electron systems, the classical examples being ethidium and the aminoacridines. Intercalation is an unusual type of binding between the DNA polyanion and the dye cations, in which the cation undergoes insertion between the DNA base pairs.

Evidence to support the intercalation model came from X-ray crystallographic data of intercalated fibers. [67,160] These findings showed that the planar acridine dyes sit between two planar base pairs, pushing the base pairs apart so as to accommodate the dye. Further evidence supporting the intercalation model are based on spectroscopic studies using fluorescence, [161] polarized fluorescence, flow dichroism, absorption, NMR, CD and ORD.[162]

Intercalation is believed to involve binding of the probe drug between two base pairs. In other words, the binding site consists of four nucleotides. This can occur via either the major or minor groove. In addition, from Scatchard [77] and X-ray analyses, it is believed that the nearest neighbor sites exclude binding, [163] because the base pairs are pushed apart to accommodate the intercalator, and the adjacent sites do not allow binding via an intercalative mode.

Several studies have confirmed intercalation as a strong binding process and electrostatic binding as a weak binding process, which was first described by Peacocke and Skerrett [164] as a stacking interaction. Stacking of he dye along the helix was found to be a very weak interaction, [165] and was completely lost when ionic strength was increased. The model of intercalation first proposed by Lerman [67] is now supported by researchers as the most stable type of interaction of planar aromatic dyes and drugs with DNA, yet it is generally accepted that electrostatic interactions must also be present to promote intercalative binding.

Surface (Groove Binding)

Surface binding is also believed to occur with certain drugs and dyes. [166,167] Binding in this fashion is believed to involve both electrostatic and hydrophobic interactions. This binding mode is much more difficult to characterize because the physical and spectroscopic properties of the bound molecule would not be expected to change significantly in this process. Further complicating the characterization of this mode, it would be expected to have a binding affinity to DNA similar to the weak electrostatic process, and may not be distinguishable from purely electrostatic binding. Binding of this type can take place either in the major or minor groove, and planarity is not necessary to induce this type of binding.

Binding of Transition Metal Complexes to DNA

The binding of heterocyclic compounds to DNA by intercalation, where the planar aromatic cation stacks between adjacent base pairs of the duplex, [67] has been the subject of considerable investigation. [73, 168-169] Intercalative drugs can be strongly mutagenic, and some such as adriamycin and duanomycin, serve as potent chemotherapeutic agents. [170] The small intercalators such as ethidium and proflavine in addition provide useful chemical probes of nucleic acid structure. [171-172]

Metallointercalators have also been particularly useful in probing DNA structure and the intercalation process itself, because the ligands or metal may be varied in an easily controlled manner to facilitate the individual application. [173] The aromatic chromophore of the intercalative cation can provide a sensitive handle to monitor the conformation and flexibility of the helix. Many intercalators show antibacterial or

anticancer activity and, because the inserted residue often resembles a base pair in shape and thickness, intercalators are commonly frame shift mutagens. [169] Intercalation appears to require, simply, a planar heterocyclic residue, [73] and in fact cationic metal complexes, which contain aromatic ligands, bind to DNA by intercalation as well. [170]

The original studies of metallointercalators centered on square-planar platinum (II) complexes containing aromatic terpyridyl or phenanthroline ligands [40,174-176], and single crystal studies of terpyridylplatinum (II) species stacked with nucleotides showed the platinum complex to insert almost fully between the base pairs.[177,178] Also, the reagent methidiumpropyl-Fe(II)EDTA, which contains a redox-active metal center tethered to an organic intercalator, has been applied in "footprinting" experiments to determine the sequence specificities of small drugs bound to DNA.[179-181] Bis(phenanthroline)-cuprous ion has similarly been employed in DNA cleavage experiments, [182] and this reagent also presumably binds to DNA by intercalation.

Studies on the binding of polypyridyl complexes to Zn(II), [183] Co(III), [184,185,186] Cr(III), [186] Rh(III), [187] and Ru(II) [20,21,27,29] to DNA have led to a binding model of partial intercalation of one of three planar polypyridyl chelating ligands in the tris complexes of 1,10-phenanthroline (phen) and related complexes. In addition, electrostatic and surface bound modes were proposed. Studies with tris(bipyridyl) complexes indicated that the bpy ligand was not sufficiently extended from the metal core to bind in this fashion.[22] Some $Ru(bpy)_2L^{2+}$ (bpy = 2,2'-bipyridine) complexes appear to bind intercalatively, if the ligand L is sufficiently extended from the Ru core. However, with these complexes, the ancillary (non-intercalating) bpy ligands do not restrict insertion by interaction with the sugar-phosphate backbone to the same extent as in the $Ru(phen)_2L^{2+}$ complexes.

Reagents of high specificity and even stereoselectivity are desirable in the design both of potent drugs and of structural probes. For the chiral complex $(phen)_2Zn^{2+}$ (phen = 1,10-phenanthroline) an enantiomeric preference in binding to B-DNA has been observed. [188] As for the tetrahedral $(phen)_2Cu^{+}$ complex, and in contrast to the square-planar platinum intercalators, the octahedral coordinaton in the tris(phenanthroline) metal cations can permit a partial insertion of only one coordinated ligand. Thus while one ligand is stacked between the base pairs, the remaining nonintercalated phenanthroline ligands should be available to direct the enantiomeric selection.

Enantiomeric selectivity has been observed in the inetractions of tris(phenanthroline) metal complexes with B-DNA[19,188,189] Experiments with tris(phenanthroline)zinc(II) have indicated stereoselectivity;[188] dialysis of B-DNA against the racemic mixture leads to the optical enrichment in the lambda enantiomer. Subsequent luminescence, electrophoretic, and equilibrium dialysis studies of the well-characterized ruthenium (II) analogues have suggested that the tris(phenanthroline) metal isomers bind to DNA by intercalation and it is the delta enantiomer that binds preferentially to the right-handed duplex [19,189] via the major groove. The enantiomeric selectivity as predicted by Barton et al. is based on the steric clash between the nonintercalated (ancillary) phenanthroline ligands and the phosphate backbone. Although the right-handed propeller-like isomer intercalates with facility into a right-handed helix, steric repulsions interfere with a similar intercalation of the lambda enantiomer.

A number of subsequent studies, [190,191] including a recent study [192] of $Ru(phen)_3^{2+}$ (and methylated analogs) binding with DNA have called into question the basic interpretation of the results concerning the enantioselectivity of $Ru(phen)_3^{2+}$. Even the

intercalative nature of both the delta and lambda isomers has been questioned. Also, a study on the effect of the ancillary ligands on enantioselectivity was conducted in this laboratory[85]. In this study the binding constant of the complexes Ru((+)-chiragen[6]ppz)+2 , Λ-$[Ru(bpy)_2ppz]^{2+}$ and Δ-$[Ru(bpy)_2ppz]^{2+}$ (bpy = 2,2'-bipyridine; ppz = 4,7-phenanthrolino-[6,5-b]-pyrazine; (+)-chiragen[6][193]) were determined by fluorescence titrations at varied salt concentrations. The result from this experiment showed a four-fold difference in binding between the enantiomers favoring the Λ-enantiomer. Therefore, this must be attributed to structural interactions which are non-electrostatic in nature, and clearly shows that the ancillary ligands are not sufficient to predict which enantiomer will bind more strongly to DNA as have been suggested by Barton et al. This proves that more subtle interactions with the double stranded DNA structure, involving not only the ancillary ligands, but also the partially intercalated diimine ligand, are evidently involved.

The intercalative nature of binding of a specific complex has been firmly established via studies [15, 194, 195] of the complex $Ru(phen)_2(dppz)^{2+}$ (dppz = dipyrido-[3,2-a;2',3'-c]phenazine). At issue is whether the site of access is via the major or the minor groove of the duplex. Both NMR studies and binding studies with T4-DNA have been interpreted in terms of a model whereby the dppz ligand intercalates via access from the minor groove of double stranded DNA. Competitive binding studies with distamycin (a minor groove binder) and a complex of Rh(III) known to be a major groove binder were interpreted as indicative of major groove access for the dppz complex.

Based on the premise of stereoselectivity, metal complexes appear useful in the design of probes to distinguish left-handed and right-handed DNA duplexes. The

design flexibility inherent in metallointercalation reagents, in which both ligand and metal may be varied easily, makes coordination complexes attractive probes. [173,196,197] In this dissertation we will concentrate on bipyridine complexes of ruthenium(II) which like those of phenanthroline have high luminescence associated with their intense metal-to-ligand charge-transfer bands, [198,199] and minimal racemization [200] due to the exchange-inert character of low-spin d^6 complexes.

Evidence for the Binding of Probes to DNA

Introduction

Spectroscopic pertubations of a molecular probe on binding report on the local environment of the chromophore, and serve to indicate the DNA duplex conformation.[66] Several spectroscopic observations have been made with "classic " intercalators and Ru(II) polypyridyl complexes when bound to DNA. Characterization of the binding as being intercalative, surface or electrostatic is supported by various spectral pertubations. These spectral changes do not lead to the description of the binding as intercalative in nature, but is highly suggestive of this binding mode. Several techniques have been used for describing the binding of dyes and metal complexes to DNA. [19,22,31,36,66,67-75] In this chapter we would limit our discussion to a few of these techniques which include the effects of binding on absorption, emission, fluorescence titration, equilibrium dialysis, and fluorescence quenching by an anionic quencher ($K_4Fe(CN)_6$).

1. Effects of Binding on Absorption (UV/Vis)

Upon binding to DNA, intercalation tends to decrease the intensity of the absorption bands of the molecular probe.[76] This has been attributed to a hypochromic effect (i.e. less color), which has been attributed to a decrease in absorbance due to ordering (stacking) of the chromophore which is absorbing light. A shift in energy of the absorption bands of the chromophore involved in the intercalative binding is also observed. Typically these shifts are to lower energy (bathochromic). For example, the ethidium bromide absorption band shifts from 480 nm to 520 nm upon DNA binding, [70] accompanied by a hypochromic effect.

Ru (II) polypridyl complexes generally show a much smaller hypochromic effect than intercalators such as ethidium bromide. [19,36] This has been attributed [19] to only partial intercalation occuring for the metal complexes, and also due to the symmetry of the molecule. For example, with Ru $(phen)_3^{2+}$, a D_3 complex ion, the predominant polarization of the visible MLCT charge transfer band is perpendicular to the molecular C_3 axis, rather than parallel to the plane of the intercalator as it is with organic intercalators. This reduces the hypochromic effect seen in Ru $(phen)_3^{2+}$ and several other Ru (II) complexes. Furthermore, charge transfer of the two non-intercalated ligands would lead to a smaller hypochromic effect, since these ligands are not thought to be perturbed upon binding to DNA to the same extent as the intercalated phen ligand. The absence of hypochromism in the absorption band of the Ru $(bpy)_3^{2+}$ complex ion is indicative of a lack of intercalative binding for this cation. [19, 22] It is thought that the bpy ligand is not sufficiently extended from the metal to promote intercalative binding and this evidence supports the theory.

Electrostatic binding, however, does not induce a hypochromic effect, since the Ru $(bpy)_3^{2+}$ complex ion must bind this way to some extent due to the dipositive (2+) charge on the Ru ion. Therefore, the presence of hypochromism in an absorption spectrum indicates binding modes that differ from purely electrostatic binding.

2. Effects of Binding on Emission.

Upon binding to DNA, intercalating molecular probes often exhibit blue shifts in the emission maxima, accompanied by emission enhancement, similar to effects observed upon going from polar to non- polar solvents. Emission bands tend to be narrower due to the redistribution and decrease in intensity of the vibrational modes of the excited state that occur when going from a polar to a non- polar solvent. Similar shifts have been observed with intercalators such as ethidium bromide, [72] where the binding to DNA shifts the emission maximum to higher energy (blue shift). This is consistent with the chromophore luminescencing from a more non polar environment, such as the interior of the double helix of DNA, when intercalatively bound. For Ru $(phen)_3^{2+}$ emission increases of 48% and 87% were observed respectively for the lambda and delta isomers bound to DNA, while a band shift of ~2nm to the red was observed.[19] This small shift does not disprove intercalation, since luminescence in this complex ion may originate from MLCT states associated with the non-intercalated ligands, and van der Waals and electrostatic interactions of these ligands within the major groove can possibly shift emission maxima to lower energy (red shift).

3. Fluorescence Titration

Studies by fluorescence titration on Ru(II) polypyridyl complexes lead to linear Eadie-Hofste plots. [201-203] From these plots the binding constant of the Ru(II) complex with DNA is determined from the slope of the line. The binding constant is usually determined at varying salt (NaCl) concentration. Since Ru(II) complexes are dications, their binding to DNA is thermodynamically linked to Na^+ binding to DNA, and as a result, its DNA binding constant will depend on the total Na^+ concentration. Also, analysis of the sodium ion concentration dependence of the binding constants using polyelectrolyte theory [204] indicates the degree to which the binding is electrostatic in nature.

4. Equilibrium Dialysis

Equilibrium dialysis studies on organic dyes and Ru (II) polypyridyl complexes lead to non-linear Scatchard plots, [19] which have been instrumental in estimating the binding constant of the probe to DNA.[77] The non- linearity in these plots is attributed to the existence of multiple binding sites. Average binding constants of the DNA duplex are obtained by fitting the binding curve to the McGhee and Von Hippel equation, [78] which is modeled after the non-cooperative nearest- neighbor exclusion model.

$r/C_f = (K_b/2)(1-2lr)[(1-2lr)/(1-2(l-1)r]^{l-1}$ (McGhee and Von Hippel Equation)

In the above equation, r is the fraction of bound sites, C_f is the concentration of ruthenium free in the solution, K_b is the intrinsic binding constant, and the integer

l measures the degree of anticooperativity, which is the size of the binding site in base pairs.

For Ru $(phen)_3^{2+}$, a binding constant of 6.3×10^3 was found corresponding to a site size of l = 4 (8 base pairs). [19] The value of the binding constant for Ru $(phen)_3^{2+}$ is quite low in comparison to values of 3×10^5 and 5×10^4 for ethidium and $[(phen)Pt\text{-}(en)]^{2+}$, respectively. [205] The lower affinity of $Ru(phen)_3^{2+}$ is not surprising since only partial stacking of the phenanthroline ligand is feasible in this octahedral complex; greater overlap of the phenanthroline with the base pairs may be achieved in the square-planar platinum (II) species. The steric bulk of the nonintercalated ligands determine also the large four base pair site size compared to a two base pair (neighbor excluded) site for basically planar reagents. [46, 163, 174-176]

5. Enantioselectivity

Equilibrium dialysis experiments of racemic mixtures of Ru(II) complexes provide pertinent information on the relative binding of the enantiomers to DNA. This is determined by using circular dichroism to measure the degree of optical enrichment of the unbound enantiomer in the dialysate. If a CD signal is found, the binding of one enantiomer is stronger than the other, and enantioselectivity is the cause. The weaker binding enantiomer is enriched in the dialysate, since the stronger binding enantiomer binds well to DNA, and decreases the concentration of the stronger binder in the dialysate.

In the case of $Ru(phen)_3^{2+}$ the delta enantiomer was found to bind preferentially to the right handed helix.[19,22,81] Molecular modeling [19] and calculations [34] also suggest that the right-handedness of B-DNA accommodates the delta enantiomer better than the lambda enantiomer for intercalative binding. This is based on the model by Barton et al., which basically says that the lambda isomer has its ancillary (non-intercalating) ligands opposed to the direction of the groove, while the delta isomer has its non-intercalating ligands along the major groove. This implies that enantioselectivity is favored for the delta isomer simply because it has a better fit in the major groove of the right-handed helix.

Other than $Ru(phen)_3^{2+}$, preferred binding of the delta enantiomer is found to be favored for a number of complexes and has been rationalized [21,29] based largely on viewing of molecular models and/or three-dimensional structures. However, this general picture must be questioned as a result of data presented by our group and others, which shows a four fold preference for the lambda configuration of Ru (bpy) $_2$(ppz)(+2) in binding to DNA.[85] A four-fold difference in binding favoring the lambda enantiomer must therefore be attributed to differences in structural interaction, which are non-electrostatic in nature. Therefore, the configuration of the two ancillary ligands is not sufficient to predict which enantiomer will bind more strongly, as has been suggested. Therefore, prediction of which enantiomer will bind more strongly depends on the configuration of the two ancillary ligands as has been suggested and also on the nature of the partially intercalated diimine ligand. [85]

5. Fluorescence Quenching by Ferrocyanide Anion ($Fe(CN)_6^{4-}$)

Additional support for the binding mode of Ruthenium (II) complexes to DNA is through steady-state emission quenching experiments. The negatively charged quencher is expected to be repelled by the negatively charged phosphate backbone, and therefore a bound (intercalated) Ru(II) cation should be protected from quenching from the anionic quencher. On the other hand, anionic quenchers would readily quench "free" or aqueous complexes.

Quenching by ferrocyanide ion has been used [206, 207] to infer an intercalative mode of binding for the isomers of $Ru(phen)_3^{2+}$ (phen = 1,10-phenanthroline). The predicted binding mode was deduced from the non-linear Stern-Volmer plots created with the data from fluorescence quenching experiments (see experimental). The Stern-Volmer plots exhibited a downward curvature which has been attributed to the differential accessibility of the bound complex to the quencher due to a variety of binding sites (intercalative, surface, and electrostatic) on DNA. [207] For $Ru(phen)_3^{2+}$ a pronounced decrease in the effectiveness of the anion $Fe(CN)_6^{4-}$ to quench the emission of Δ- $Ru(phen)_3^{2+}$ in the presence of DNA led Barton and others to the conclusion that the chromophore responsible for the emission is shielded from the quencher and is therefore more fully intercalated within the DNA duplex. [206, 207] While a decrease in the quenching ability of $Fe(CN)_6^{4-}$ with Λ- $Ru(phen)_3^{2+}$ was also observed, it was less pronounced than that for the Δ-isomer, and this led to the conclusion that the Λ-isomer was groove bound but not intercalated.

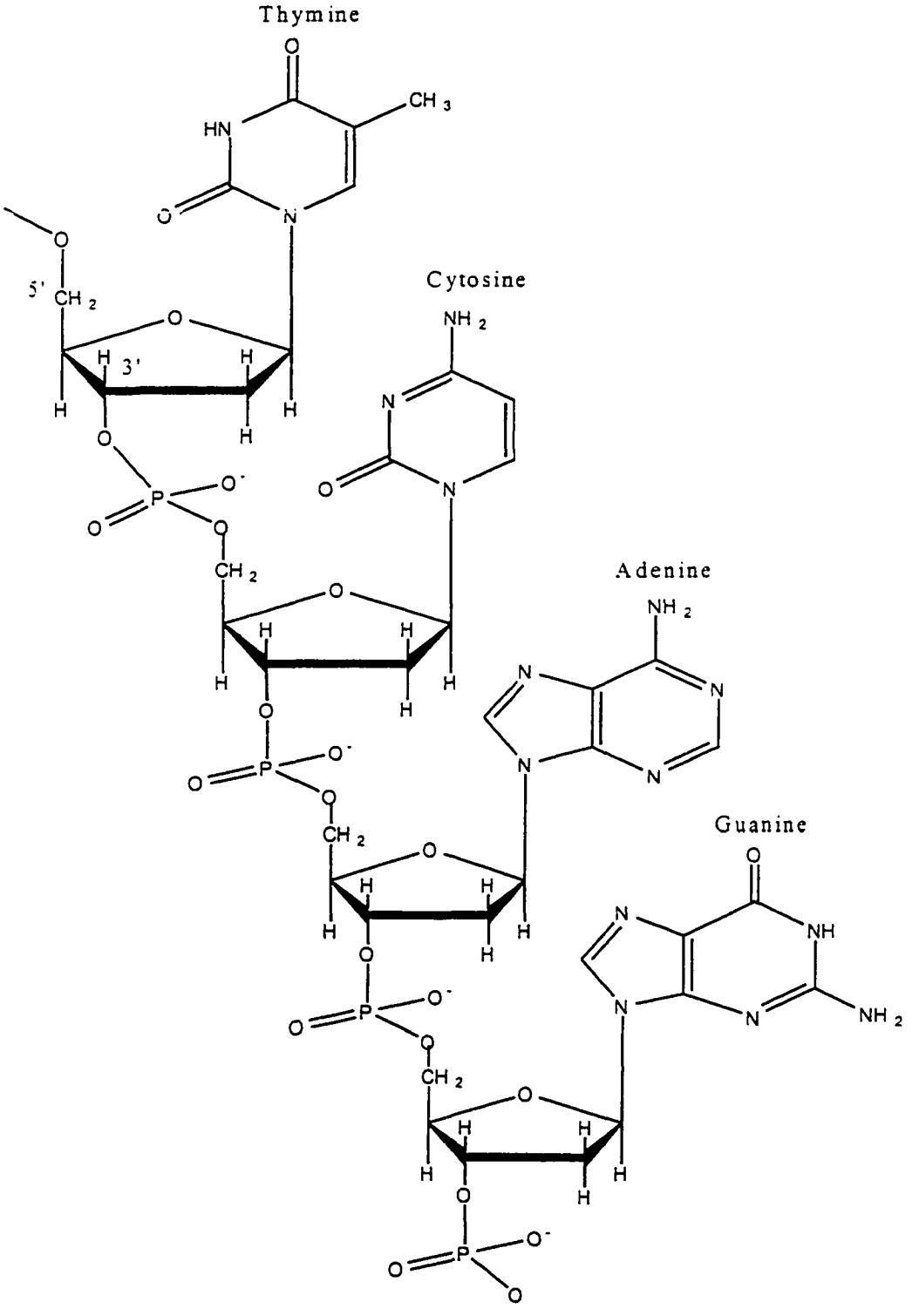

Fig. 1 Nucleotides

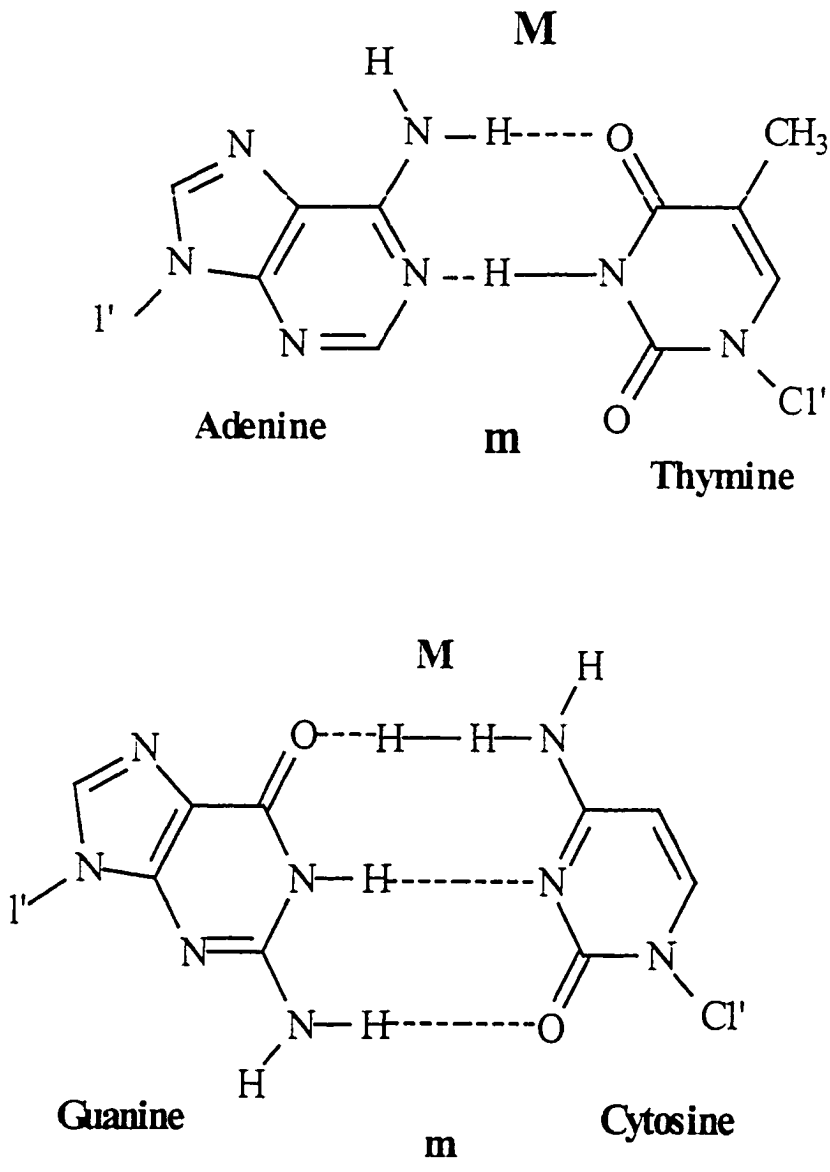

Fig. 2 Watson-Crick base pairing in DNA. M and m indicate major and minor grooves respectively.

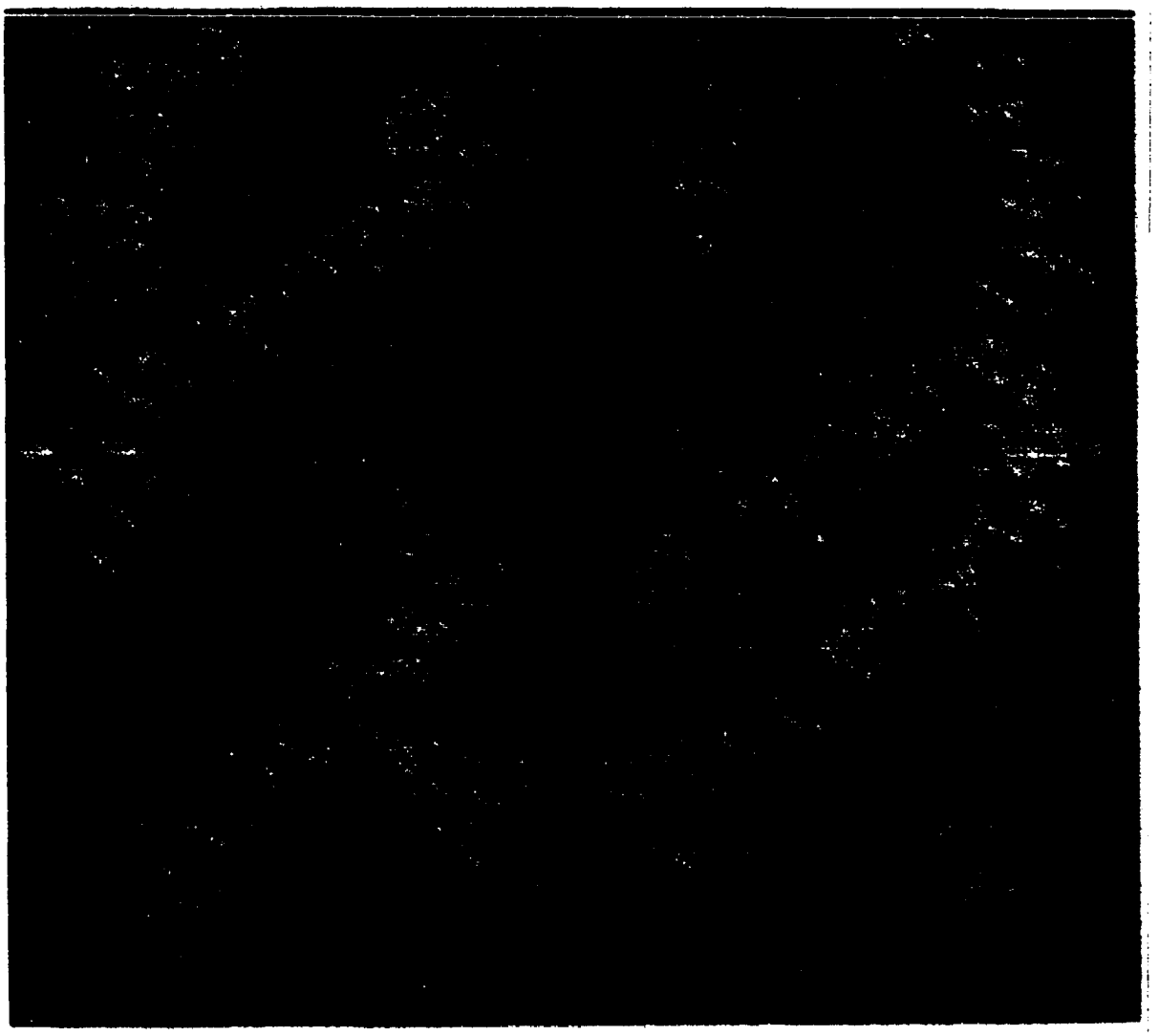

Fig. 3 Major and Minor grooves in B-DNA.

Molecular Probes

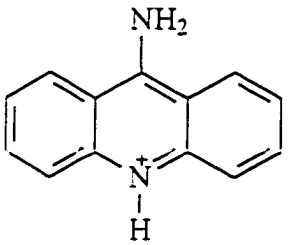

9- Aminoacridine

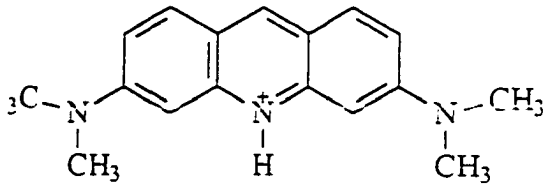

Acridine Orange

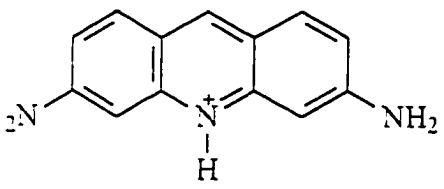

Proflavine

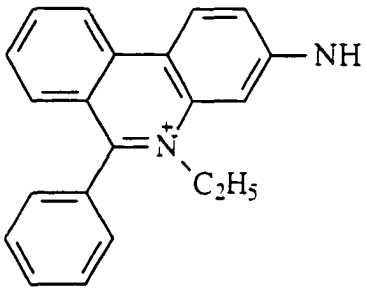

Ethidium

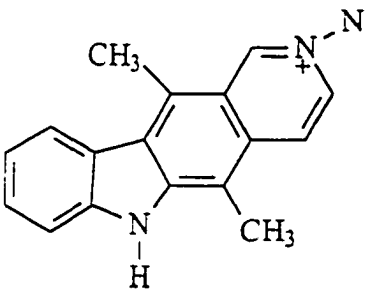

Ellipticine

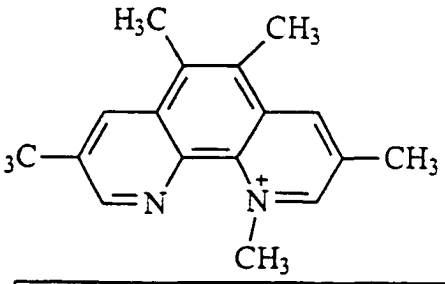

3,5,6,8-tetramethyl N-methyl phenanthrolinium

Figure 4. Molecular Probes.

Chapter VII

DNA binding of $Ru(bpy)_2L^{2+}$ Complexes.

Introduction

The binding of cationic transition metal polypyridyl complexes to DNA, RNA, and synthetic polynucleotides has been extensively studied.[208] It has been proposed that the binding of these cations may occur via partial intercalation if one or more of the ligands is planar or nearly planar. Work performed in our laboratory strongly suggest an intercalative interaction in the case of $[Ru(bpy)_2ppz]^{2+}$. For example, this complex shows significant spectroscopic changes when added to DNA, while the complex containing the structurally similar but non planar ligand dpp (Fig. 1) in place of ppz does not. Partial intercalation is also a fundamental feature of a model proposed by Barton et al. where one of the planar ligands of a tris chelate ion is considered to be inserted between adjacent DNA base pairs in the major groove. [20] The binding of the delta and lambda enantiomers of $[Ru(phen)_3]^{2+}$ (phen = 1,10-phenanthroline) to several native DNA's was examined by Barton et al. [20,21] Analysis of spectroscopic and physical data led these workers to conclude that the delta isomer favors binding in a partially intercalative fashion, with the non intercalated (ancillary) ligands providing van der Waals interactions with the atoms lining the major groove. In contrast, they suggested that the non-intercalated ancillary ligands of the lambda isomer are repelled sterically by the atoms lining the major groove of the duplex. Therefore, minor groove surface binding was thought to be the most favored binding mode for the lambda isomer. However, the generality of this picture must be questioned as a result of the subsequent data presented by various groups[190-192] including our group as will be described here. [85]

In accordance with the early picture proposed by Barton et al. where the Δ isomer of $[Ru(phen)_3]^{2+}$ was proposed as fitting better into the right handed helical structure of DNA, we initially assumed that the Δ enantiomer of $[Ru(bpy)_2ppz]^{2+}$ was the isomer that bound more strongly to DNA. However, to make a definitive assignment, we needed to elucidate the configuration of the more strongly binding isomer. To do this we prepared the (Δ) and (Λ) isomers of $Ru(bpy)_2ppz^{2+}$ as described in Chapter III and also a ruthenium (II) complex with a chiral bis-bpy-like ligand, ((+)-chiragen[6]).[193] The structure of (+)-chiragen[6] (see Figure 2) is such that it can "wrap around" Ru in only a Δ sense. Circular dichroism (CD) spectrum of the chiragen complex was similar to the $[Ru(bpy)_2ppz]^{2+}$ complex that binds less strongly to DNA suggesting that it is the Δ isomer of $[Ru(bpy)_2ppz]^{2+}$. Therefore, we conclude that the Λ isomer binds more strongly to DNA. The binding constant of these complexes to DNA was determined by fluorescence titration at varying salt concentration. [85] Results from these experiments showed a four-fold preference for the lambda isomer in binding to DNA. Therefore, more subtle interactions than those proposed by Barton et al., must be involved in the binding of these complexes to DNA.

This chapter is a report on spectroscopic evidence collected for the resolved enantiomers of $[Ru(bpy)_2L]^{2+}$ (L = ppz, bppz, mbppz, bzp, ippz) complexes. Also reported in this chapter is the spectroscopic data collected for the non-planar and non-aromatic $[Ru(bpy)_2L]^{2+}$ (L= bis-oxazoline (bisoxazo), pyridyl-oxazoline (pyoxazo), dimethylpyridyl-oxazoline (dmpyoxazo)) complexes.

Results

Effects of Binding to DNA on Absorption

Visible absorption spectra of the complexes studied in buffer alone, and in the presence of calf thymus DNA, are presented in Figures 3 to 9. As observed for the ppz complex, [36, 71] both enantiomers (Δ and Λ) of the Ru(II) complexes based on the ligands bppz, and mbppz exhibited a red shift and a decrease in absorbance (hypochromic effect) at the MLCT band (in the 500-600nm region) in the presence of B-DNA. In each case these effects were more pronounced for the lambda isomer. In addition, the complexes based on bppz and mbppz also exhibited hypochromicity of the intra-ligand bands (π-π^*, in the 350-400nm region).

The enantiomers (Δ and Λ) of the $[Ru(bpy)_2L]^{2+}$ (L = ippz, bzp) complexes also exhibited a decrease in absorbance (hypochromic effect) at the MLCT band in the presence of B-DNA. The spectral shift and hypochromicity observed was larger for the Λ isomers of $[Ru(bpy)_2bzp]^{2+}$ and $[Ru(bpy)_2ippz]^{2+}$. On the other hand, only an increase in absorbance at the MLCT band was observed for the $[Ru(bpy)_2L]^{2+}$ (L= bisoxazo, pyoxazo, dmpyoxazo). A summary of the binding data from absorption experiments is presented in Table 1.

Effects of Binding to DNA on Emission

The emission spectra for the $[Ru(bpy)_2L]^{2+}$ complexes studied in buffer alone, and in the presence of B-DNA, are presented in Figures 10 to 17. In the presence of B-DNA, enantiomers of the Ru(II) complexes based on the ligands bppz, and mbppz exhibited a blue shift (lower energy) in the emission maxima, accompanied by large emission

enhancement. The blue shift in the emission maximum was more apparent for the lambda isomers in each case. Similar effects were also observed for the complex containing ppz.[36, 71]

Upon binding to DNA, luminescence enhancement of the emission maximum was also observed for the enantiomers of $[Ru(bpy)_2bzp]^{2+}$ and $[Ru(bpy)_2ippz]^{2+}$. In addition, a shift in emission maximum to lower energy (blue shift) was observed for both complexes but was more apparent for the isomers of $[Ru(bpy)_2bzp]^{2+}$ than that of $[Ru(bpy)_2ippz]^{2+}$. Although a spectral shift to the blue was observed for the enantiomers of $[Ru(bpy)_2ippz]^{2+}$ and $[Ru(bpy)_2bzp]^{2+}$ there was no distinction between the enantiomers with respect to spectral shift at similar [DNA]/[Ru] ratio. On the other hand, the Δ isomer exhibited a larger enhancement in emission maximum in each case.

Because the $[Ru(bpy)_2L]^{2+}$ (L= bisoxazo, pyoxazo, dmpyoxazo) complexes do not luminescence in aqueous solution or in the presence of DNA, we were unable to use luminescence spectroscopy to study the DNA binding. A summary of the emission maxima, I/Io values, and spectral shift in emission maxima for DNA- phosphate to ruthenium ratio greater than 60 ([P]/[Ru]) is represented in Table 2.

Equilibrium Dialysis

The binding constant, K_b, and the average site size in base pairs, *l*, was determined by fitting the data collected from equilibrium dialysis experiments to the McGhee and von Hippel equation ($r/C_f = [(K_b/2)(1-2lr)/(1-2(l-1)r]^{l-1}$), as was also used by Barton et. al.[4] The binding constant for the $[Ru(bpy)_2L]^{2+}$ (L= ppz, ippz, bppz, mbppz, bzp) complexes studied were of the order 10^3, which is of the same order that Barton et

al. found for $[Ru(phen)_3]^{2+}$, but relatively low compared to many other complexes in the literature (10^4 to 10^6). [205] The site size for all complexes studied was of the order of l = 3 to 5. The large site size found with Ru (II) complexes is partly attributed to the steric bulk of the opposing non-intercalating ligands compared to the two base-pair (neighbor excluded) site for planar aromatic intercalators, and also to the degree of disruption of the DNA structure. [46, 163, 174-176] The binding constants for all the complexes studied, with the exception of Δ-$[Ru(bpy)_2ippz]^{2+}$, showed stronger binding for the lambda isomer.

For the non-planar $[Ru(bpy)_2L]^{2+}$ (L= bisoxazo, pyoxazo, dmpyoxazo) complexes studied, the binding constants were also of the order 10^3 with a site size of l = 3-4. However, they were smaller in magnitude than those obtained for the stronger binding isomers of $[Ru(bpy)_2L]^{2+}$ (L= bppz, mbppz. bzp) complexes. The binding constants and site size for the Ru(II) complexes studied by equilibrium dialysis are listed in Table 3. The binding isotherms fitted to the McGhee and von Hippel equation are presented in Figures 17 to 24.

Enantioselectivity

(1) As studied by Eqilibrium Dialysis.

In the following discussion enantioselectivity refers to the preferential binding of one enantiomer of the metal complex to DNA. This effect was observed for the $[Ru(bpy)_2L]^{2+}$ (L= ppz, bppz, mbppz, bzp) complexes. Equilibrium dialysis was one of several techniques we used to study this phenomenon. The racemic complex was dialyzed against B-DNA (calf thymus DNA) and the circular dichroism (CD) spectrum of the solution outside the dialysis bag (dialysate) was measured. For the Ru(II) complexes

containing ppz, bppz, and mbppz the CD signal observed was oriented in the negative direction corresponding to the Δ isomer. This indicates that the Λ isomer was more strongly bound and therefore binding is enantioselective, with the Λ isomer favored. However, for the complex containing bzp enantioselectivity was observed favoring the Δ isomer and no significant preference in binding was observed for the complexes containing ippz, bisoxazo, pyoxazo, and dmpyoxazo. Circular dichroism spectra showing enantioselectivity for the complexes studied are represented in figure 25-27. A summary of the enantioselectivity for the $[Ru(bpy)_2L]^{2+}$ complexes studied are represented in Table 4.

(2) As Studied by Fluorescence Titrations

The binding constant, K_b, for $[Ru(bpy)_2L]^{2+}$ (L= ppz, bppz, mbppz, bzp, ippz) to calf thymus DNA from fluorescence titrations are listed in Table 5. Eadie Hofstee plots representing the binding of the Ru(II) complexes studied by fluorescence titration are presented in Figures 28 to 31. The sodium ion concetrations used were 10, 25, 50, and 100mM. Since K_b values are determined as −1/slope, in each case as the salt concentration increased from 10 to 100mM there was a progressive increase in the slope indicating a decrease in the binding constant, thus illustrating the dependence of the value K_b on the sodium ion concentration. Here again, in agreement with equilibrium dialysis results, stronger binding was observed for the Λ isomers of the complexes containing ppz, bppz, mbppz and for Δ-$[Ru(bpy)_2ippz]^{2+}$. However, using this method, the binding constant was larger for Δ-$[Ru(bpy)_2bzp]^{2+}$. Since the $[Ru(bpy)_2L]^{2+}$ (L = bisoxazo,

pyoxazo, dmpyoxazo) complexes do not luminescence in aqueous solution we were unable to determine their respective binding constants by this method.

(3) As Studied by Steady State Luminescence Quenching by $Fe(CN)_6^{4-}$

Further data used to infer intercalative binding of Ru(II) complexes to DNA is obtained through steady-state emission quenching experiments with $Fe(CN)_6^{4-}$. The negatively charged quencher is expected to be repelled by the negatively charged phosphate backbone, and therefore an intercalatively bound ruthenium cation should be protected from quenching by an anionic quencher. On the other hand, anionic quenchers would readily quench "free" or aqueous complexes or near the DNA surface. Negatively charged ferrocyanide ion was chosen for this purpose, since it has been proven to be an excellent quencher for Ru(II) complexes in the presence of DNA. [206-207]

Figures 32-35 shows the Stern-Volmer plots, Io/I vs $[FeCN_6]^{4-}$, of luminescence quenching of Ru-DNA solutions with increasing concentrations of ferrocyanide ion. The Stern-Volmer plots for Δ-$[Ru(bpy)_2bppz]^{2+}$, Δ/Λ-$[Ru(bpy)_2ippz]^{2+}$, and Δ/Λ-$[Ru(bpy)_2bzp]^{2+}$ were practically linear, whereas a downward curvature was found for Λ-$[Ru(bpy)_2bppz]^{2+}$and both isomers of $[Ru(bpy)_2mbppz]^{2+}$. The curvature is interpreted as reflecting differing degrees of protection or relative accessibility of bound Ru cations. For the complexes studied, with the exception of the complex containing bzp, the degree of quenching was greater for the delta isomer indicating a greater degree of penetration of the binding site (presumably in the major groove) for the Λ isomer as was observed for $[Ru(bpy)_2ppz]^{2+}$.

Discussion

Results from the experiments above show similar effects to those observed for $[Ru(bpy)_2ppz]^{2+}$ and other intercalators. For intercalating organic dyes stacking interactions with the base pairs in DNA lead to hypochromism in the π -π^* transitions. This was also observed at the MLCT band for both isomers of the Ru(II) polypyridyl complexes containing ppz, bppz, mbppz, ippz, and bzp accompanied by a red shift in the spectra. In each case (ppz, bppz, mbppz, bzp, ippz) greater hypochromicity and spectral shift was observed for the lambda isomer. For the ligands bppz and mbppz hypochromicity was also observed at the intra ligand bands, which further indicates that the effect was due to the partially intercalated bppz or mbppz ligand and not the ancillary ligands (bpy). In contrast, Ru(II) complexes containing bisoxazo, pyoxazo, and dmpyoxazo exhibited a small *increase* in absorbance at the MLCT band and no spectral shift was observed. This may indicate that the ligands of these complexes are not sufficiently extended from the metal to partially intercalate between the base pairs of B-DNA and perturb the system. Evidence for intercalation includes planarity, and aromaticity, of ligand along with hypochromicity and spectral shifts on binding to DNA. The latter two are not present and we can infer that the Ru(II) complexes containing bisoxazo, pyoxazo, and dmpyoxazo bind to B-DNA mainly via electrostatic interactions.

For the intercalative mode of binding to DNA an enhancement in emission and corresponding increased luminescent lifetimes is usually observed, which reflects the decreased mobility of the complex when sandwiched into the helix as well as the hydrophobic nature of the environment. A blue shift in the emission maximum is also observed on binding to DNA. An enhancement in emission and shift to lower energy

(blue shift) was observed for each enantiomer of the $[Ru(bpy)_2L]^{2+}$ (L = ppz, bppz, mbppz, bzp, ippz) complexes. For the Ru(II) complexes containing ppz, bppz, and mbppz the enhancement in emission intensity and spectral shift was maximal for the lambda configuration. However, the greatest effect was observed for mbppz as the partially intercalated α-diimine ligand, followed by ppz and bppz. For the enantiomers of the complexes containing bzp and ippz the blue spectral shift was almost identical but a slightly larger enhancement of emision maximum was observed for the Δ isomers. Luminescence lifetime in DNA was previously measured only for $[Ru(bpy)_2ppz]^{2+}$. A maximal value of 950ns was obtained for the lambda isomer and a maximal value of ~550ns for the delta isomer (see Stephen Tysoe's thesis).

Emission quenching by ferrocyanide ion was also used to probe the intercalative mode of binding of tris–chelates with DNA. An intercalated Ru(II) complex within the major groove should be less accessible to anionic quenchers in solution, than are electrostatic or surface bound complexes. The data gathered from luminescence experiments suggests that the delta isomer of the Ru (II) complexes containing ippz and bzp were preferably binding to DNA. However, by anionic quenching experiment the I_o/I values at high concentration of ferrocyanide was higher for the Δ isomer in each case indicating more efficient quenching, therefore less protected in the major groove. Therefore, the Δ isomers containing bppz, mbppz, ppz, bzp, and ippz are probably bound more extensively bound via the minor groove, whereas the Λ isomers of the Ru(II) complexes containing ppz, ippz, bzp, bppz, mbppz, are probably bound via the major groove.

Binding constants obtained from equilibrium dialysis and fluorescence titration at varying salt concentration showed a higher binding constant for the Λ isomer for each of the Ru(II) complex containing ppz, bppz, and mbppz. However, the Δ isomer of the complex containing ippz exhibited the higher binding constant from both methods. In the case of the Ru(II) complex containing bzp a higher binding constant was observed for the Δ isomer by fluorescence titrations but the opposite was observed by equilibrium dialysis. Since equilibrium dialysis is a longer process, this may reflect chemistry involving DNA and the bzp complex. Binding constants for $[Ru(bpy)_2L]^{2+}$ (L= bppz, mbppz, bzp, ippz, bisoxazo, pyoxazo, dmpyoxazo) determined by equilibrium dialysis were of the order 10^3 ($[Na^+] = 0$). Although the constants for complexes containing bisoxazo, pyoxazo, and dmpyoxazo were of the order 10^3, they were numerically smaller than those obtained for the stronger binding isomer of the complexes containing bppz, mbppz, and bzp.

The binding constants observed (order 10^3) are similar to those for $[Ru(phen)_3]^{2+}$, which are resonable for a weak intercalative mode of binding. From equilibrium dialysis a site size of ~3-5 was observed for all complexes. For metal complexes the octahedral coordination around the metal precludes effective stacking of the entire complex between base pairs. If the complex is pictured with one of the α-diimine ligands (ppz, ippz, bppz, mbppz, bzp, bisoxazo, pyoxazo,dmpyoxazo) inserted into the helix, then the other two ligands (bpy) actually protrude above and below the face of this α-diimine ligand and decrease the effective area of overlap. Hence only partial insertion is possible, which accounts for the low binding. The base-pair site size is similarly consistent with the structural model for the bound complex, where one ligand intercalates and the remaining

two span the groove of the helix, the degree of intercalation distorting the secondary structure of DNA.

Differential binding studies of the enantiomers of Ru(II) polypyridyl complexes to DNA has been informative on the description of the strong binding process as intercalative. Determination of the stronger binding enantiomer was achieved by dialyzing the racemic complex against B-DNA and measuring the circular dichroism (CD) of the dialysate. For the Ru(II) polypyridyl complexes containing ppz, bppz, and mbppz the CD signal corresponded to that of the Δ isomer, thus indicating that binding was enantioselective favoring the Λ isomer in each case. However, for the complexes containing bzp and ippz (both ligands similar to ppz in structure) enantioselectivity was observed favoring the Δ isomer of $[Ru(bpy)_2bzp]^{2+}$ and none was observed for the isomers of $[Ru(bpy)_2ippz]^{2+}$. Also, enantioselectivity was not observed for the complexes containing bisoxazo, pyoxazo, and dmpyoxazo. Table 6 gives a summary of the evidence collected pertaining to enantioselectivity.

Conclusion

The lambda isomer of $[Ru(bpy)_2ppz]^{2+}$ is the isomer that binds most strongly to B-DNA. Based on spectroscopic data gathered for $[Ru(bpy)_2bppz]^{2+}$ and $[Ru(bpy)_2mbppz]^{2+}$ we also conclude that the lambda isomers of these complexes bind more effectively to DNA, most probably by intercalation via the major groove. Intercalation via the minor groove or surface binding is likely the favored binding modes for the delta isomers. In contrast, from spectroscopic data gathered for the complexes $[Ru(bpy)_2bzp]^{2+}$ and $[Ru(bpy)_2ippz]^{2+}$ we can conclude that the Δ isomer binds more

effectively to DNA which is most probably via the minor groove. Clearly, very subtle effects determine which of the enantiomers of these complexes binds more strongly to DNA, because ppz, ippz, and bzp are isoelectronic and isosteric. Surface binding is probably the favored mode of binding for the Λ isomers. However, electrostatic surface binding is most likely the favored mode of binding for the $[Ru(bpy)_2L]^{2+}$ (L = bisoxazo, pyoxazo, and dmpyoxazo) complexes on the basis of spectroscopic data gathered. These results further demonstrate that the early Barton model is inadequate for understanding the binding of α-diimine complexes to DNA.

Table 1. Absorption data

	λ_{max}, nm			
Complex	**without DNA**	**with DNA**	**Δλ, nm**	**Hypochromicity,%**
Δ-ppz	422(477)sh	422(485)sh	+8	~12
Λ-ppz	422(477)sh	422(495)sh	+18	~25
Δ-bppz	544	550	+6	~9.5 (16 ; 360nm)
Λ-bppz	544	552	+8	~13.4 (20 ; 360nm)
Δ-mbppz	534	540	+6	~5.1(10.4 ; 366nm)
Λ-mbppz	534	542	+8	~12.5 (20.4; 366nm)
Δ-bzp	452	454	+2	~5
Λ-bzp	452	460	+8	~11
Δ-ippz	450	454	+4	~8
Λ-ippz	450	458	+8	~14
Bisoxazo	450	450	0	0 (~3% incr. in abs.)
Pyoxazo	456	456	0	0 (~2% incr. in abs.)
Dmpyoaxzo	454	454	0	0
T-pyoxazo	466	466	0	0
T-dmpyoxazo	456	456	0	~2
T-bzp	454	458	+4	1

Absorption measurements for all the complexes studied was carried out in 5mM Tris buffer, 50mM NaCl, and at pH 7.4.

Table 2. Fluorescence Data

	λ_{max}, *nm*			
Complex	**without DNA**	**with DNA**	**Δλ, nm**	**I/Io**
Δ-ppz	690	670	-20	5.2
Λ-ppz	690	660	-30	17
Δ-bppz	817	799	-18	5.2
Λ-bppz	817	795	-22	8.5
Δ-mbppz	807	769	-38	5.5
Λ-mbppz	807	759	-48	9.7
Δ-bzp	607	598	-9	2.3
Λ-bzp	607	598	-9	2.2
Δ-ippz	612	612	0	4.2
Λ-ippz	614	613	-1	3.9
Tris-bzp	598	594	-4	2.2

Fluorescence measurements for all the complexes studied was carried out in 5mM Tris buffer, 50mM NaCl, and at pH 7.4.

Table.3 Equilibrium Dialysis

Complex	K_b	L = site size in base pairs
Δ-ppz	6.0×10^3	3,4
Λ-ppz	1.2×10^4	3
Δ-bppz	1.8×10^3	3
Λ-bppz	3.2×10^3	4
Δ- mbppz	3.45×10^3	3
Λ-mbppz	4.85×10^3	4
Δ-bzp	1.2×10^3	5
Λ-bzp	4.4×10^3	4,5
Δ-ippz	1.7×10^3	4
Λ-ippz	7.5×10^2	3
Bisoxaz	2.5×10^3	4
Pyoxaz	2.8×10^3	4
Dmpyoxaz	3.4×10^3	4

Equilibrium Dialysis measurements for $[Ru(bpy)_2ppz]^{2+}$ was carried out in 5mM Tris buffer, [NaCl] = 50mM, and at pH 7.4. All the other measurements were carried out in 5mM Tris buffer, [NaCl] = 0, and at pH 7.4.

Table. 4 Enantioselectivity by Equilibrium Dialysis.

Complex	Evidence for Enantioselectivity
ppz	Λ- preferred isomer
bppz	Λ- preferred isomer
mbppz	Λ-preferred isomer
bzp	Δ-preferred isomer
ippz	No evidence of preference
Bisoxazo	No evidence of preference
Pyoxazo	No evidence of preference
Dmpyoxazo	No evidence of preference

Determination of enantioselectivity by equilibrium dialysis for $[Ru(bpy)_2ppz]^{2+}$ was carried out in 5mM Tris buffer, [NaCl] = 50mM, and at pH 7.4. All the other measurements were carried out in 5mM Tris buffer, [NaCl] = 0, and at pH 7.4.

Table 5. Fluorescence Titration

	K_b			
Complex	**10mM NaCl**	**25mM NaCl**	**50mM NaCl**	**100mM NaCl**
Δ-ppz	2.1×10^4	4.2×10^3	2.8×10^3	1.2×10^3
Λ-ppz	6.3×10^4	2.9×10^4	1.1×10^4	3.9×10^3
Δ-bppz	9.3×10^3	2.7×10^3	2.4×10^3	1.1×10^3
Λ-bppz	1.4×10^4	2.7×10^3	2.4×10^3	1.7×10^3
Δ-mbppz	2.1×10^4	7.9×10^3	2.1×10^3	5.5×10^2
Λ-mbppz	2.5×10^4	8.96×10^3	3.1×10^3	7.9×10^2
Δ-bzp	2.2×10^5	1.3×10^5	1.1×10^5	3.4×10^4
Λ-bzp	1.3×10^5	1.1×10^5	7.6×10^4	2.7×10^4
Δ-ippz	1.6×10^5	1.1×10^5	3.4×10^4	9.4×10^3
Λ-ippz	1.0×10^5	7.8×10^4	2.8×10^4	7.7×10^3
Tris-bzp	1.19×10^5	9.48×10^4	8.49×10^4	7.24×10^4

Table 6. Summary of Enantioselectivity

$Ru(bpy)_2L^{2+}$ L	K_b Equilibrium Dialysis (no salt except ppz)	K_b Fluorescence Titration (10-100mM salt)	Fluorescence with DNA (I_{em} greater; 50mM NaCl)	Absorbance with DNA (hypo-shift greater; 50mM NaCl)	Dialysate CD (signal in dialysate) (no salt)	$[Fe(CN)_6]^{4-}$ Quenching (least quenched; 50mM NaCl)
ppz	Λ	Λ	Λ	Λ	Λ	Λ
i-ppz	Δ	Δ	Δ	Λ	No evidence	Λ
bzp	Λ	Δ	Δ	Λ	Λ	Λ
bppz	Λ	Λ	Λ	Λ	Λ	Λ
mbppz	Λ	Λ	Λ	Λ	Λ	Λ

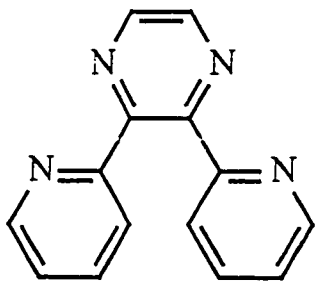

Fig.1 Structure of dpp

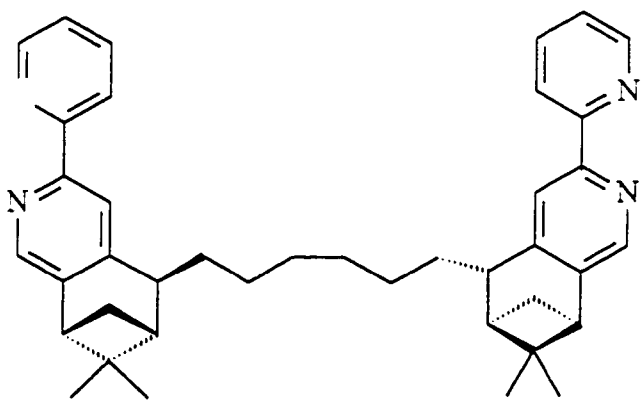

Fig. 2 Structure of (+)-chiragen[6]

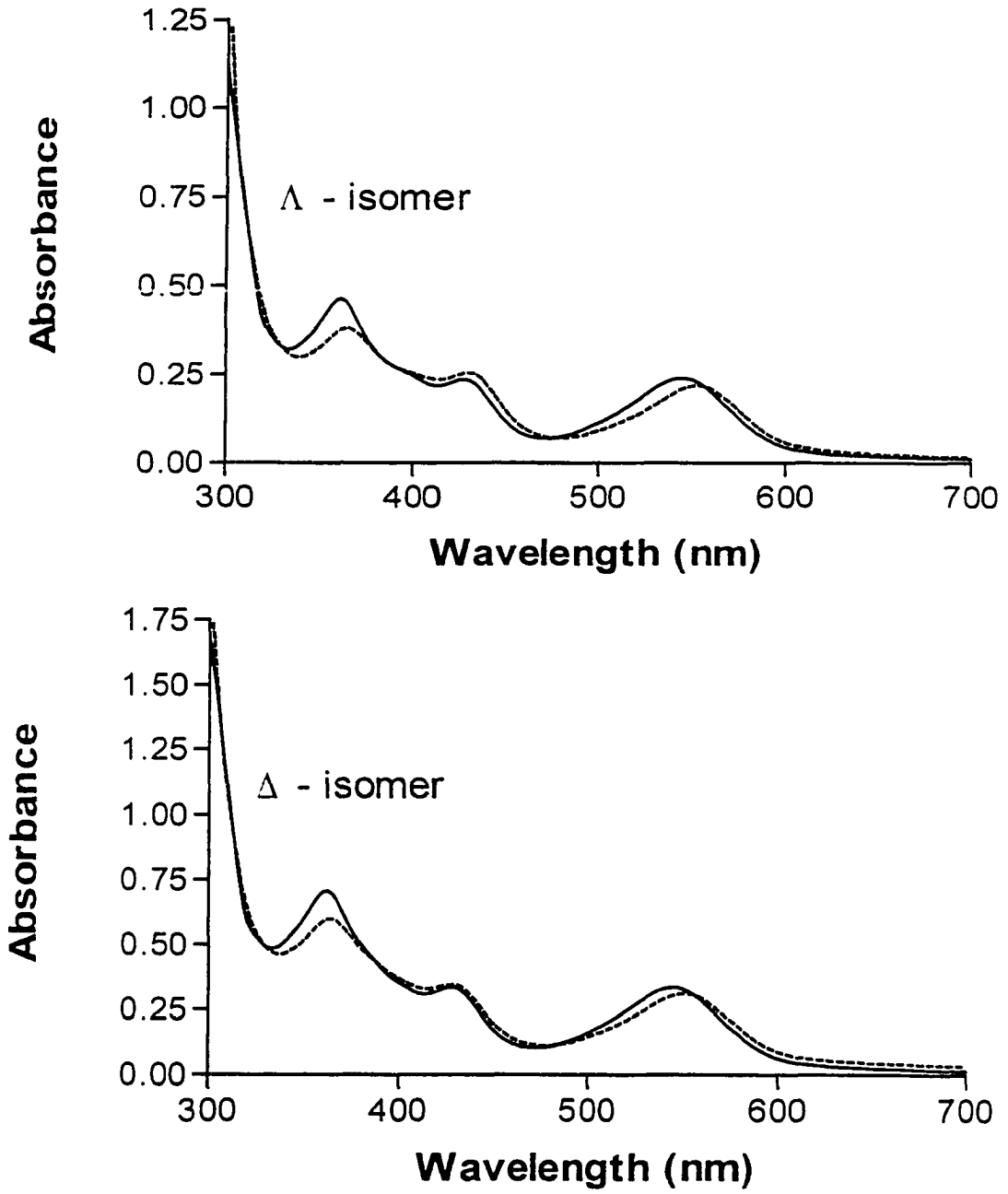

Fig.3. Absorption Spectra of Λ-$[Ru(bpy)_2bppz]^{2+}$ (top, [P]/[Ru] = 91) and Δ-$[Ru(bpy)_2bppz]^{2+}$ (bottom, [P]/[Ru] = 74) in the presence of DNA (---) and absence of DNA (__). All spectra were measured in 5mM Tris buffer, 50mM NaCl, and at pH 7.4.

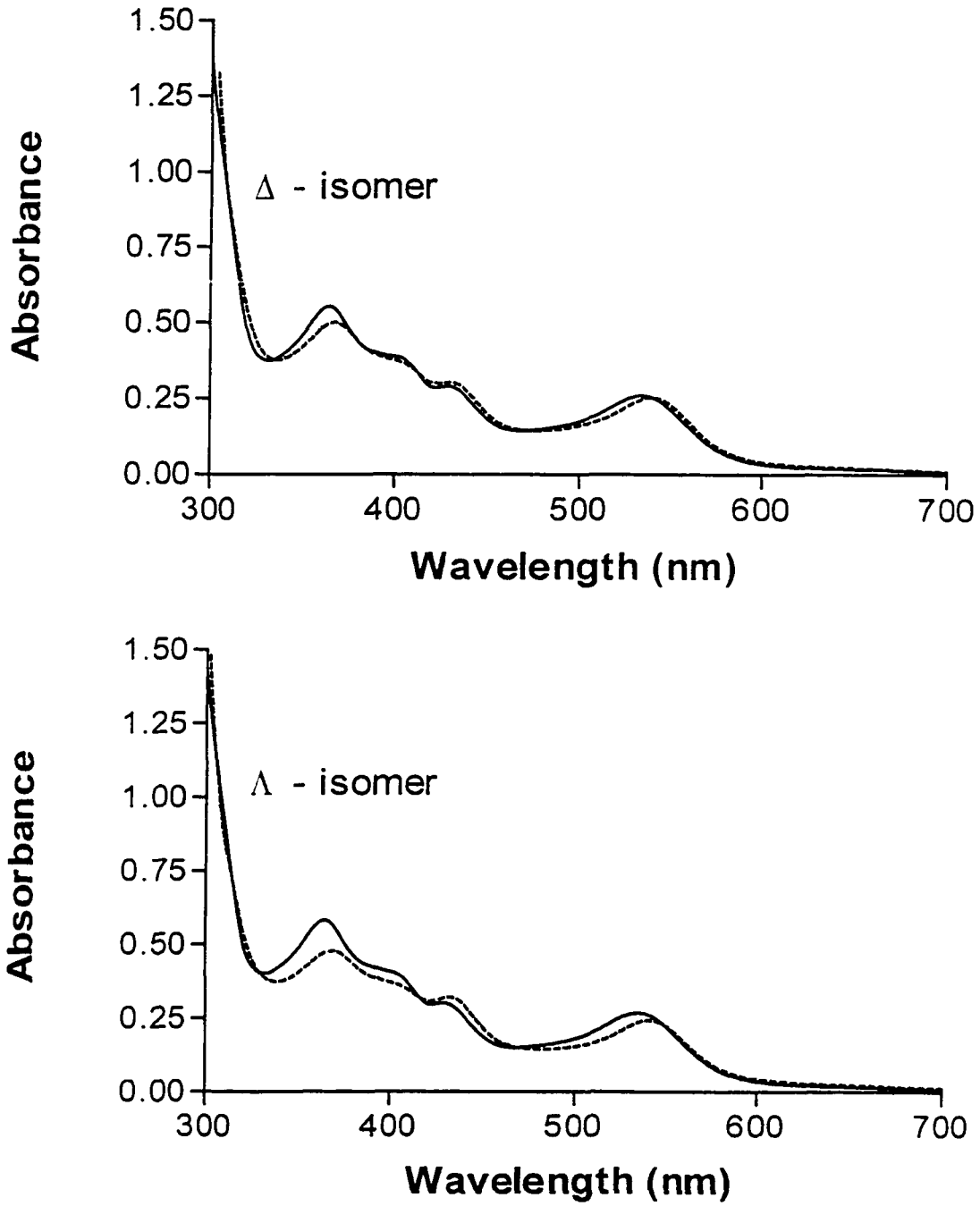

Fig.4. Absorption Spectra of Δ-$[Ru(bpy)_2mbppz]^{2+}$ (top, [P]/[Ru] = 91) and Λ-$[Ru(bpy)_2mbppz]^{2+}$ (bottom, [P]/[Ru] = 89) in the presence of DNA (---) and the absence of DNA (__). All spectra were measured in 5mM Tris buffer, 50mM NaCl, and at pH 7.4.

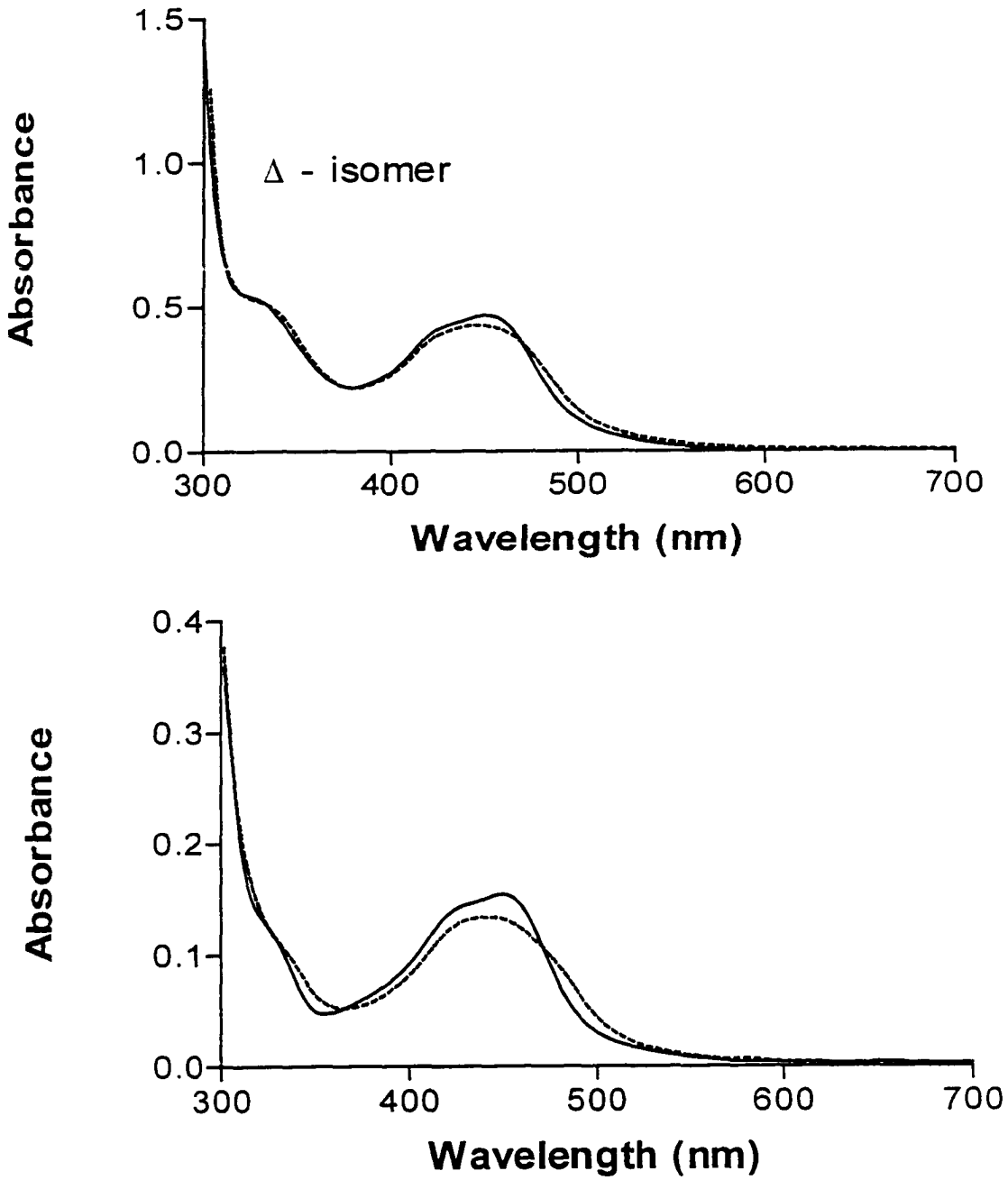

Fig.5. Absorption spectra of Δ-$[Ru(bpy)_2ippz]^{2+}$ (top; [P]/[Ru] = 64) and Λ-$[Ru(bpy)_2ippz]^{2+}$ (bottom; [P]/[Ru] = 54) in the presence of DNA (---) and absence of DNA (__). All spectra were measured in 5mM Tris buffer, 50mM NaCl, and at pH 7.4.

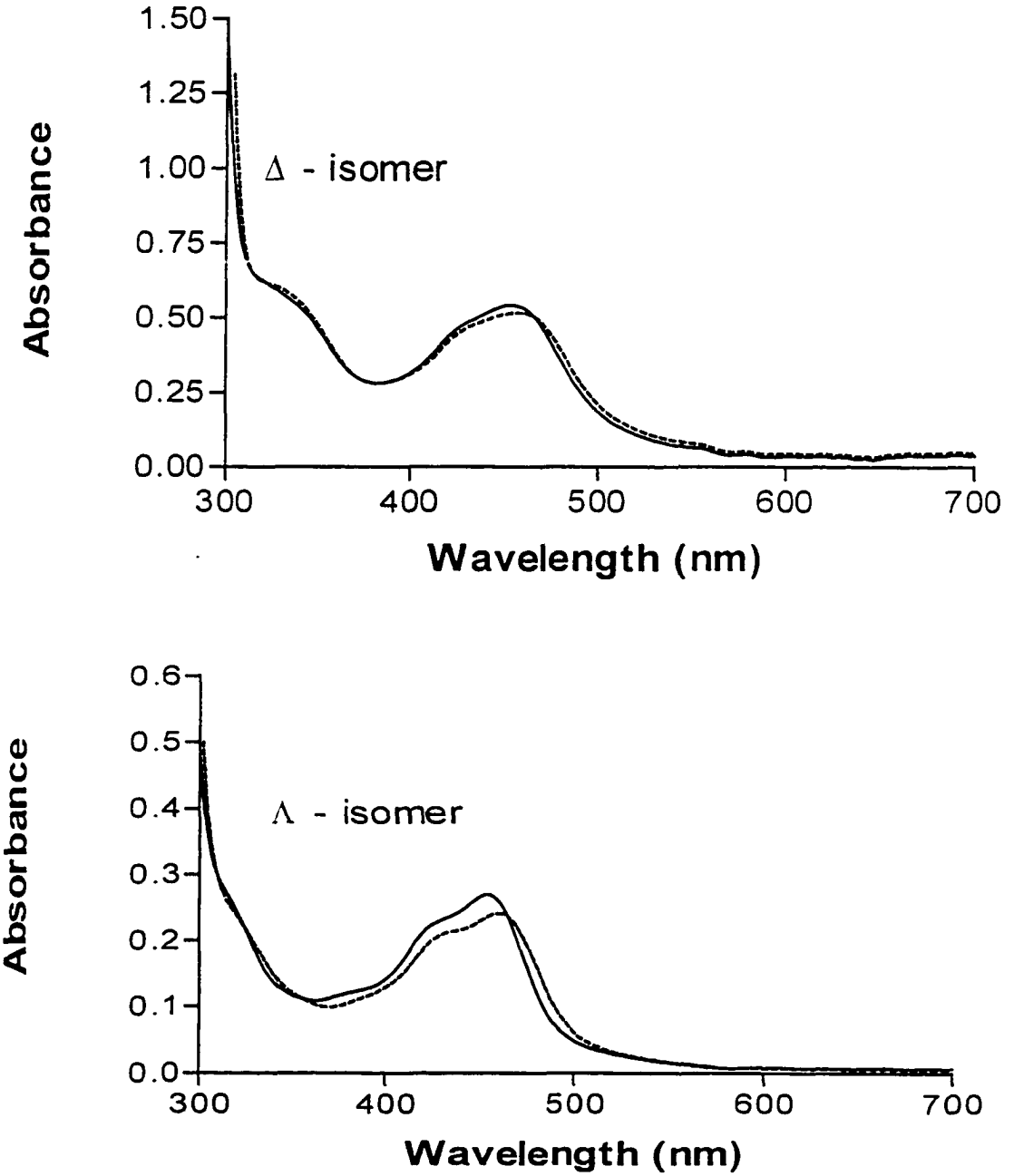

Fig.6. Absorption Spectra of Δ-$[Ru(bpy)_2bzp]^{2+}$ ([P]/[Ru] = 68) and Λ-$[Ru(bpy)_2bzp]^{2+}$ (bottom, [P]/[Ru] = 67) in the presence of DNA (---) and the absence of DNA (__). All spectra were measured in 5mM Tris buffer, 50mM NaCl, and at pH 7.4.

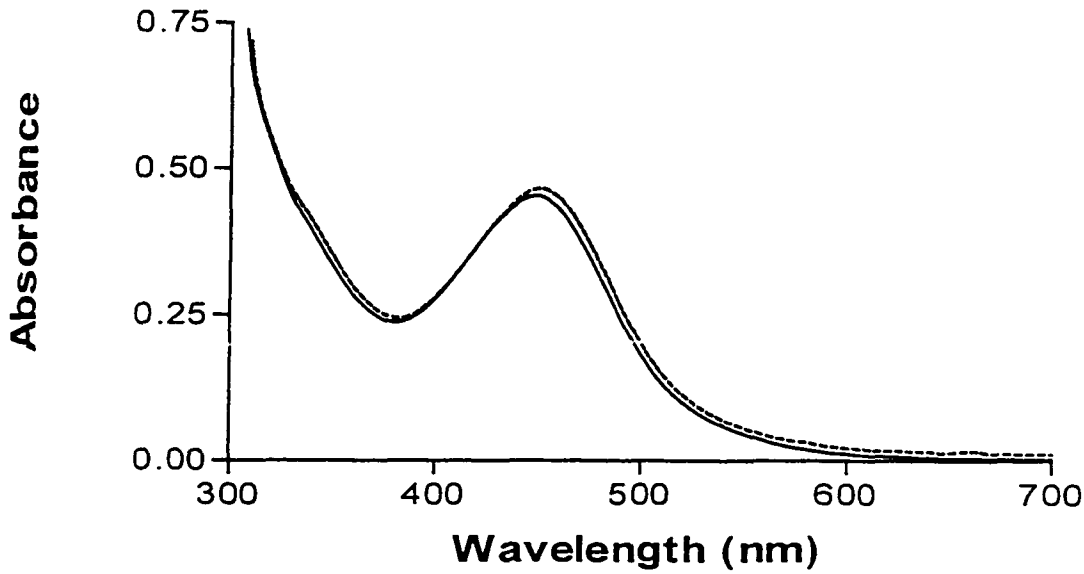

Fig.7 Absorption Spectra of $[Ru(bpy)_2(bisoxazo)]^{2+}$,[P]/[Ru] = 80, in the presence of DNA (---) and absence of DNA (__). All spectra were measured in 5mM Tris buffer, 50mM NaCl, and at pH 7.4.

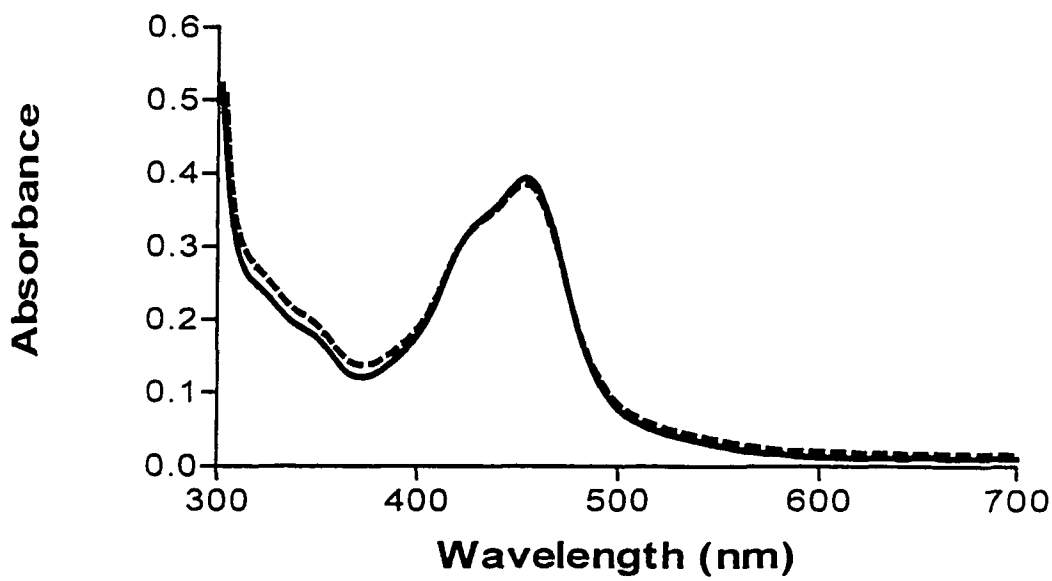

Fig.8 Absorption Spectra of $[Ru(bpy)_2(dmpyoxazo)]^{2+}$,[P]/[Ru] = 47, in the presence of DNA (---) and absence of DNA (__). All spectra were measured in 5mM Tris buffer, 50mM NaCl, and at pH 7.4.

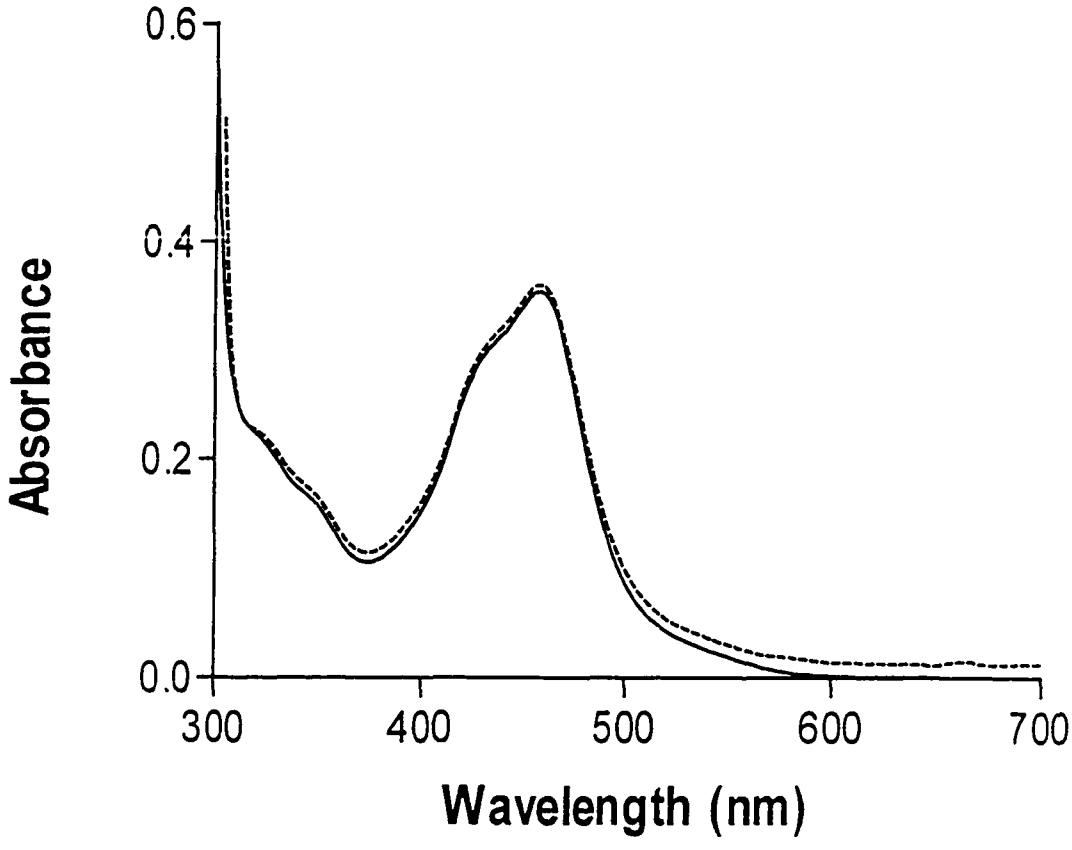

Fig.9 Absorption Spectra of $[Ru(bpy)_2(pyoxazo)]^{2+}$,[P]/[Ru] = 55, in the presence of DNA (---) and absence of DNA (__). All spectra were measured in 5mM Tris buffer, 50mM NaCl, and at pH 7.4.

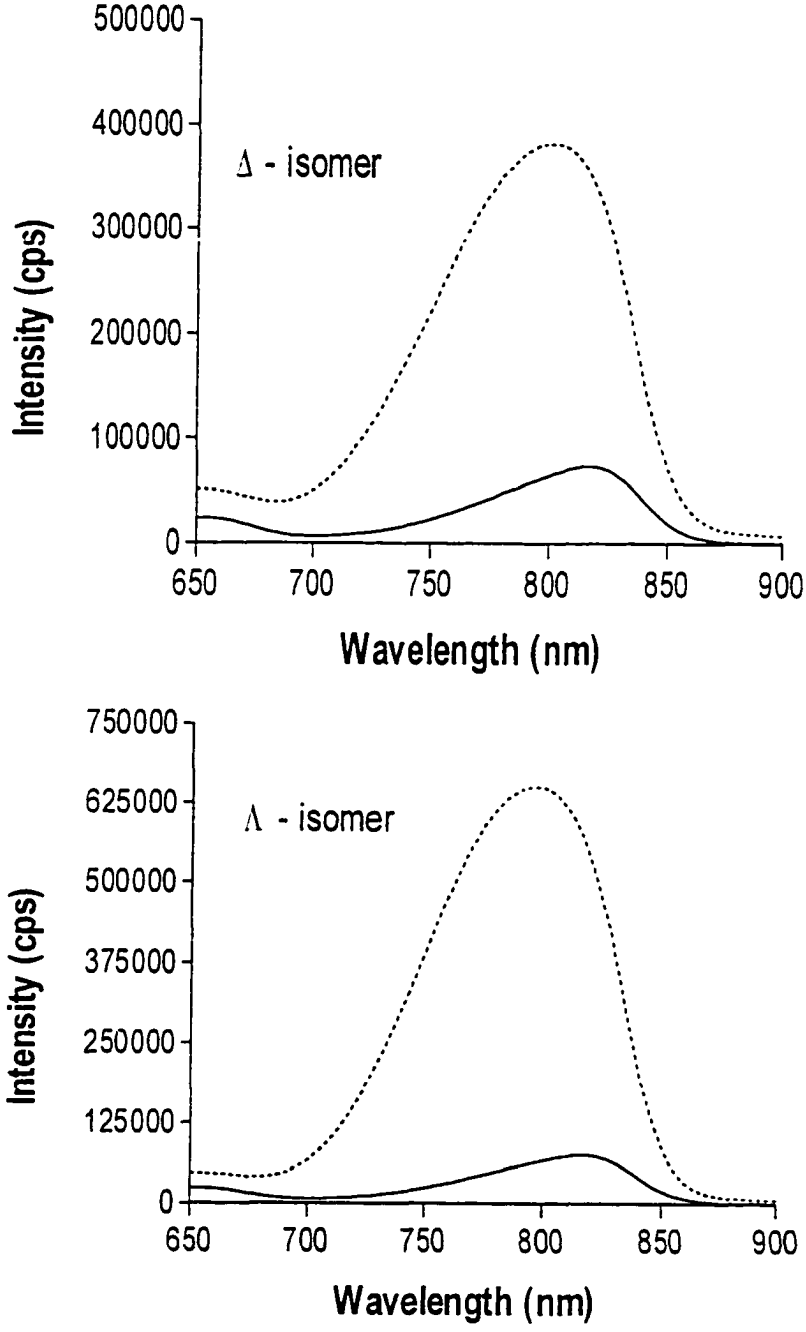

Fig.10. Emission Spectra of Δ-$[Ru(bpy)_2bppz]^{2+}$ and Λ-$[Ru(bpy)_2bppz]^{2+}$ ([P]/[Ru] = 65) in the presence of DNA (---) and the absence of DNA (___). All spectra were measured in 5mM Tris buffer, 50mM NaCl, and at pH 7.4.

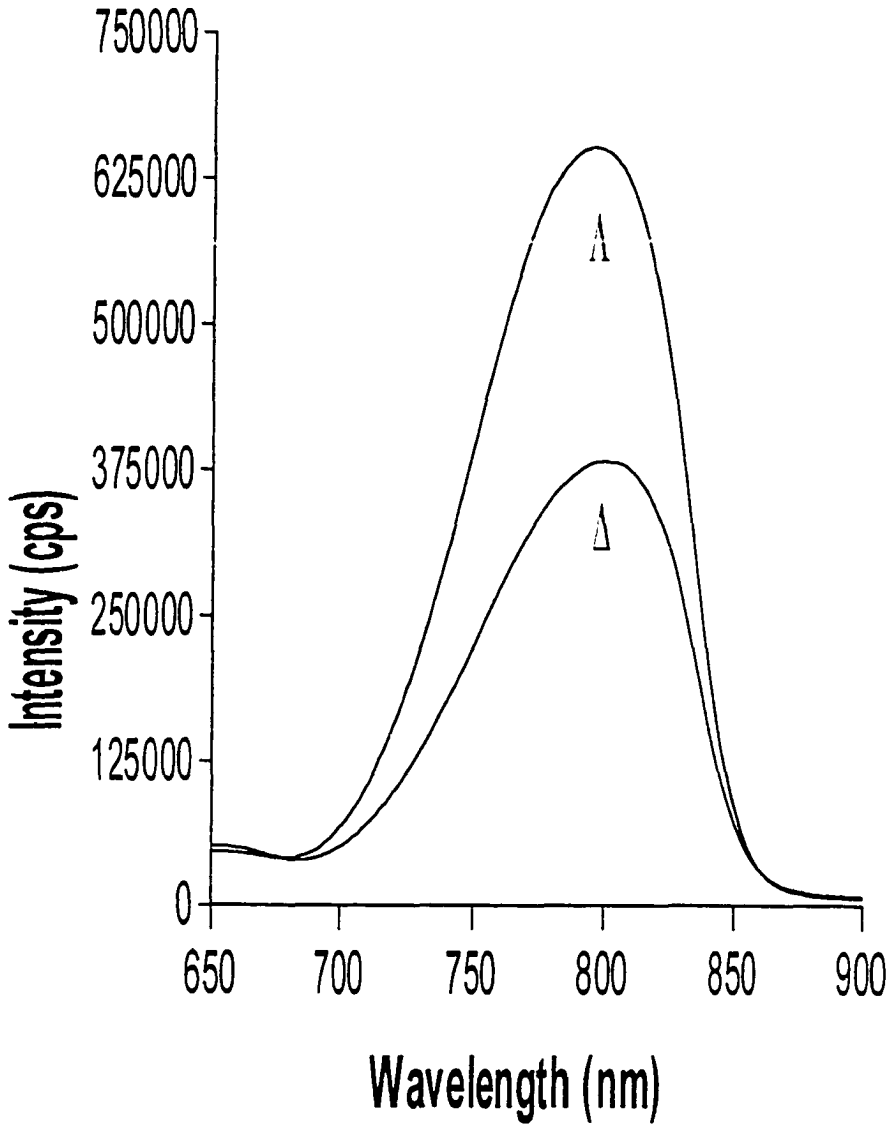

Fig.11. Emission Spectra of Δ-$Ru(bpy)_2bppz]^{2+}$ (Em. = 799nm) and Λ-$[Ru(bpy)_2bppz]^{2-}$ (Em. = 795) in the presence of DNA , [P]/[Ru] = 65. All spectra were measured in 5mM Tri buffer, 50mM NaCl, and at pH 7.4. [Ru] identical in both samples.

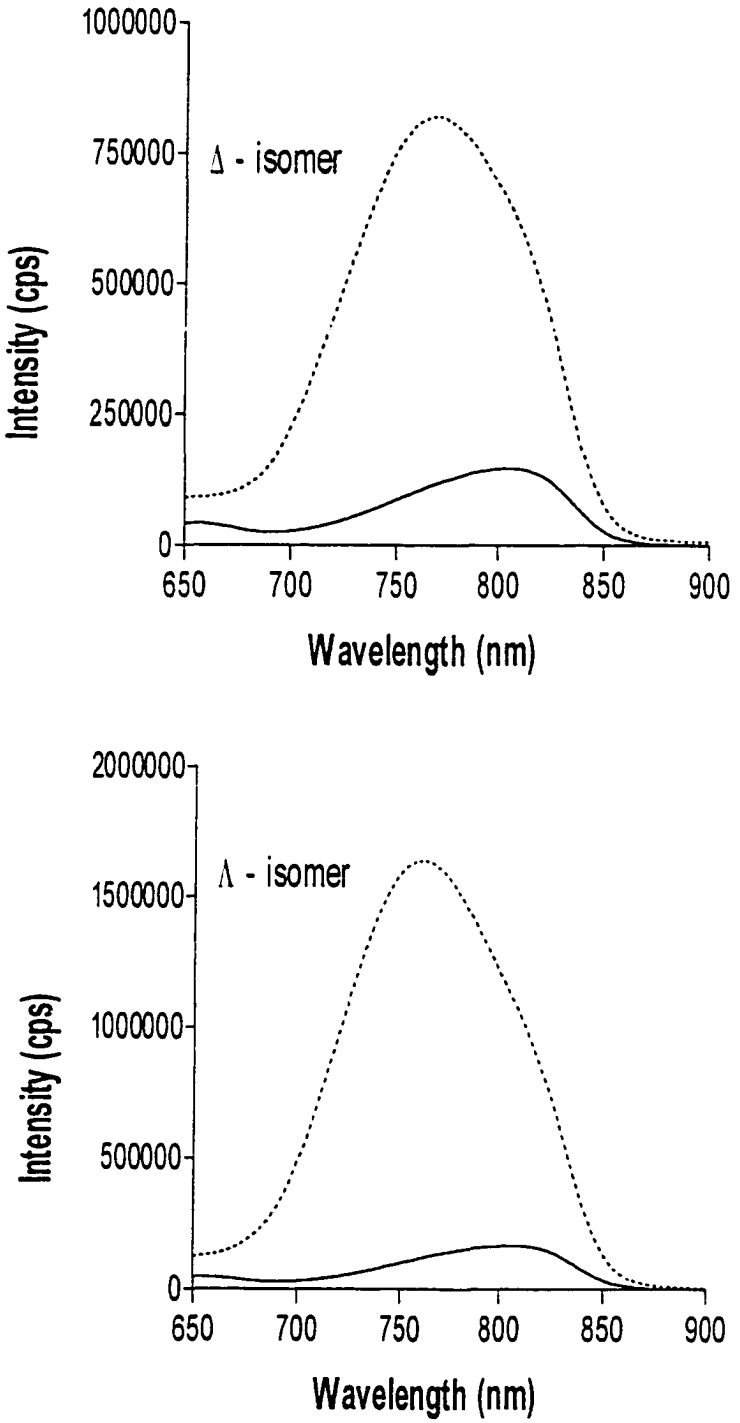

Fig.12. Emission Spectra of Δ-$[Ru(bpy)_2mbppz]^{2+}$ and Λ-$[Ru(bpy)_2mbppz]^{2-}$ ([P]/[Ru] = 77) in the presence of DNA (---) and the absence of DNA (___). All spectra were measured in 5mM Tris buffer, 50mM NaCl, and at pH 7.4.

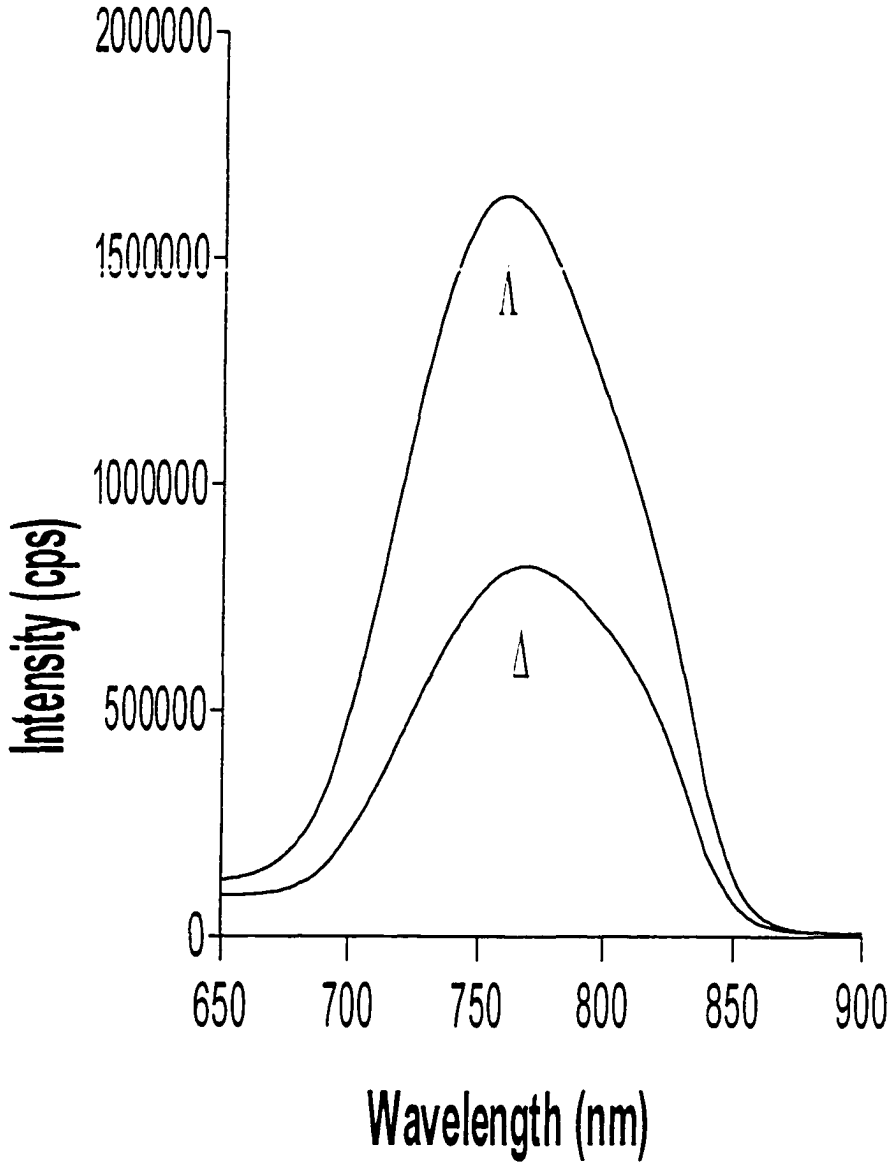

Fig.13. Emission Spectra of Δ-$Ru(bpy)_2mbppz]^{2+}$ (Em. = 769nm) and Λ-$[Ru(bpy)_2mbppz]^{2+}$ (Em. = 761) in the presence of DNA , [P]/[Ru] = 77. All spectra were measured in 5mM Tri buffer, 50mM NaCl, and at pH 7.4. [Ru] identical in both samples.

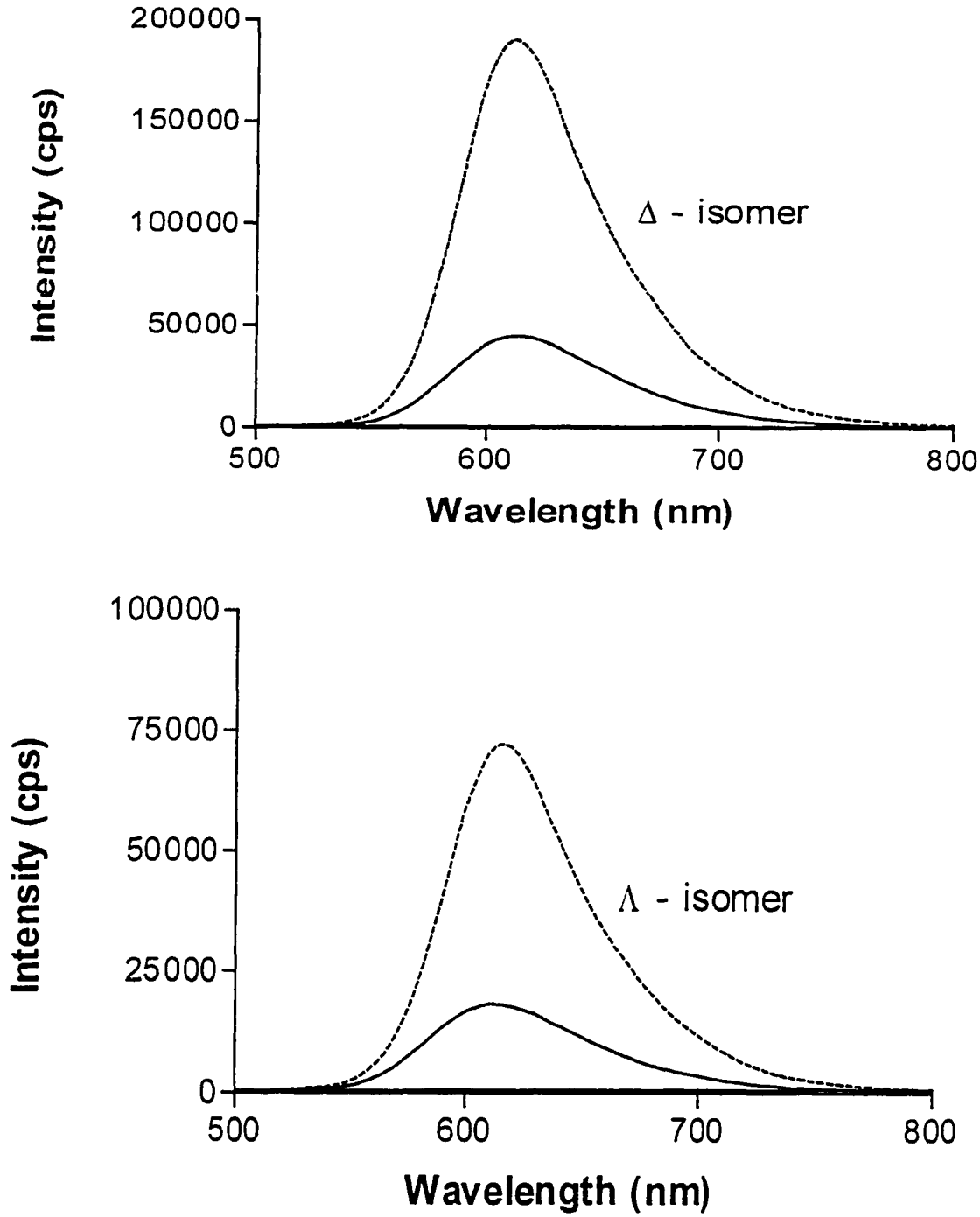

Fig.14. Emission Spectra of Δ-$[Ru(bpy)_2ippz]^{2+}$ and Λ-$[Ru(bpy)_2ippz]^{2+}$ ([P]/[Ru] = 80) in the presence of DNA (---) and the absence of DNA (___). All spectra were measured in 5mM Tris buffer, 50mM NaCl, and at pH 7.4.

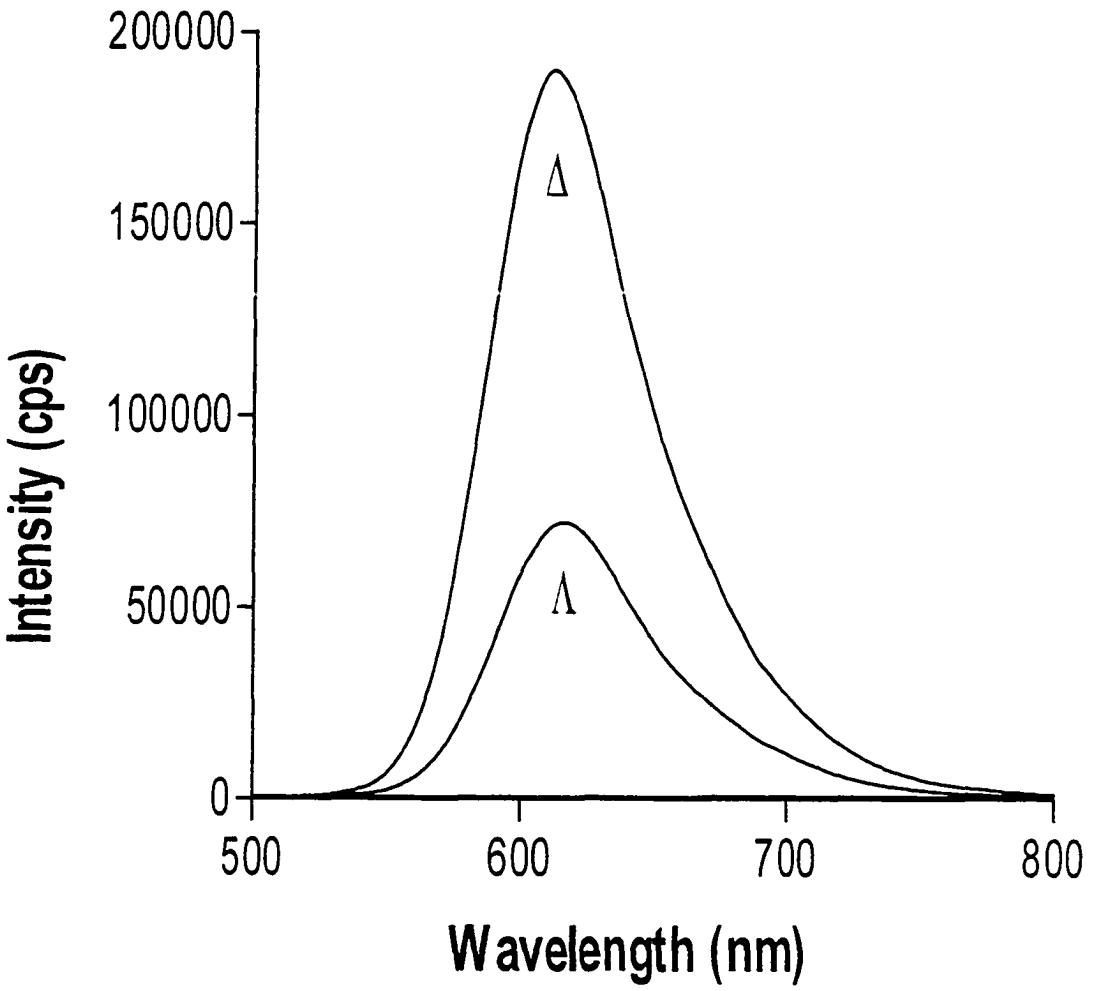

Fig.15. Emission Spectra of Δ-$Ru(bpy)_2ippz]^{2+}$ (Em. = 612) and Λ-$[Ru(bpy)_2ippz]^{2+}$ (Em. = 616) in the presence of DNA , [P]/[Ru] = 80. All spectra were measured in 5mM Tris buffer, 50mM NaCl, and at pH 7.4. [Ru] identical in both samples.

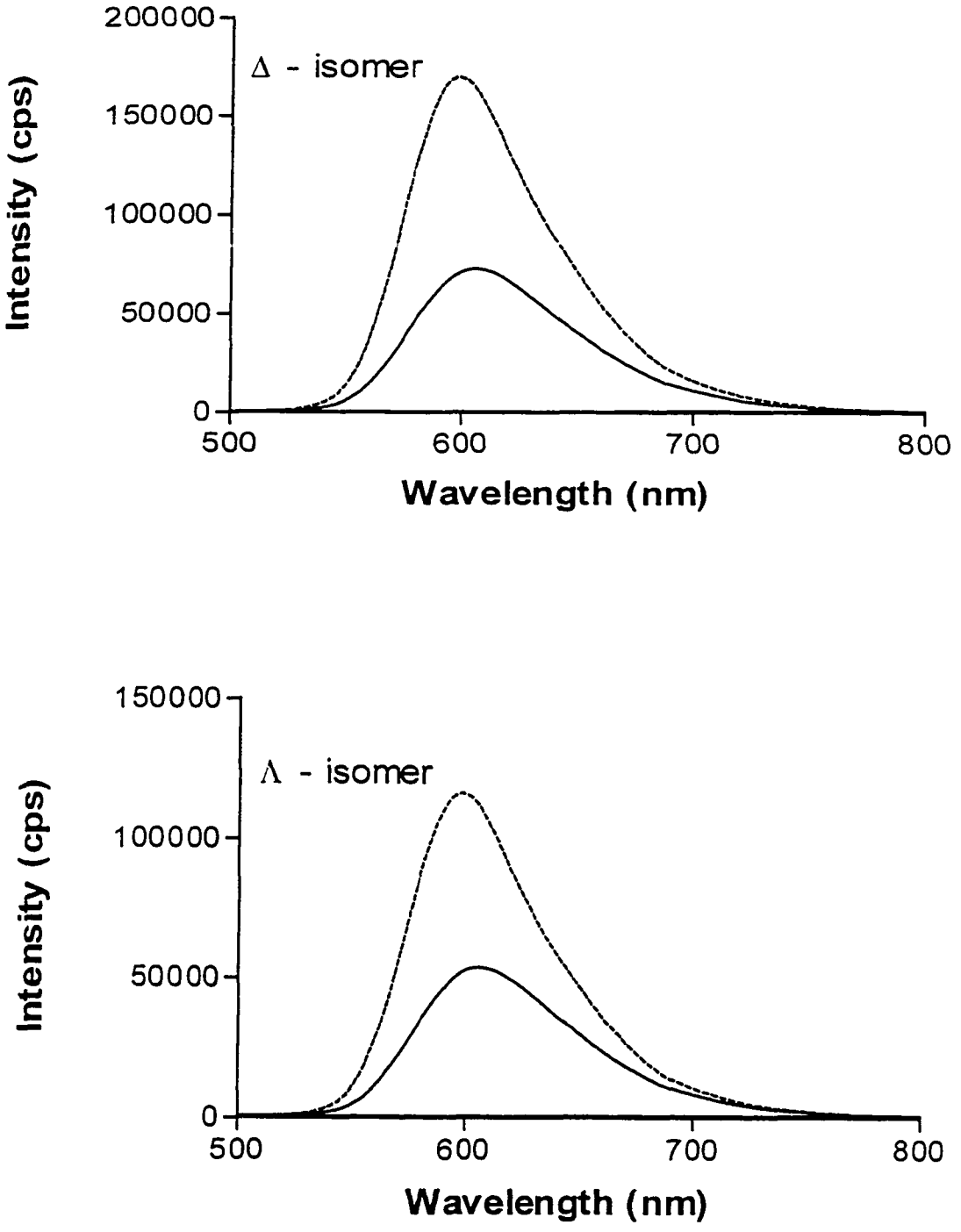

Fig.16. Emission Spectra of Δ-$[Ru(bpy)_2bzp]^{2+}$ ([P]/[Ru] = 78) and Λ-$[Ru(bpy)_2bzp]^{2+}$ ([P]/[Ru] = 73) in the presence of DNA (---) and the absence of DNA (___). All spectra were measured in 5mM Tris buffer, 50mM NaCl, and at pH 7.4.

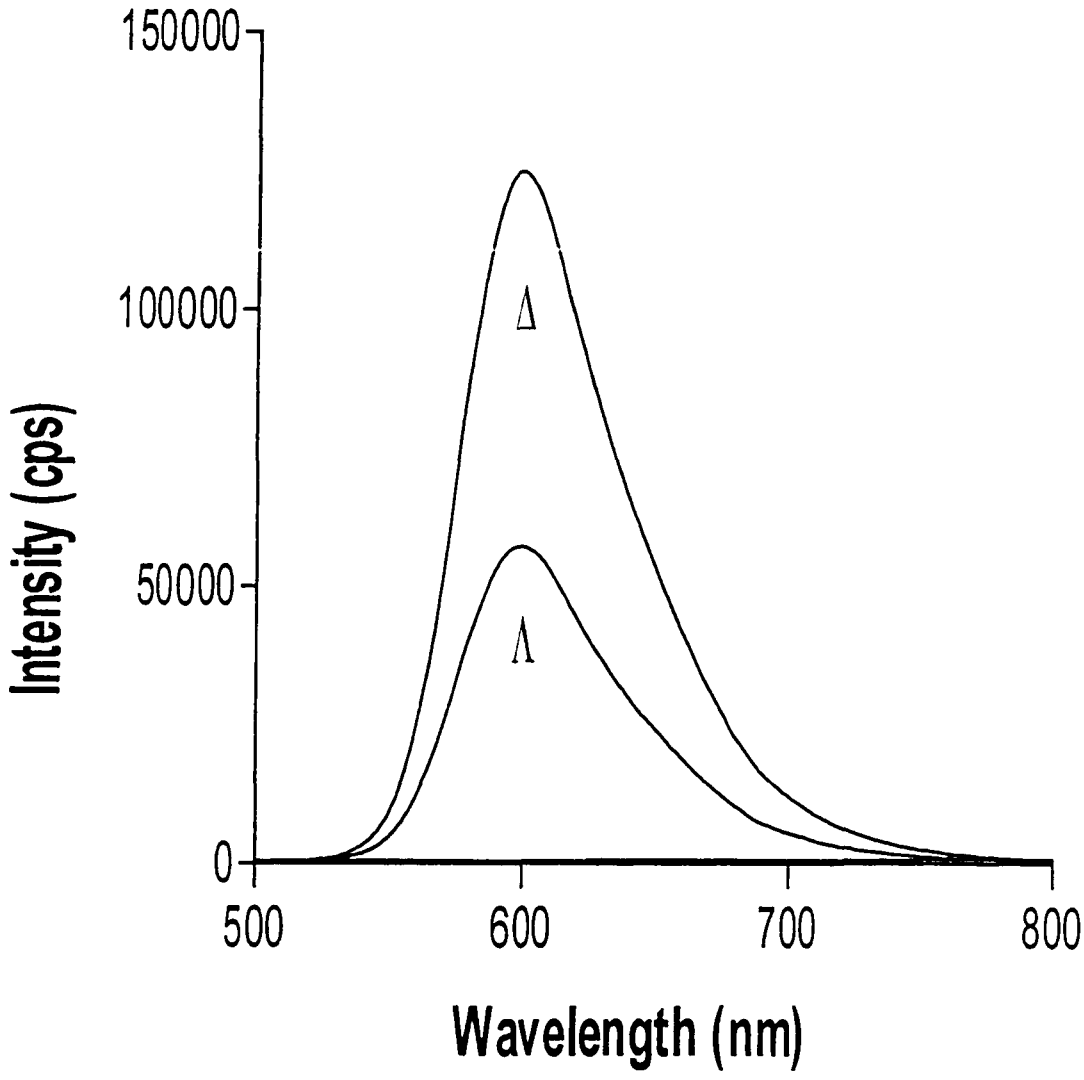

Fig.17. Emission Spectra of Δ-$Ru(bpy)_2bzp]^{2+}$ (Em. = 598nm) and Λ-$[Ru(bpy)_2bzp]^{2+}$ (Em. = 598) in the presence of DNA , [P]/[Ru] = 22. All spectra were measured in 5mM Tris buffer, 50mM NaCl, and at pH 7.4. [Ru] identical in both samples.

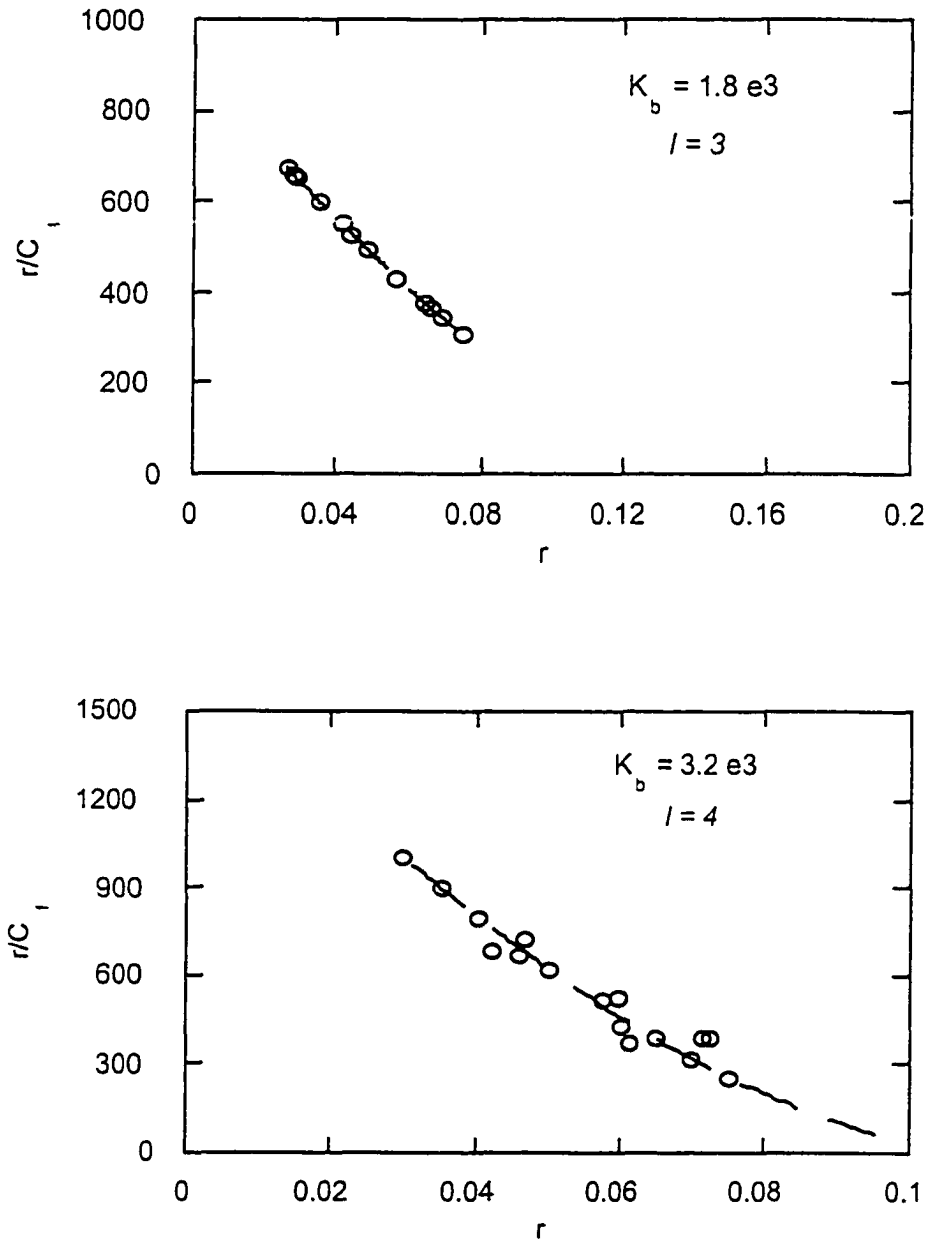

Fig.18. Scatchard analysis from equilibrium dialysis for Δ (top) and Λ (bottom) $[Ru(bpy)_2bppz]^{2+}$. Actual data (o), best fit to the McGhee and von Hippel equation (---). Site sizes and binding constants are indicated in the plot.

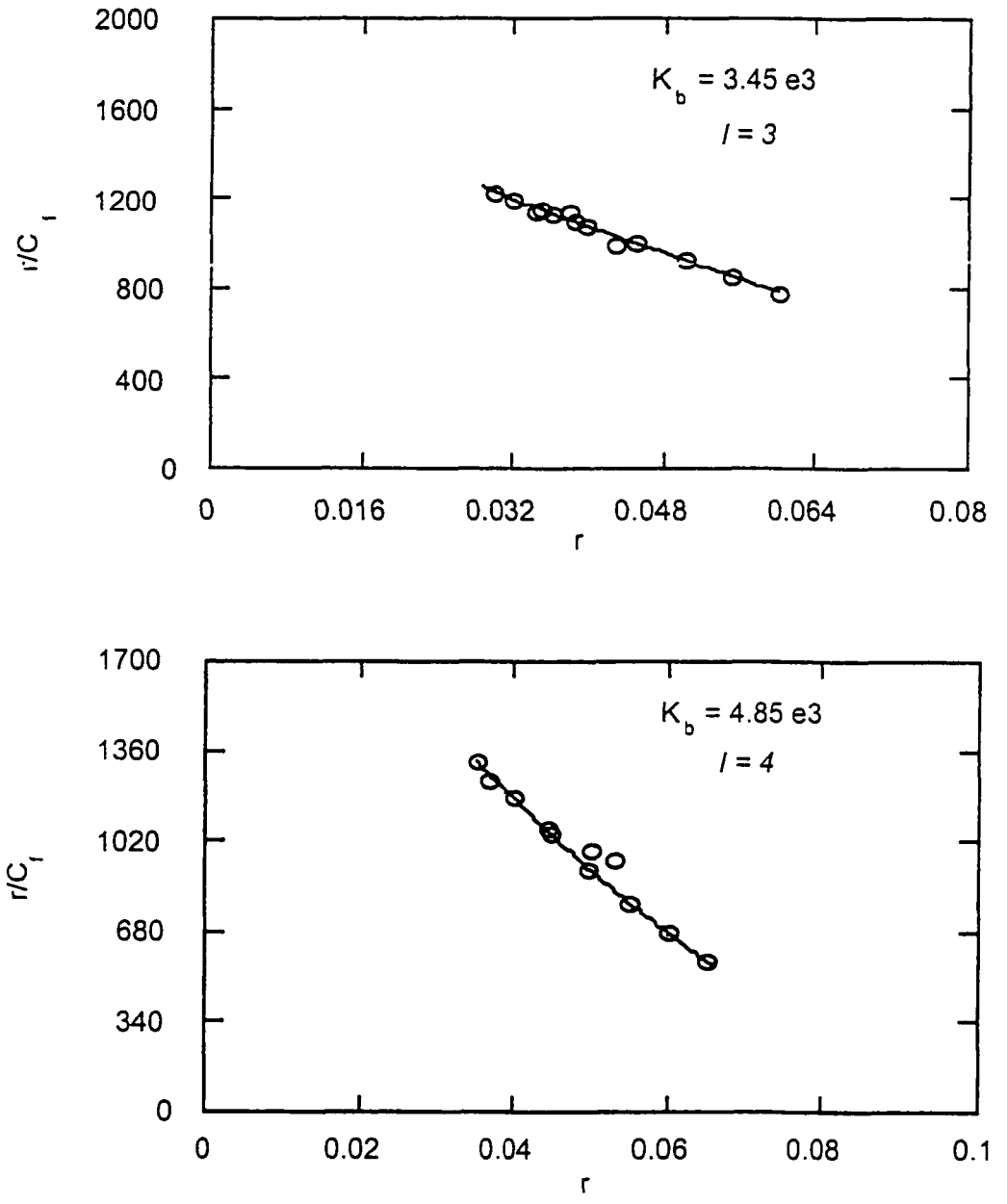

Fig. 19 Scatchard analysis from equilibrium dialysis for Δ (top) and Λ (bottom $[Ru(bpy)_2mbppz]^{2+}$. Actual data (o), best fit to the McGhee and von Hippel equation (---). Site sizes and binding constants are indicated in the plot.

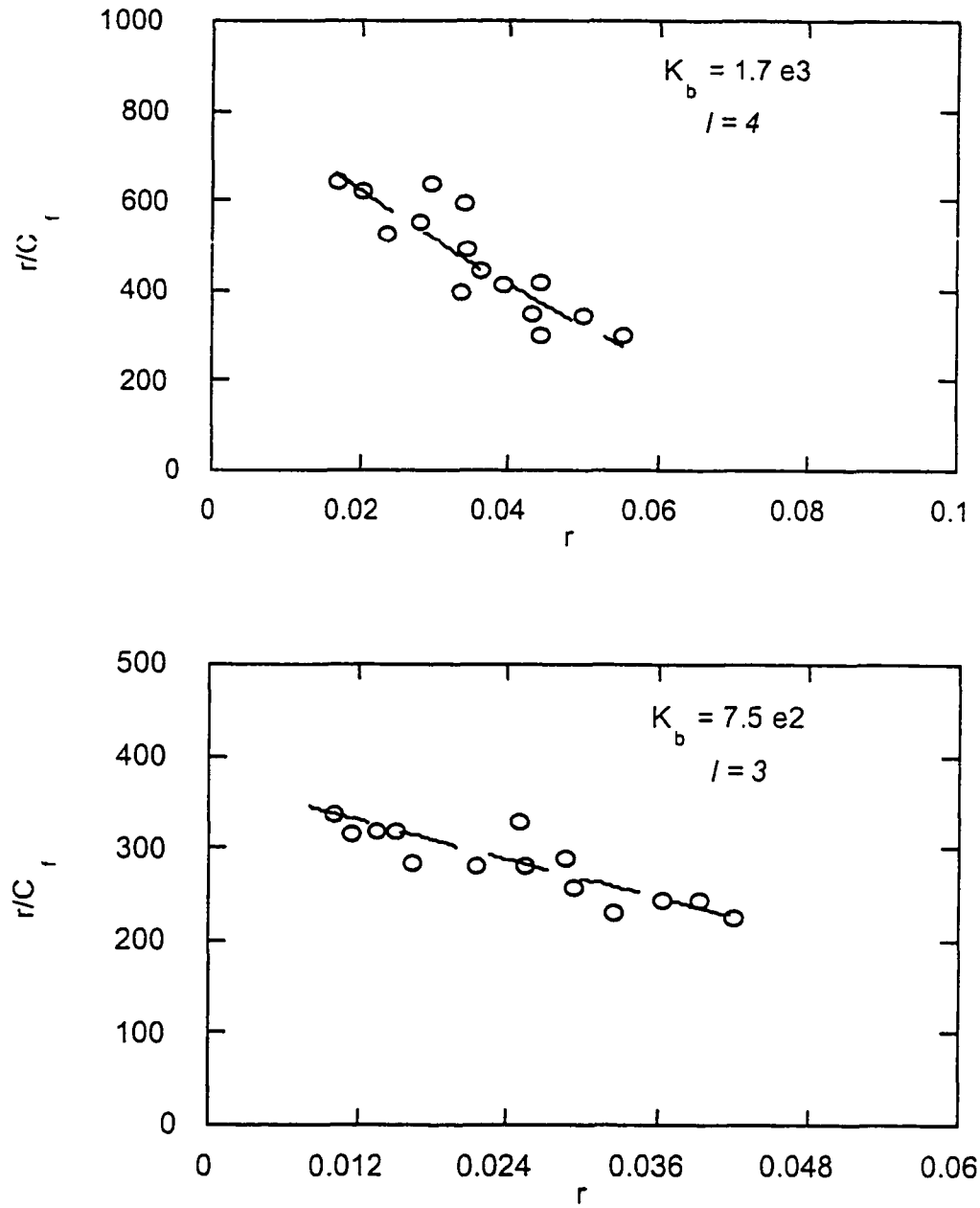

Fig.20 Scatchard analysis from equilibrium dialysis for Δ (top) and Λ (bottom) $[Ru(bpy)_2ippz]^{2-}$. Actual data (o), best fit to the McGhee and von Hippel equation (---). Site sizes and binding constants are indicated in the plots.

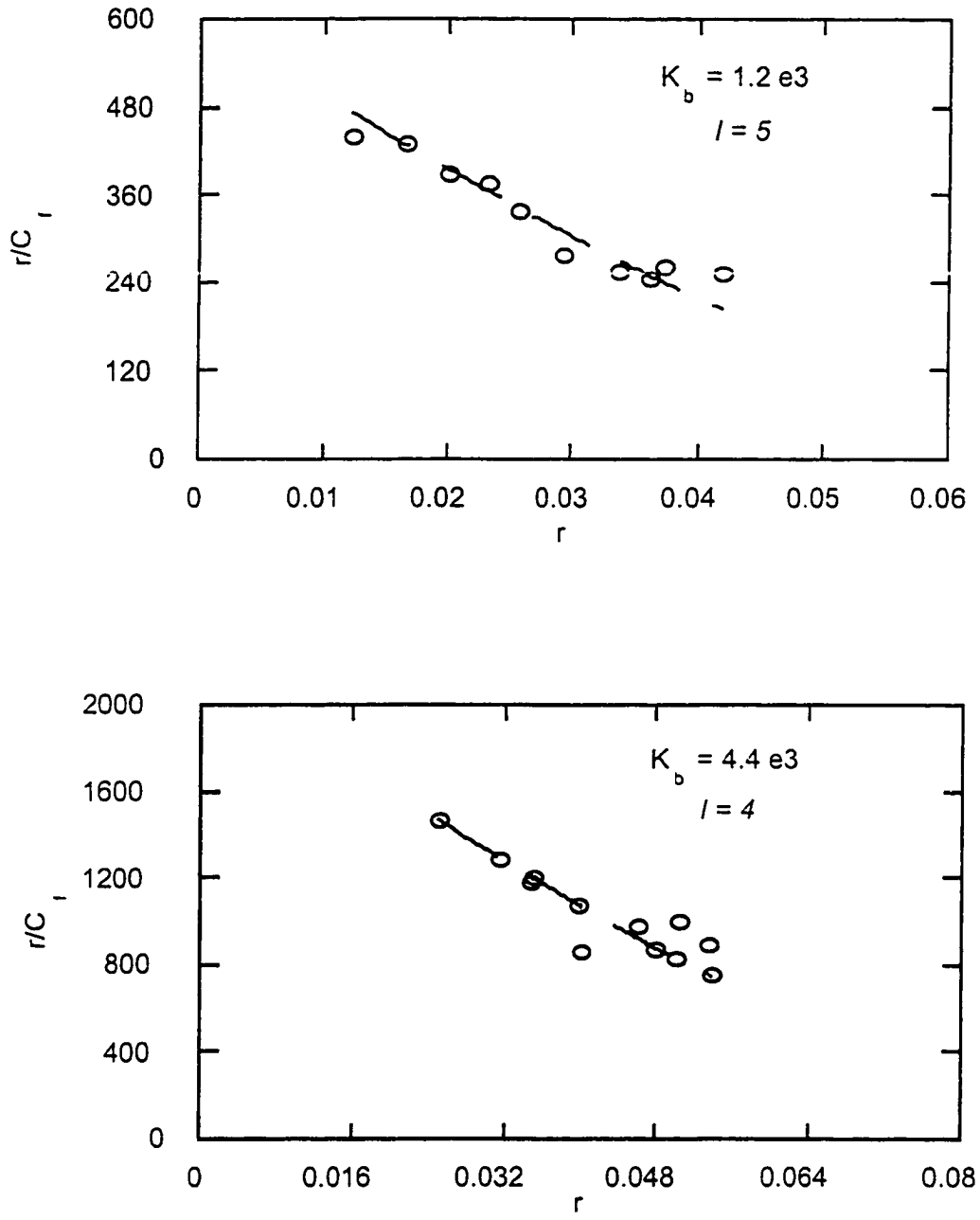

Fig. 21 Scatchard analysis from equilibrium dialysis for Δ (top) and Λ (bottom) $[Ru(bpy)_2bzp]^{2+}$. Actual data (o), best fit to the McGhee and von Hippel equation (---). Site sizes and binding constants are indicated in the plots.

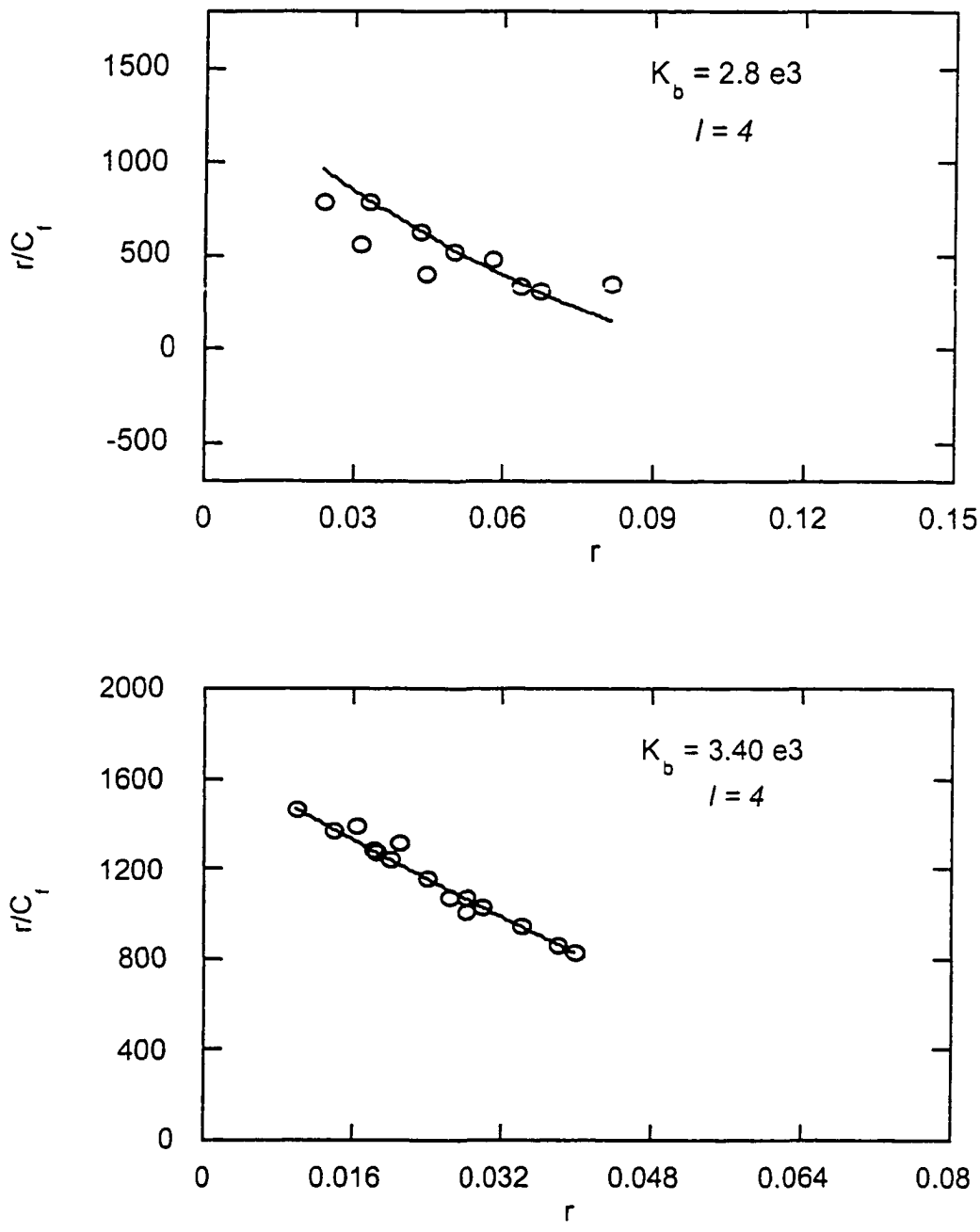

Fig.22 Scatchard analysis from equilibrium dialysis for $[Ru(bpy)_2(pyoxazo)]^{2+}$ (top) and $[Ru(bpy)_2(dmpyoxazo)]^{2+}$ (bottom). Actual data (o), best fit to the McGhee and von Hippel equation (---). Site sizes and binding constants are indicated in the plot.

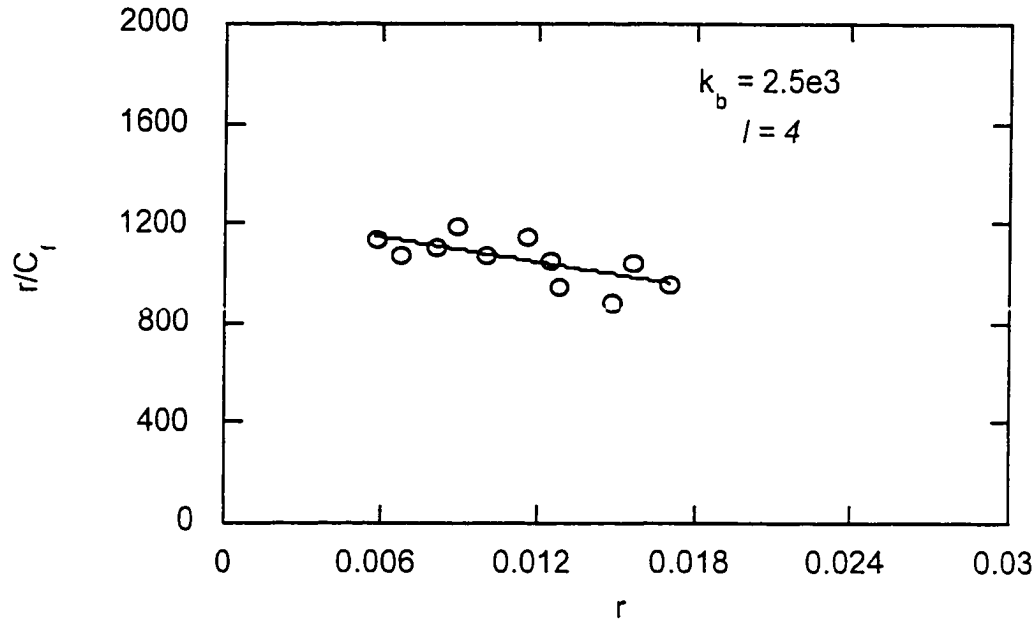

Fig 23. Scatchard analysis from equilibrium dialysis for [Ru(bpy)2(bisoxazo)]2+. Actual data (o), best fit to the McGhee and von Hippel equation (---). Site sizes and binding constants are indicated in the plot.

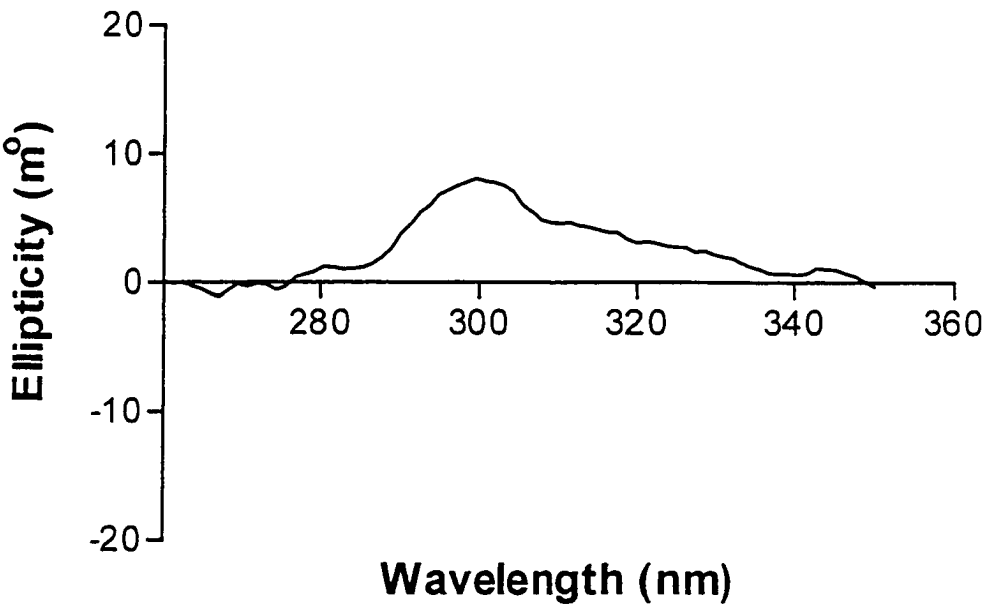

Fig. 24 Circular Dichroism Sectra for 48 hour dialyzates vs. calf thymus DNA for racemic $[Ru(by)_2bzp]^{2+}$.

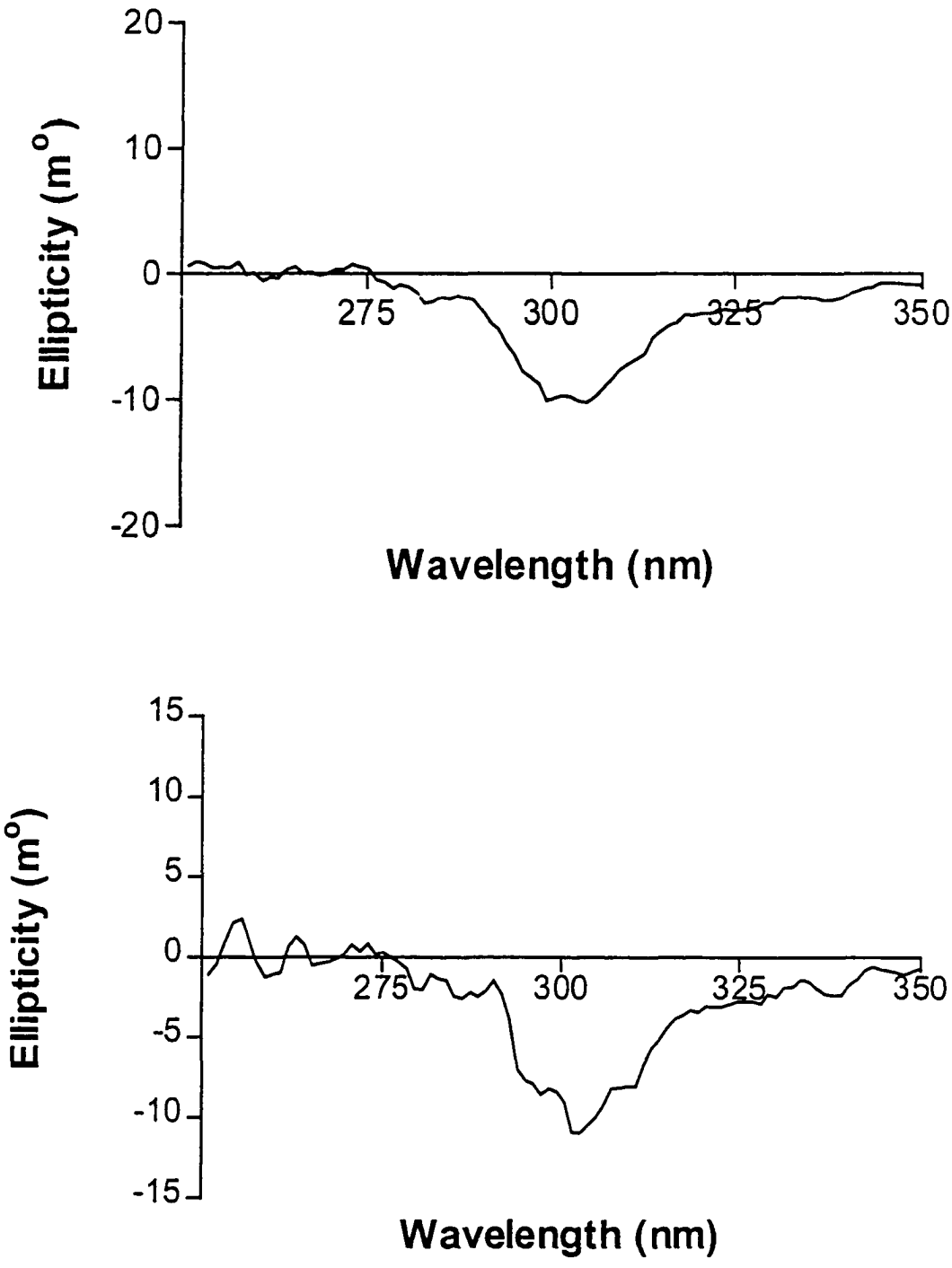

Fig. 25 Circular Dichroism Sectra for 48 hour dialyzates vs. calf thymus DNA for racemic $[Ru(by)_2bppz]^{2+}$ (top) and $[Ru(bpy)_2mbppz]^{2+}$ (below).

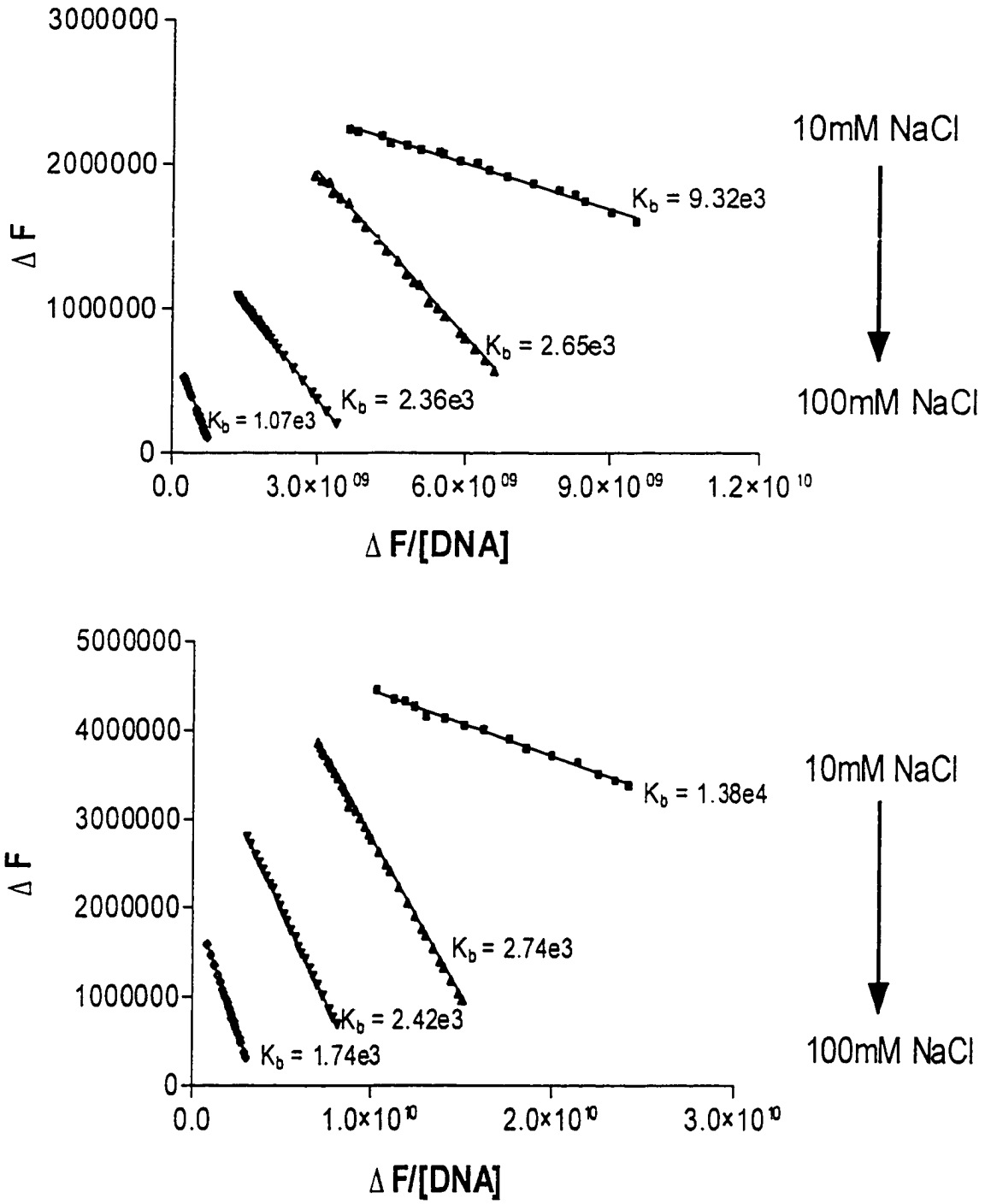

Fig.26 Eadie-Hofstee plots for the binding of Δ-$[Ru(bpy)_2bppz]^{2+}$ (top) and Λ-$[Ru(bpy)_2bppz]^{2+}$ (bottom) with calf thymus DNA.

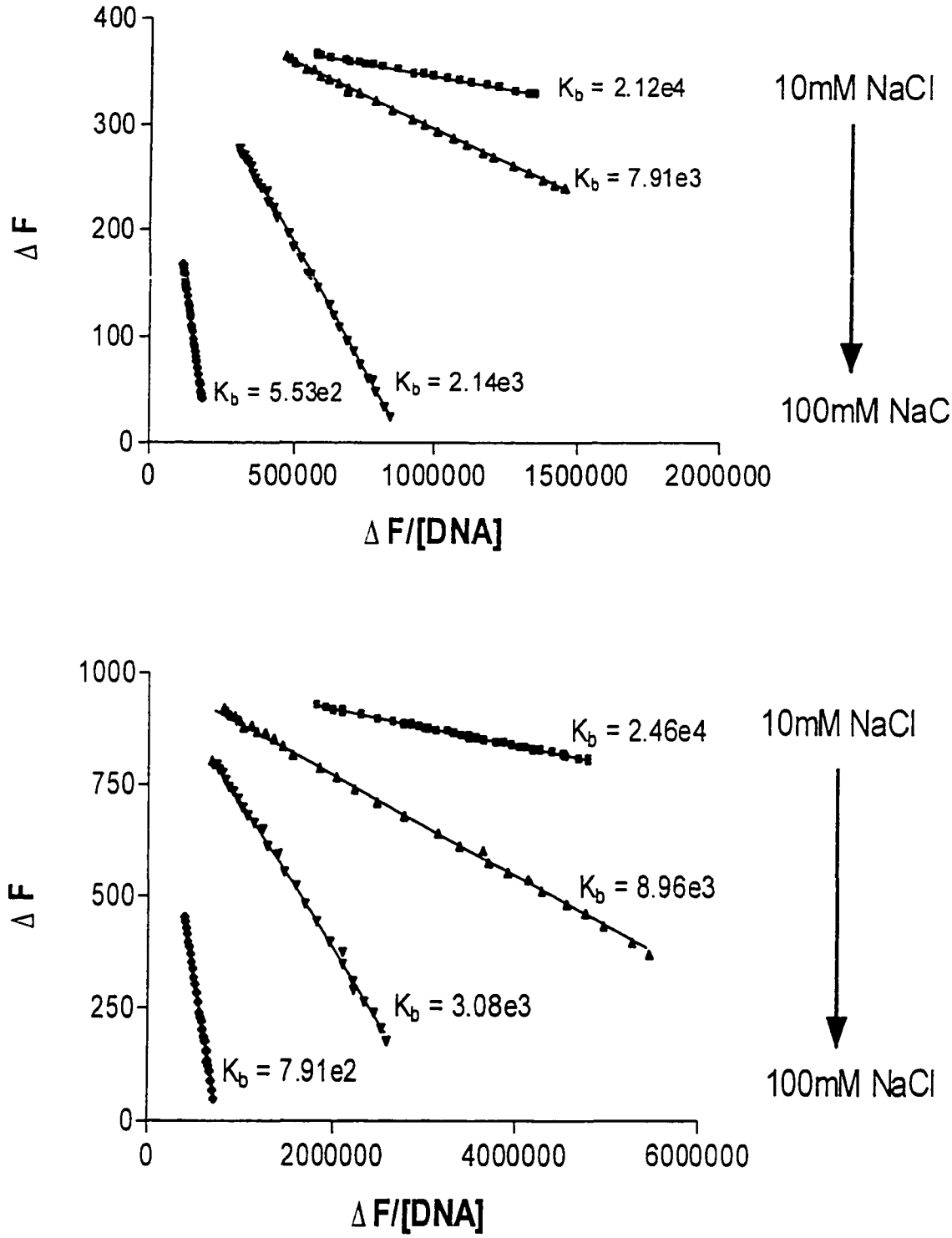

Fig.27 Eadie-Hofstee plots for the binding of Δ-$[Ru(bpy)_2mbppz]^{2+}$ (top) and Λ-$[Ru(bpy)_2mbppz]^{2+}$ (bottom) with calf thymus DNA.

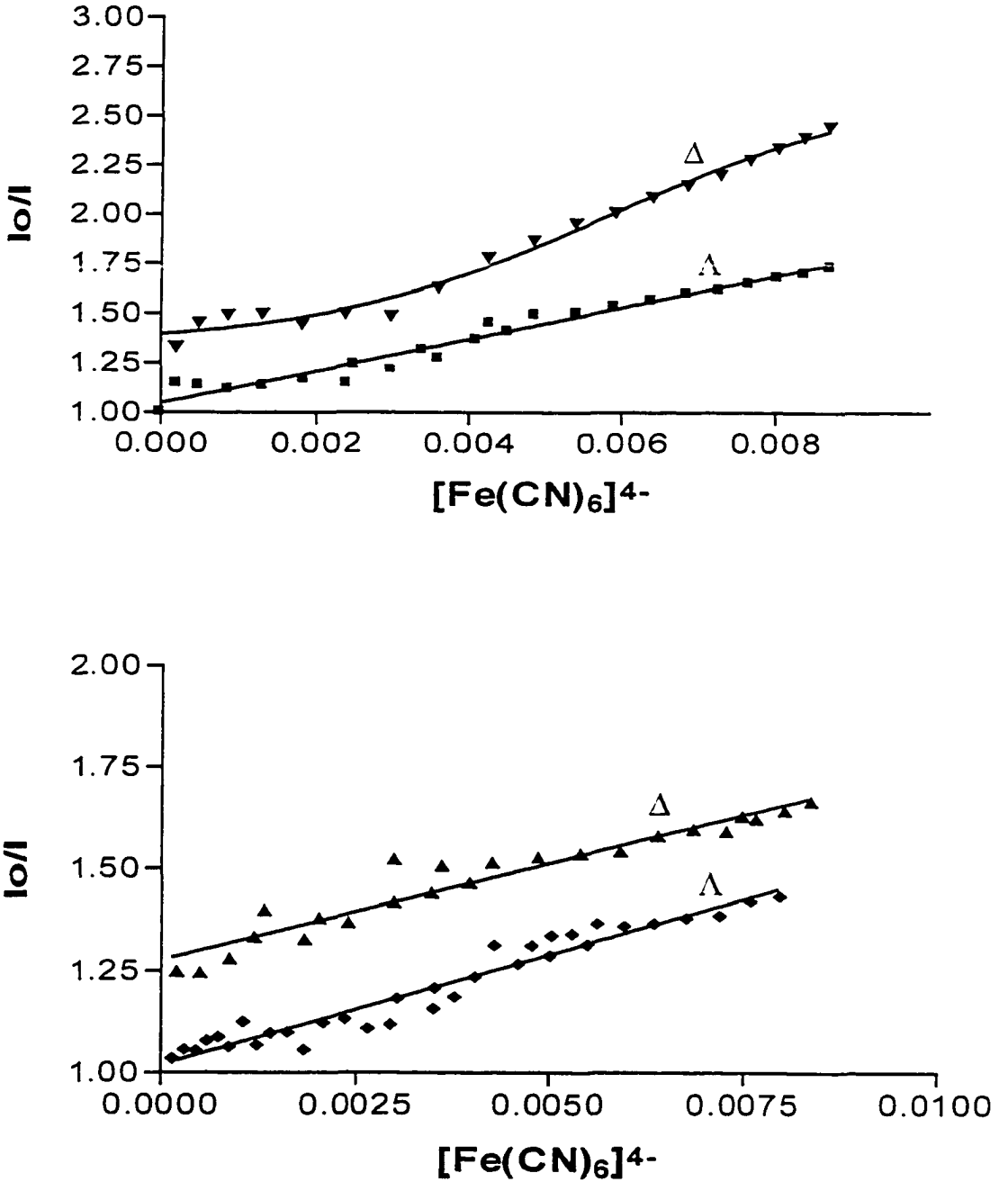

Fig.28 Quenching with $Fe(CN)_6^{4-}$ ion for Δ and Λ-$[Ru(bpy)_2ippz]^{2+}$ (top, [P]/Ru] = 54) and Δ and Λ-$[Ru(bpy)_2bzp]^{2+}$ (bottom, [P]/[Ru] = 52). All samples measured at 20°C in 5mM Tris buffer, 50mm NaCl, pH 7.4.

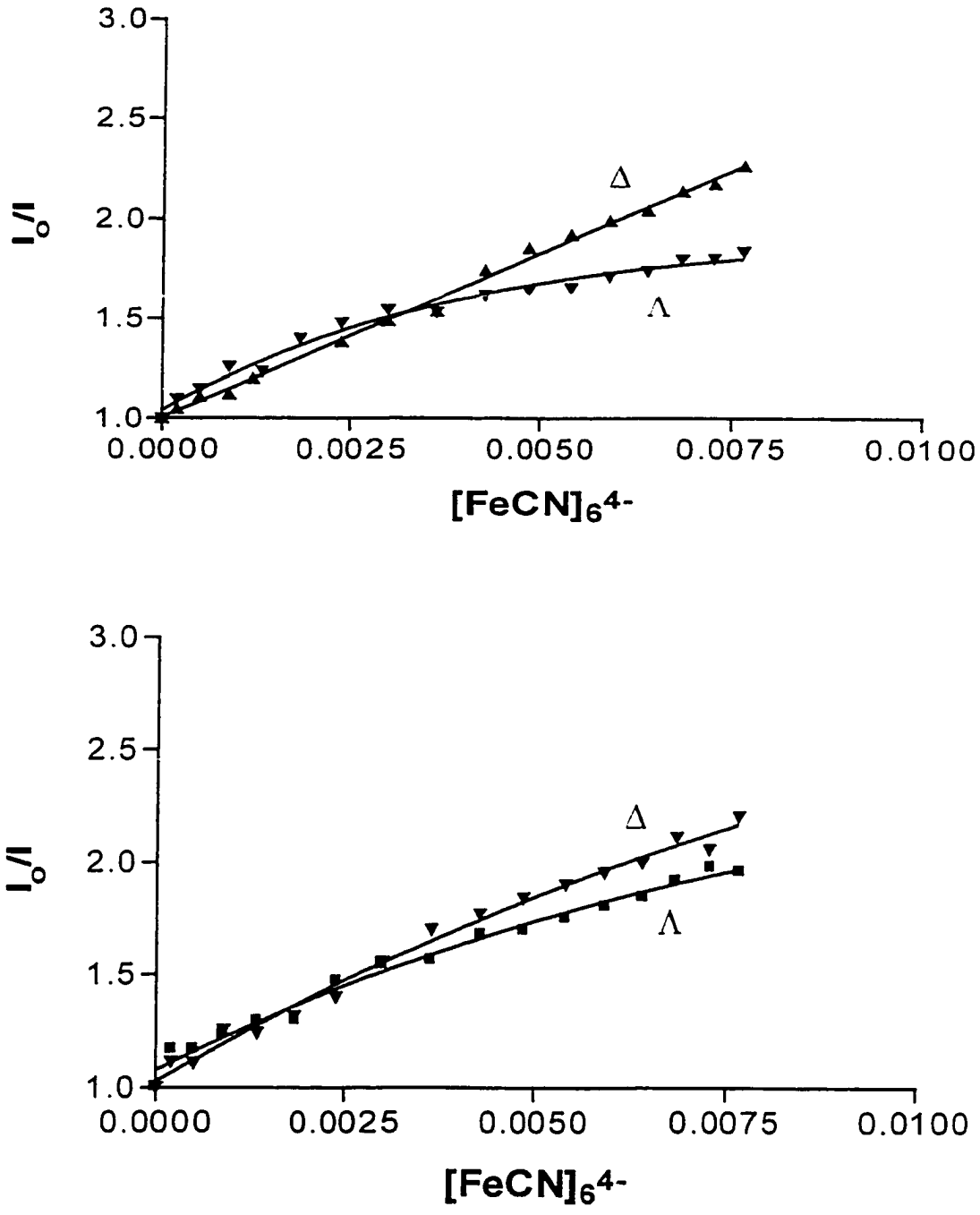

Fig.29 Quenching with $Fe(CN)_6^{4-}$ ion for Δ and Λ-$[Ru(bpy)_2bppz]^{2+}$ (top, [P]/Ru] = 55) and Δ and Λ-$[Ru(bpy)_2mbppz]^{2+}$ (bottom, [P]/[Ru] = 55). All samples measured at 20°C in 5mM Tris buffer, 50mm NaCl, pH 7.4.

Chapter VIII
Binding of RuL_3^{2+} Complexes with B-DNA

Introduction

The binding of $[Ru(L)_3]^{2+}$ (L= bzp, pyridyl-oxazoline (pyoxazo), dimethyl pyridyl-oxazoline (dmpyoxazo)) to B-DNA are considered in this chapter. These complexes have similar symmetry (C_3 axis) but the bzp ligand is planar and aromatic whereas pyoxazo and dmpyoxazo are neither planar nor aromatic. Comparing the binding of these complexes would provide useful information on the binding of tris non-planar probes and tris planar probes. Also, since bzp differs from phen (1,10-phenanthroline) in length by a benzene ring it is of interest to compare the binding results of $[Ru(bzp)_3]^{2+}$ and $[Ru(phen)_3]^{2+}$.

Results

Effects of Binding to DNA on Absorption

Visible absorption spectra of the complexes studied, in buffer alone, and in the presence of calf thymus DNA are presented in Figures 1 to 3. Upon binding to B-DNA $[Ru(pyoxazo)_3]^{2+}$ exhibited a 2% increase in absorbance at the MLCT band (in the 500-600nm range) whereas a 2.5% decrease in absorbance (hypochromic effect) at the MLCT band was observed for $[Ru(dmpyoxazo)_3]^{2+}$. For both complexes no spectra shift was observed. However, in the presence of DNA practically no hypochromicity was observed for $[Ru(bzp)_3]^{2+}$, but an increase in absorbance at the UV bands was observed. In addition a red spectral shift of 4nm at the MLCT band was observed. A summary of the binding data from absorbance experiments is listed in Table 1.

Effects of Binding to DNA on Emission

The complexes $[Ru(pyoxazo)_3]^{2+}$ and $[Ru(dmpyoxazo)_3]^{2+}$ do not luminescence in aqueous solution or in the presence of DNA. Therefore, we were unable to study their binding to DNA based on emission measurements. However, $[Ru(bzp)_3]^{2+}$ complex do luminescence in aqueous solution and in the presence of DNA. As DNA phosphate to ruthenium ratio increases the emission maximum is blue shifted (4nm) and an enhancement of the emission intensity is also observed (I/I_o = 2.2). The emission spectrum of $[Ru(bzp)_3]^{2+}$in the presence of DNA and in buffer alone is represented in Figure 4.

Equilibrium Dialysis

The binding constant, K_b, and the average site size in base pairs, *l*, for $[Ru(bzp)_3]^{2+}$, $[Ru(pyoxazo)_3]^{2+}$ and $[Ru(dmpyoxazo)_3]^{2+}$ were determined by fitting the data collected from equilibrium dialysis experiments to the McGhee and von Hippel equation ($r/C_f = [(K_b/2)(1-2lr)/(1-2(l-1)r]^{l-1}$) (see Table 2). The binding constant for $[Ru(pyoxazo)_3]^{2+}$ and $[Ru(dmpyoxazo)_3]^{2+}$ were of the order 10^3 whereas that of $[Ru(bzp)_3]^{2+}$ was of the order 10^4. The site size for the complexes containing pyoxazo and dmpyoxazo was of the order l=4 whereas the site size for the complex containing bzp was of the order l=2. Figures 5-7 represents the binding isotherms fitted to the McGhee and von Hippel equation.

Enantioselectivity

Enantioselectivity refers to the preferential DNA binding of one enantiomer. This is determined by dialyzing the racemic complex against DNA and measuring the circular dichroism (CD) of the dialysate. If a CD signal is found, the binding of one enantiomer is stronger than the other, and enantioselectivity is the cause. The weaker binding enantiomer is enriched outside the dialysis bag, since the stronger binding enantiomer binds well to DNA, and decreases the concentration of the stronger binder outside the bag. For the tris complexes studied this effect was not observed thus indicating that there was no preference in binding.

Fluorescence Titration

Fluorescence titrations were used to determine the binding constant, K_b, at varying salt concentration (10, 25, 50, and 100mM). The binding constant obtained by this method for $[Ru(bzp)_3]^{2+}$ from 10 to 100mM NaCl were 1.19×10^5, 9.48×10^4, 8.49×10^4, and 7.24×10^4 respectively. Eadie-Hofstee plots representing the binding of $[Ru(bzp)_3]^{2+}$ studied by fluorescence titration are represented in Figure 8. Since K_b values are determined as -1/slope, in each case as the salt concentration increased from 10 to 100mM there was a progressive increase in the slope indicating a decrease in the binding constant, thus illustrating the dependence of the value K_b on salt concentration. Since the Ru(II) complexes containing pyoxazo and dmpyoxazo do not luminescence in aqueous solution we were unable to determine their respective binding constants by this method.

Steady State Luminescence Quenching by $Fe(CN)_6^{4-}$

Figure 9 represents the Stern-Volmer plot, Io/I vs $[Fe(CN)_6]^{4-}$, of luminescence quenching of $[Ru(bzp)_3]^{2+}$ with increasing concentrations of ferrocyanide ion. The plot obtained exhibited a downward curvature, which is interpreted as reflecting differing degrees of protection or relative accessibility of bound Ru cations. Therefore, the $[Ru(bzp)_3]^{2+}$ complex is protected from the anionic quencher. Here again we were unable to carry out quenching experiment on the complexes containing pyoxazo and dmpyoxazo since they do not emit in aqueous solution.

Discussion

Upon binding to DNA, intercalation tends to decrease the intensity of the absorption bands (hpyochromic effect) of the molecular probe, which is sometimes accompanied by a shift in energy of the absorption bands to lower energy (bathchromic shift). For the complex $[Ru(bzp)_3]^{2+}$ there was practically no decrease in absorbance (hypochromicity) but an increase in absorbance at the UV bands was observed. A 4nm spectral shift to the red at the MLCT band was also observed. In comparison, $[Ru(phen)_3]^{2+}$ also exhibited a 4nm spectral shift to the red but its hypochromic effect was approximately 12%. Since $[Ru(phen)_3]^{2+}$ is believed to bind by intercalation as indicated by Barton et al we can infer from the absorption data that $[Ru(bzp)_3]^{2+}$ may be electrostatically or surface bound to DNA. For the Ru(II) complexes containing pyoxazo and dmpyoxazo no spectral shift was observed. However, a decrease in absorbance (2.5%) was observed for $[Ru(dmpyoxazo)_3]^{2+}$ and an increase in absorbance (2%) for $[Ru(pyoxazo)_3]^{2+}$. Since very little hypochromicity and no spectral shift was observed we

can infer that the Ru(II) complexes containing pyoxazo, and dmpyoxazo do not bind to DNA by intercalation but its binding is probably through electrostatic interactions.

On binding to B-DNA a shift in emission maximum of 2nm to longer wavelength (red) was observed for $[Ru(phen)_3]^{2+}$ accompanied by a large emission enhancement. In accordance with the intercalative mode of binding an enhancement in emission maximum and shift to lower energy (blue) is normally observed. This was observed for $[Ru(bzp)_3]^{2+}$, thus indicating that the bzp ligand may be surface bound or intercalatively bound to B-DNA.

The binding constants determined by equilibrium dialysis and fluorescence titrations indicate how strongly Ru(II) complexes bind to DNA. In the case of equilibrium dialysis the binding constant observed for $[Ru(bzp)_3]^{2+}$ was 1.8×10^4 whereas that of $[Ru(phen)_3]^{2+}$ was of the order 6.2×10^3. Although the binding constants obtained for $[Ru(pyoxazo)_3]^{2+}$ and $[Ru(dmpyoxazo)_3]^{2+}$ were 3.77×10^3 and 3.40×10^3 respectively, their values were numerically smaller then that of $[Ru(phen)_3]^{2+}$. For planar aromatic intercalators, site sizes are typically $l = 2$ (4 base pairs) but larger site sizes are normally found with Ru(II) complexes. However for the Ru(II) complexes containing bzp and dmpyoxazo the site size was of the order l = 2, whereas those of $[Ru(phen)_3]^{2+}$ and $[Ru(pyoxazo)_3]^{2+}$ was of the order $l = 3 - 4$. It is thought that electrosatatic binding would be expected to have a smaller relative site size, *l*, due to the increased availability of sites compared to the intercalative binding mode (major groove). Although, the site size of $[Ru(bzp)_3]^{2+}$ is of the order $l = 2$, binding is believed to be by intercalation since the data gathered from emission and the relatively large binding constant obtained by equilibrium dialysis are all consistent with the intercalative mode of binding. Also, results from

anionic quenching experiments of $[Ru(bzp)_3]^{2+}$ exhibit a Stern-Volmer plot with a downward curvature. These results further indicate that the bound complex is somewhat protected and therefore binding may be through an intercalative fashion. However, due to the non-luminescent property of the Ru(II) complexes containing pyoxazo and dmpyoxazo anionic quenching experiments were not possible.

Conclusion

Intercalative binding via the major groove has been the proposed mode of binding of $[Ru(phen)_3]^{2+}$ by Barton et al. This proposed mode of binding has been challenged by other groups [190-192] who believe that intercalation is via the minor groove. Based on the spectroscopic data gathered for $[Ru(bzp)_3]^{2+}$ we can conclude the biding to B-DNA is probably by intercalation which may be via the minor groove. As seen with $[Ru(bpy)_3]^{2+}$ no spectral shift and practically no hypochromicity was observed for $[Ru(pyoxazo)_3]^{2+}$ and $[Ru(dmpyoxazo)_3]^{2+}$. This has been attributed to the length of the ligand, which is not sufficiently extended from the metal to perturb the system. Therefore, like $[Ru(bpy)_3]^{2+}$ electrostatic binding is most likely the preferred mode of binding for the Ru(II) complexes containing pyoxazo and dmpyoxazo.

Table 1. Absorption Data

Complex	without DNA λmax, nm	with DNA λmax, nm	Δλ, nm	Hypochromicity, %
Bzp	454	458	+4	1
Pyoxazo	466	466	0	0
Dmpyoxazo	456	456	0	~2

Table 2. Equilibrium Dialysis

Complex	K_b, binding constant	*l* = site size in base pairs
Bzp	1.8×10^4	2
Pyoxazo	3.77×10^3	3
Dmpyoxazo	3.42×10^3	2

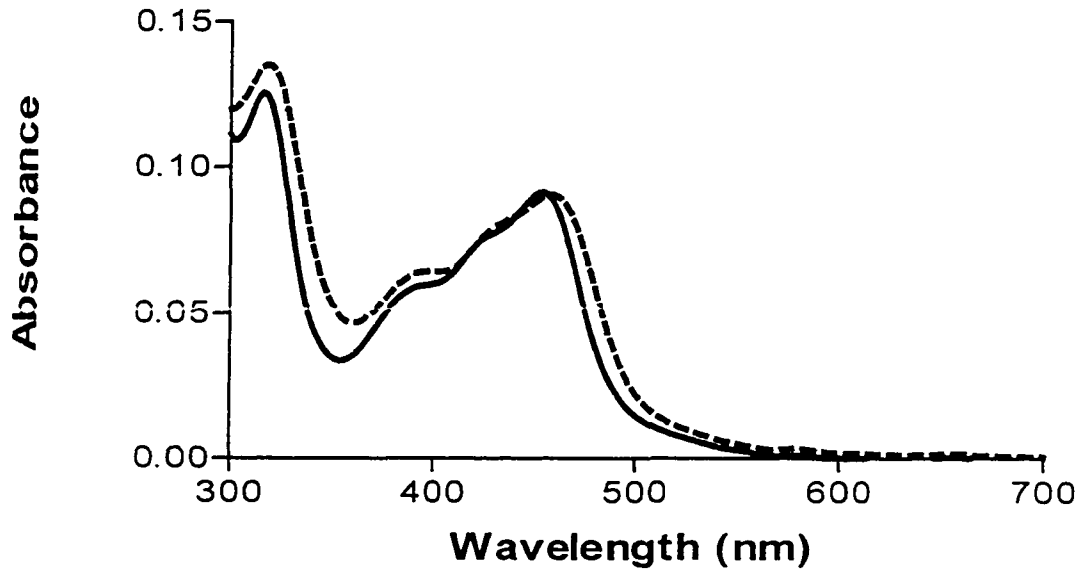

Fig.1 Absorbance Spectra of $[Ru(bzp)_3]^{2+}$ ([P]/[Ru] = 47) in the presence of DNA (----) and absence of DNA (___). All spectra were measured in 5mM Tris buffer, 50mM NaCl, pH 7.4.

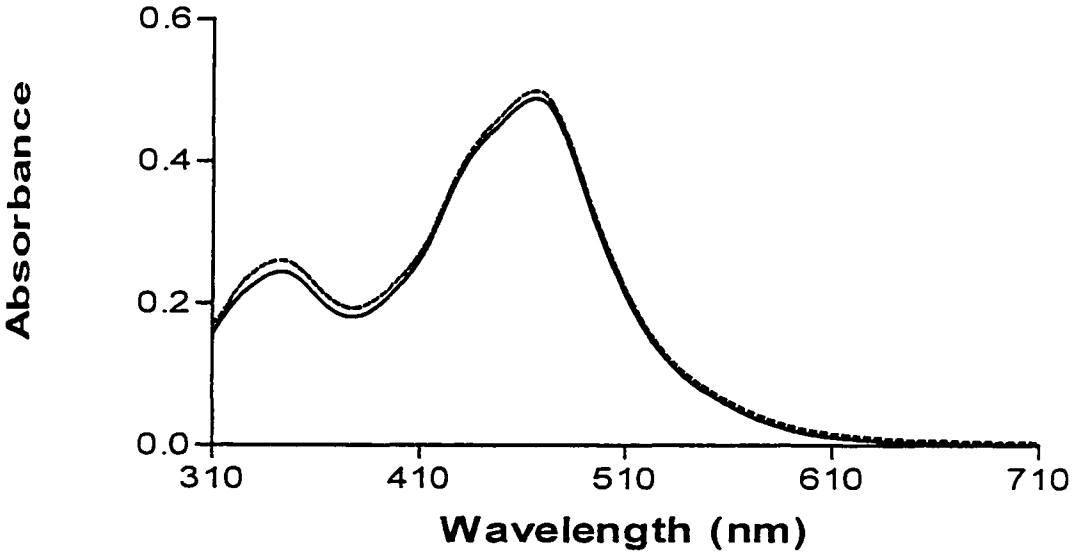

Fig.2 Absorbance Spectra of $[Ru(pyoxazo)_3]^{2+}$ ([P]/[Ru] = 55) in the presence of DNA (----) and absence of DNA (___). All spectra were measured in 5mM Tris buffer, 50mM NaCl, pH 7.4.

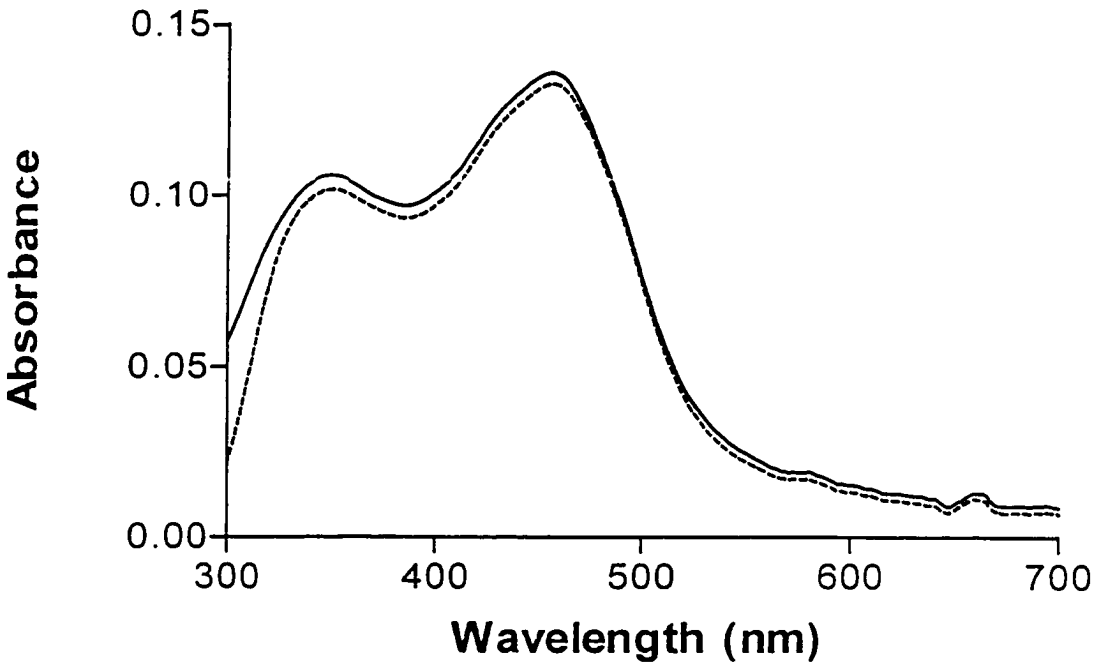

Fig.3 Absorbance Spectra of $[Ru(dmpyoxazo)_3]^{2+}$ ([P]/[Ru] = 55) in the presence of DNA (----) and absence of DNA (___). All spectra were measured in 5mM Tris buffer, 50mM NaCl, pH 7.4.

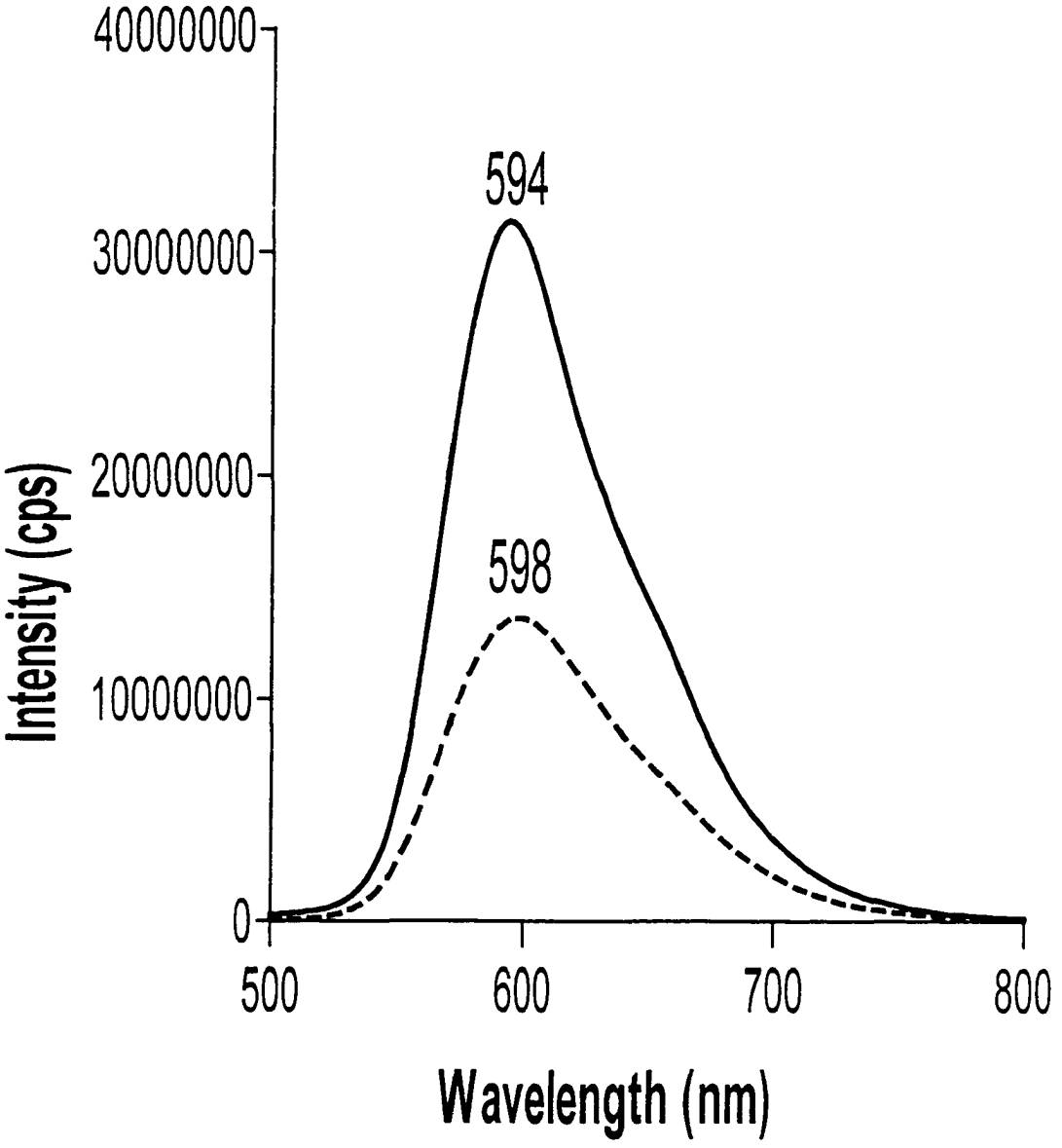

Fig.4. Emission Spectra of $[Ru(bzp)_3]^{2+}$ with DNA (___) and in buffer (---).

Excitation vavelength = 450nm; Emission in buffer only = 598nm; Emission in the presence of DNA ([P]/[Ru] = 35) = 594nm; I/I_o = 2.2. All spectra were measured in 5mM Tris buffer, 50mM NaCl, and pH 7.4.

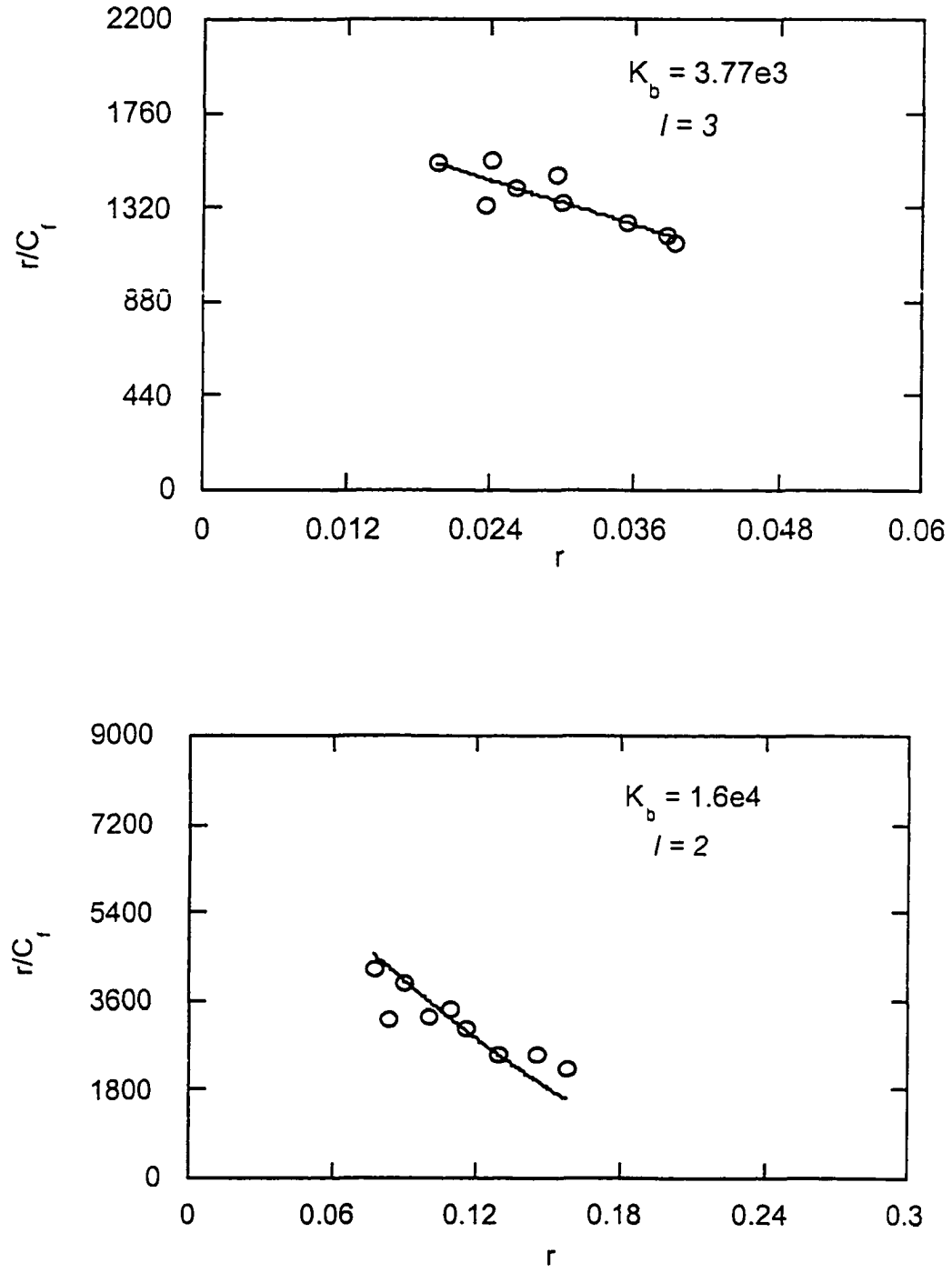

Fig. 5 Scatchard analysis from equilibrium dialysis for $[Ru(bzp)_3]^{2+}$ (top) and $[Ru(pyoxazo)_3]^{2+}$ (bottom). Actual data (o), best fit to the McGhee and von Hippel equation (----). Site sizes and binding constants are indicated in the plot.

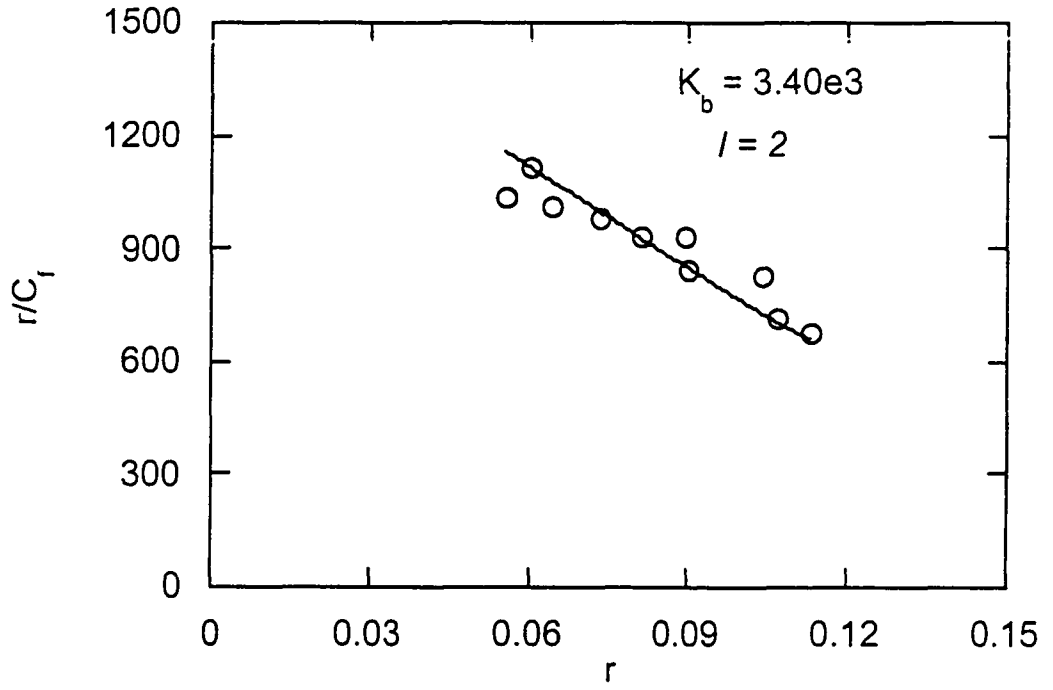

Fig. 6 Scatchard analysis from equilibrium dialysis for $[Ru(dmpyoxazo)_3]^{2+}$. Actual data (o), best fit to the McGhee and von Hippel equation (----). Site sizes and binding constants are indicated in the plot.

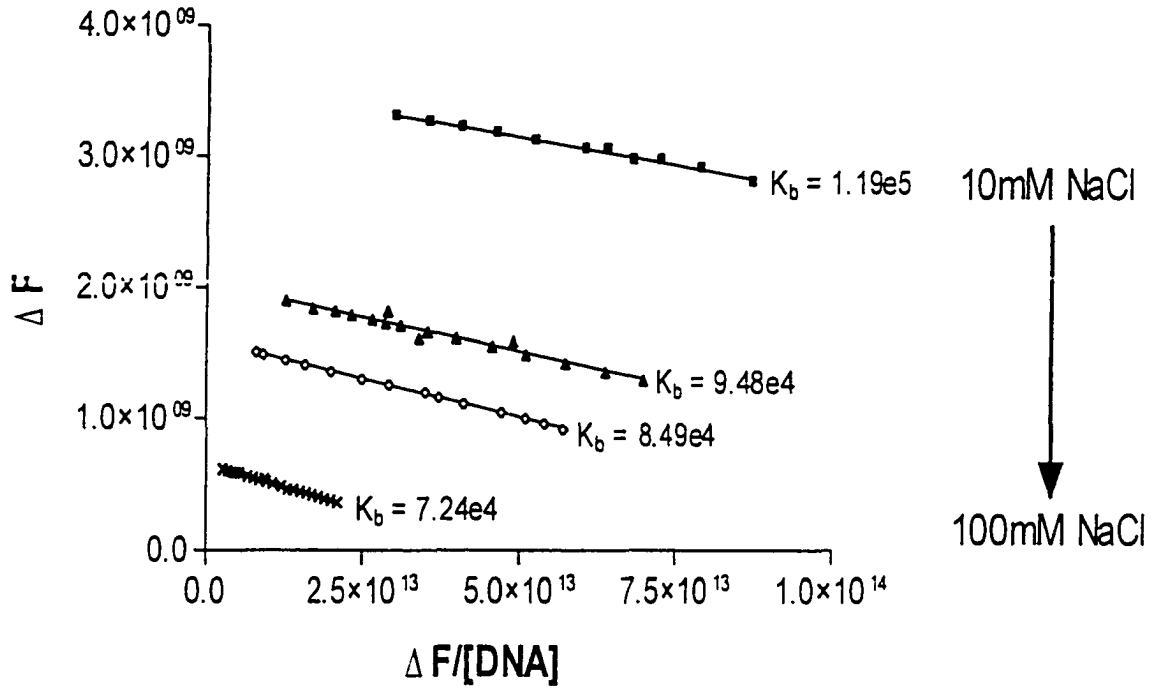

Fig.7 Eadie-Hofstee plots for the binding of $[Ru(bzp)_3]^{2+}$ with calf thumus DNA.

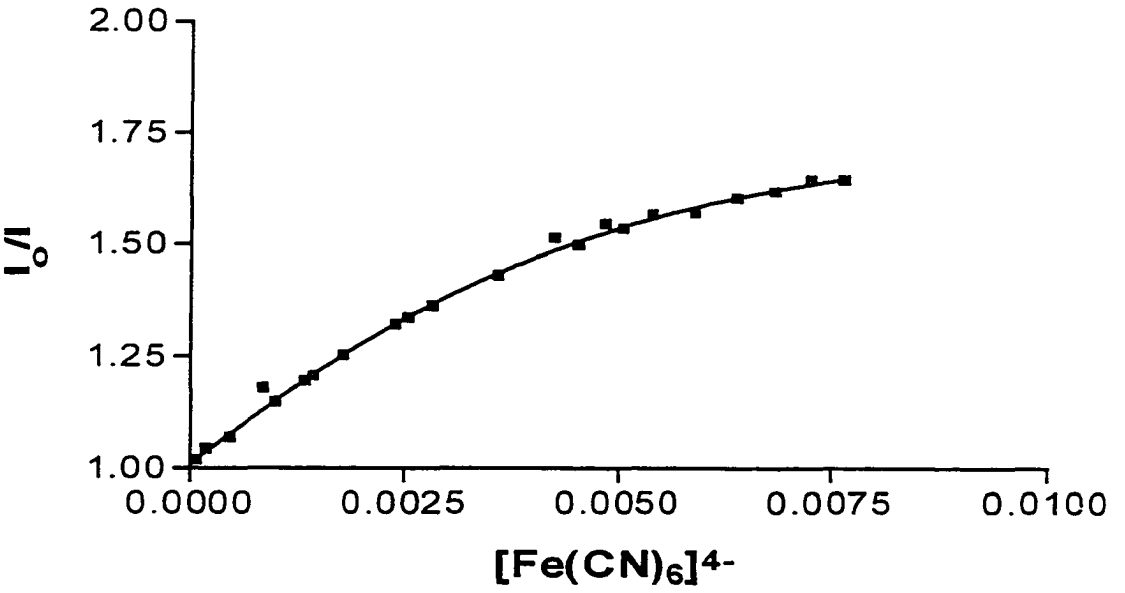

Fig.8 Quenching with $Fe(CN)_6^{4-}$ ion of $[Ru(bzp)_3]^{2+}$ at [DNA-phosphate]/[Ru] =52. All samples measured at 20°C in 5mM Tris buffer, 50mM NaCl, and pH 7.4.

Chapter IX
Experimental

Materials and Methods

$Ru(bpy)_2Cl_2$ was either purchased as the hexahydrate from Aldrich, or prepared by following existing literature procedures.[174] Acetonitrile was Baker HPLC grade. Calf Thymus DNA was purchased from Sigma Chemical. All solutions used for the DNA experiments consisted of a 'Tris" buffer (5mM tris acetate, 50mM NaCl, pH 7.4). All other chemicals used were purchased from Aldrich.

Acidity Measurements

A stock solution of the complex to be studied, either $[Ru(bpy)_2\ bppz]^{2-}\ (PF_6)_2$, or $[Ru(bpy)_2\ mbppz]^{2-}\ (PF_6)_2$ was adjusted to absorbance 0.8 to 1.5 for absorption measurements, and to 0.6 for emission experiments. The solution was made slightly acidic to solubilize them. Standard solutions of sulfuric acid and sodium hydroxide were prepared for the use as titrants.

A Corning 135 pH meter was used for pH measurements in both cases, the meter was first calibrated with standard buffer solutions obtained from Fischer. The pH meter was calibrated using the two-point method. The stock solution of the complex was adjusted to a convenient initial pH. Small aliquots of standard acid or base were added in portions to the stock solution so as to adjust the pH, and its spectrum was recorded. After several measurements, the solution was returned to its original pH, whereupon spectra identical to that of the original solution were obtained. This was the case whether the original solution was first made basic with sodium hydroxide solution or acidic with

sulfuric acid. After each series of measurements, the pH meter was rechecked with known buffers to ensure that no significant drift had occurred.

Absorption and Luminescence Measurements

All UV/Vis spectra were recorded on a Perkin Elmer 320 spectrophotometer. Emission spectra were recorded on a Fluorolog Jobin Yvon-Spex spectrophotometer.

Column Chromatography

Samples of all the ruthenium complexes described here can be purified by column chromatography on alumina (neutral, Brockman Activity I, obtained from Baker). The general procedure is to place a plug of glass wool in the column, make a slurry of alumina in acetonitrile, and pour the slurry into the column. Th column is packed by allowing the acetonitrile to pass through; thus allowing the alumina to settle. Two centimeters of sand is then added to the top of the column. The complex to be purified is dissolved in acetonitrile, in the case of the hexafluorophosphate or tetrafluoroborate salt, or acetonitrile/methanol in the case of the chloride. The sample is then added to the column and allowed to enter the stationary phase, by adding small quantities of acetonitrile. The column is then developed with acetonitrile. If the material does not move down the column with acetonitrile, an acetonitrile/methanol (90/10) mixture is used. To increase movement of the bands down the column the amount of methanol is increased. The column can be cleaned by passing a volume of methanol through it, and prepared for another sample, with a volume of acetonitrile.

Equilibrium Dialysis

The binding constant to DNA was determined by adding 1.0mL (1mg/mL) DNA solution dissolved in buffer (5mM Tris, pH 7.4) to a dialysis bag of MWCO 12000-14000 and sealing it. Dialysis vs 2.0mL of the Ru (II) complex for 48-72 hours were carried out and the concentration of Ru (II) complex inside and outside the bag was determined by absorption spectroscopy. Enantioselectivity was determined by dialysis of the racemic mixture against DNA for 48 to 72 hours, and measuring the circular dichroism (CD) of the dialysate.

Circular Dichroism

Circular dichroism spectra were collected on a Jasco Model 500-C spectropolarimeter, and also on an Olis Cary-16 spectropolarimeter. CD was primarily used to determine the purity of enantiomers and detection of enantioselectivity in binding to DNA.

Fluorescence Titration

This technique was used to determine the binding constant of Ru (II) complexes to DNA at varying salt concentration (10mM, 25mM, 50mM, and 100mM). Fluorescence titrations are run by adding aliquots of a solution containing Ru complex, DNA, and NaCl in buffer (solution 1) to a solution containing only the Ru complex plus NaCl in buffer (solution 2) whose fluorescence spectrum has already been run. All stock solutions were prepared in buffer (5mM Tris buffer, pH 7.4).

Steady State Luminescence Quenching by $FeCN_6^{4-}$

Quenching experiments were done by adding aliquots (5-20μL) of a solution containing Ru complex, DNA (1.5mg/mL), $K_4Fe(CN)_6$ (20mM), and NaCl (50mM) in buffer (solution 1) to a solution containing only the Ru complex, DNA, and NaCl in buffer (solution 2) whose fluorescence spectrum has already been run. All stock solutions were prepared in buffer (5mM Tris buffer, pH 7.4).

High Resolution Mass spectrometry (HRFAB)

Analysis of the compounds in this dissertation by High-resolution Fast Atom Bombardment (HRFAB) was performed by the Nebraska Center for mass Spectrometry, Department of Chemistry, University of Nebraska, Lincoln, NE 68588-0362.

Preparation of Ligands

2-(2-pyridyl)-1,3-oxazoline (pyridyl oxazoline, pyoxazo)

A 50mL round bottom flask was charged with I (prepared from 2-cyanopyridine and sodium methoxide)[60] (10 mL, 80 mmol), monoethanolamine (5 mL, 80 mmol), and concentrated HCl (1 drop).The reaction mixture was stirred while heating (60°C) at reflux for 12 hours. The solvent was evaporated under reduced pressure, and the remaining substance was chromatographed over alumina, eluting with acetonitrile. Fractions, which gave a red color with ferrous sulfate, were collected and evaporated to give pure 2-(2-pyridyl)-1,3-oxazoline (7.5g).

2-(1,3-oxazolin-2-yl)-1,3-oxazoline (bis-oxazoline , bisoxazo)

A 250mL round bottom flask was charged with dichlorodiethyl oxamide [61,62] (12g) and 1M methyl alcoholic potassium hydroxide (113mL). The mixture was boiled for one hour, after which the solution was filtered, and the filtrate was evaporated under reduced pressure to give a solid. The solid was recrystallized from 113g toluene to give white crystals (8g).

4,4-dimethyl-2-(2-pyridyl)-1,3-oxazoline (dimethylpyridyl-oxazoline, dmpyoxazo)

A 50mL round bottom flask was charged with I (prepared from cyanopyridine and sodium methoxide)[60] (10mL, 80mmol), 2-amino-2methyl-propanol (7.55mL, 80mmol), and concentrated HCl (1 drop). The reaction was stirred while heating (60°C) at reflux for 12 hr. The solvent was evaporated under reduced pressure and the remaining substance was chromatographed over alumina, eluting with acetonitrile. Fractions that gave a red color with ferrous sulfate was collected and evaporated under reduced pressure to pure 4,4-dimethyl-2-(2-pyridyl)-1,3-oxazoline (6g).

Pyridino[3,2-f]quinoxalino[2,3-h]quinoline (bppz)

A 50mL round bottom flask was charged with 1,2-phenylenediamine (257mg, 2.38mmol), 4,7-phenanthroline-5,6-dione (500mg, 2.38mmol), and 95% ethanol (20mL). The mixture was stirred and heated to reflux for six hours. The yellow-green solid formed was filtered, and the solid was recrystallized from acetone to give a beige colored solid (436.2mg, 65%).

11,12-dimethylpyridino[3,2-f]quinoxalino[2,3-h]quinoline (mbppz)

A 50 mL round bottom flask was charged with 4,5-dimethyl-1,2-phenylene diamine (323.7 mg, 2.38 mmol), 4,7-phenanthroline-5,6-dione (500 mg, 2.38 mmol), and 95% ethanol (20mL). The mixture was stirred and heated to reflux for two hours. The solution was precipitated with acetone and suction filtered to give a pale yellow solid (443 mg, 65%).

Benzo[f]pyridino[3,2-h]quinoline (benzo-1,10-phenanthroline, bzp)

A three-neck round bottom flask was charged with 2,3-diaminonapthalene (10g, 0.0632 mol), sodium m-nitrobenzene sulfonate (29.85g, 0.1326 mol), glycerol (21g, 0.228 mol), sulfuric acid (151.6 mL), and water (81.6mL). The flask was fitted with a mechanical stirrer, condenser, and the mixture was heated (130-140°C) to reflux for two hours. The resulting solution was neutralized with sodium hydroxide solution, and extracted with chloroform or methylene chloride. The organic layer was dried with anhydrous magnesium sulfate, filtered, and evaporated under reduced pressure to give a brown-yellow solid. The solid was purified by continous soxlet extraction using hexane as the solvent to give a beige solid (8.7g, 60 % yield).

Use of disodium O,O'-dibenzoyl-(R,R)-tartrate for the resolution of [Ru(II)(bpy)$_2$(py)$_2$] complexes.

To an aqueous solution of disodium O,O'-dibenzoyl-(R,R)-tartrate (19.50mL of 0.5M, 9.75mmol) was added to a solution of [Ru(II)(bpy)$_2$(py)$_2$]Cl$_2$ (1.95g, 3.03mmol) in water (39mL). The deep red solution was stirred for 10 min. and allowed to stand at room

temperature uncovered in a fume hood for 5 days. The red crystals of the pure O,O'-dibenzoyl-(R,R)-tartrate salt of Δ-[Ru(II)(bpy)$_2$(py)$_2$] which formed upon solvent evaporation were recovered by suction filtration and air dried (1.00g, 71.3% yield). This material exhibited CD spectrum where $\Delta\epsilon_{295}$ = -154M^{-1} cm^{-1} and a UV/Vis spectrum which corresponds to that previously reported.[64] The UV/Vis spectra peviously reported [64] used the dichloride salt; conversion of the O,O'-dibenzoyl-(R,R)-tartrate salt to the dichloride salt in the present work resulted in no change to either the CD or UV/Vis spectrum. The presently reported CD involves a greater ellipticity than that previously reported (+114 M^{-1} cm^{-1} at 295 nm for the Λ-enantiomer)[64] indicating a significant greater optical purity for the presently prepared material. Correspondingly, pure salts of L-[Ru(II)(bpy)$_2$(py)$_2$] ($\Delta\epsilon_{295}$ = +156 M^{-1} cm^{-1}) were generated using O,O'-dibenzoyl-(S,S)-tartrate as the resolving agent.

Preparation of [Ru(bpy)$_2$L]$^{2+}$ Complexes

(+/-) [Ru(II)(bpy)$_2$(py)$_2$]Cl$_2$

This material was prepared using a modification of a previously reported procedure.[63] A 250mL round bottom flask was charged with pyridine (23mL), water (46mL) and bis-(2,2'-bipyridine)ruthenium (II) dichloride (2.00g, 4.13mmol). The reaction mixture was stirred and heated at reflux for 4hr, filtered while hot, and the solvent was evaporated under reduced pressure. The deep red residue was dissolved in methanol (46mL) and sufficient diethyl ether was added to result in the formation of a red precipitate. The mixture was allowed to stand at room temperature for 1hr, after which the precipitate was recovered by suction filtration and the crystals were washed with

diethyl ether (2 x 50mL). The recovered solid (1.95g, 73.6%yield) was identical in properties to that previously reported [63] for (+/-) $[Ru(II)(bpy)_2(py)_2]Cl_2$.

$[Ru(bpy)_2(pyoxazo)](PF_6)_2$

A 25mL round bottom flask was charged with pyridyl-oxazoline (pyoxazo) (60.3mg, 0.413mmol), $Ru(II)(bpy)_2\ Cl_2$ (200mg, 0.413mmol) and 95% ethanol (5mL). The mixture was stirred and heated to reflux for 6 hr, after which the solution was cooled, filtered, and 10mL of water was added to the filtrate. To the filtrate was added ammonium hexafluorophosphate (1.0g), which resulted in the formation of a red colored precipitate. The precipitate was recovered by suction filtration, dried and chromatographed over alumina eluting with acetonitrile. The orange red band was collected and evaporated to give pure $[Ru(bpy)_2(pyoxazo)](PF_6)_2$ (224mg, 72% yield). The extinction coefficient determined in water at 456nm was 10200 (ε_{456} = 10200).

$[Ru(bpy)_2(bisoxazo)](PF_6)_2$

A 25mL round bottom flask was charged with bis-oxazoline (42.1mg, 0.310mmol), $Ru(II)(bpy)_2Cl_2$ (150mg, 0.310mmol) and 95% ethanol (5mL). The mixture was stirred and heated to reflux for 6 hr, after which the solution was cooled, filtered, and 10mL of water was added to the filtrate. To the filtrate was added ammonium hexafluorophosphate (1.0g), which resulted in the formation of a red colored precipitate. The precipitate was recovered by suction filtration, dried and chromatographed over alumina eluting with acetonitrile. The orange red band was colected and evaporated to

give pure $[Ru(bpy)_2(bisoxazo)](PF_6)_2$ (46mg, 40% yield). The extinction coefficients determined in water at 458nm was 14400 (ε_{458} = 14400).

$[Ru(bpy)_2(dmpyoxazo)](PF_6)_2$

A round bottom flask was charged with dimethylpyridyl-oxazoline (55mg, 0.310mmol), $Ru(II)(bpy)_2Cl_2$ (150mg, 0.310mmol) and 95% ethanol (5mL). The mixture was stirred and heated to reflux for 6hr, after which the solution was cooled, filtered, and 10mL of water was added to the filtrate. To the filtrate was added ammonium hexafluorophosphate (1.0g), which resulted in a red colored precipitate. The precipitate was recovered by suction filtration, dried and chromatographed over alumina eluting with acetonitrile. The orange red band was collected and evaporated to give pure $Ru(bpy)_2(dmpyoxazo)](PF_6)_2$ (202mg, 84% yield). The extinction coefficient determined in water at 454nm was 20400 (ε_{454} = 20400) .

$[Ru(II)(bpy)_2(bppz)](PF_6)_2$

A 25mL round bottom flask was charged with bppz (45mg, 0.160mmol (plus 10% excess)), $Ru(bpy)_2Cl_2$ (78mg, 0.160mmol), and 95% ethanol (10mL). The mixture was stirred and heated to reflux for six hours, after which the red solution was cooled, filtered, and the filtrate was diluted with 5ml of water. To the filtrate was added ammonium hexafluorophosphate (1.0g), which resulted in dark red precipitate. The precipitate was recovered by suction filtration, dried and chromatographed over alumina, eluting with acetonitrile. The purple-red colored band was collected and the solvent evaporated to give $[Ru(II)(bpy)_2(bppz)](PF_6)_2$ (85mg, 60% yield). The extinction coefficient

determined in water at 546nm was 10400 (ε_{546} = 10400).

Δ-[Ru(II)(bpy)$_2$(bppz)](PF$_6$)$_2$

A round bottom flask was charged with bppz (28.2mg, 0.100mmol (plus 10% excess)), Δ-(Ru(II)(bpy)$_2$(py)$_2$]O,O'-dibenzoyl-(R,R)tartrate salt (111mg, 0.100mmol), and 9/1 ethylene glycol/water (5 mL). The mixture was stirred and heated at reflux for six hours, after which the mixture was cooled, filtered, and the filtrate was diluted with water (5mL). To the filtrate was added ammonium hexafluorophosphate (1.0g), which resulted in the formation of a dark red precipitate. The precipitate was recovered by suction filtration, dried and chromatographed over alumina, eluting with acetonitrile. The purple/red band was collected and the solvent evaporated to give Δ-[Ru(II)(bpy)$_2$(bppz](PF$_6$)$_2$ (54mg, 60 % yield). The extinction coefficients and NMR spectra were identical to that of the racemic complex.

Λ-[Ru(II)(bpy)$_2$(bppz)](PF$_6$)$_2$

A 25mL round bottom flask was charged with bppz (28.2mg, 0.100mmol (plus 10% excess)), Λ-[Ru(II)(bpy)2(py)2]O,O'-dibenzoyl-(S,S) tartrate salt, and (9/1) ethylene glycol/water (5.0mL). The mixture was stirred and heated to reflux for six hours, after which the solution was cooled, filtered, and the filtrate was diluted with water (5.0mL). To the filtrate was added ammonium hexafluorophosphate (1.0g), which resulted in the formation of a dark red precipitate. The precipitate was recovered by suction filtration, dried and chromatographed over alumina, eluting with acetonitrile. The purple/red band was collected and the solvent was evaporated to give Λ-[Ru(II)(bpy)$_2$(bppz)](PF$_6$)$_2$ (

54mg, 60 % yield). The extinction coefficient and NMR spectra were identical to that of the racemic complex.

[Ru(II)(bpy)$_2$(mbppz)](PF$_6$)$_2$

A 25mL round bottom flask was charged with mbppz (50mg, 0.160mmol (plus 10% excess)), Ru(bpy)$_2$Cl$_2$ (78mg, 0.160mmol), and 95% ethanol (10 mL). The mixture was stirred and heated to reflux for six hours, after which the solution was cooled, filtered, and the filtrate was diluted with water (5.0mL). To the filtrate was added ammonium hexafluorophosphate (1.0g), which resulted in the formation of a dark red precipitate. The precipitate was recovered by suction filtration, dried and chromatographed over alumina, eluting with acetonitrile.The red/purple band was collected and the solvent evaporated to give [Ru(II)(bpy)$_2$(mbppz)](PF$_6$)$_2$ (110mg, 62 % yield). The extinction coefficients determined in water at 534nm was 10100 (ε_{534} = 1.01 x 10^4).

Δ-[Ru(II)(bpy)$_2$(mbppz)](PF$_6$)$_2$

A 25ml round bottom flask was charged with mbppz (31mg, 0.100 mmol), Δ-Ru(II)(bpy)$_2$(py)$_2$]O,O'-dibenzoyl-(R,R)tartrate salt (111mg, 0.100 mmol), and 9/1 ethylene glycol/water (5.0mL).The mixture was stirred and heated to reflux for six hours, after which the solution was cooled, filtered, and diluted with water (5.0mL). To the filtrate was added ammonium hexafluorophosphate (1.0g), which resulted in the formation of a dark red precipitate. The precipitate was recovered by suction filtration, dried and chromatographed over alumina, eluting with acetonitrile. The purple/red band

was collected and the solvent evaporated to give Δ-[Ru(II)(bpy)$_2$(mbppz)](PF$_6$)$_2$ (70mg, 76 % yield). The extinction coefficients and NMR spectra were identical to that of the racemic complex.

Λ-[Ru(II)(bpy)$_2$(mbppz)](PF$_6$)$_2$

A 25ml round bottom flask was charged with mbppz (31mg, 0.100 mmol), Λ-Ru(II)(bpy)$_2$(py)$_2$]O,O'-dibenzoyl-(S,S)tartrate salt (111mg, 0.100 mmol), and 9/1 ethylene glycol/water (5.0mL).The mixture was stirred and heated to reflux for six hours, after which the solution was cooled, filtered, and diluted with water (5.0mL). To the filtrate was added ammonium hexafluorophosphate (1.0g), which resulted in the formation of a dark red precipitate. The precipitate was recovered by suction filtration, dried and chromatographed over alumina, eluting with acetonitrile. The purple/red band was collected and the solvent evaporated to give Λ-[Ru(II)(bpy)$_2$(mbppz)](PF$_6$)$_2$ (65mg, 70 % yield). The extinction coefficients and NMR spectra were identical to that of the racemic complex.

[Ru(II)(bpy)$_2$(bzp)](PF$_6$)$_2$

A 25mL round bottom flask was charged with Ru(II)(bpy)$_2$Cl$_2$ (100mg, 0.206mmol), benzo-1,10-phenanthroline (bzp) (47.4mg, 0.206mmol), and 95% ethanol (10mL). The mixture was stirred and heated to reflux for six hours, after which the solution was evaporated under reduced pressure to a small volume, and chromatographed over alumina, eluting with acetonitrile. The deep orange band was collected and the solvent was evaporated to give [Ru(II)(bpy)$_2$(bzp)](PF$_6$)$_2$ (75 % yield). The extinction

coefficient determined in water at 452nm was 18000 (ε_{452} = 18000).

Δ- [Ru(II)(bpy)$_2$(bzp)](PF$_6$)$_2$

A 25ml round bottom flask was charged with benzo-1,10-phenanthroline (bzp) (58.7 mg, 0.255 mmol), Δ-Ru(II)(bpy)$_2$(py)$_2$]O,O'-dibenzoyl-(R,R)tartrate salt (250mg, 0.269 mmol), and (9/1) ethylene glycol/water (7.5L).The mixture was stirred and heated to reflux for six hours, after which the solution was cooled, filtered, and diluted with water (15.0mL). To the filtrate was added ammonium hexafluorophosphate (2.0g), which resulted in the formation of a red precipitate. The precipitate was recovered by suction filtration, dried and chromatographed over alumina, eluting with acetonitrile. The orange/red band was collected and the solvent evaporated to give Δ–[Ru(II)(bpy)$_2$(bzp)](PF$_6$)$_2$ (75% yield). The extinction coefficients and NMR spectra were identical to that of the racemic complex.

Λ- [Ru(II)(bpy)$_2$(bzp)](PF$_6$)$_2$

A 25ml round bottom flask was charged with benzo-1,10-phenanthroline (bzp) (58.7 mg, 0.255 mmol), Λ-Ru(II)(bpy)$_2$(py)$_2$]O,O'-dibenzoyl-(S,S)tartrate salt (250mg, 0.269 mmol), and (9/1) ethylene glycol/water (7.5L).The mixture was stirred and heated to reflux for six hours, after which the solution was cooled, filtered, and diluted with water (15.0mL). To the filtrate was added ammonium hexafluorophosphate (2.0g), which resulted in the formation of a red precipitate. The precipitate was recovered by suction filtration, dried and chromatographed over alumina, eluting with acetonitrile. The orange/red band was collected and the solvent evaporated to give

Λ–[Ru(II)(bpy)$_2$(bzp)](PF$_6$)$_2$ (75% yield). The extinction coefficients and NMR spectra were identical to that of the racemic complex.

[Ru(II)(bpy)$_2$(ippz)](PF$_6$)$_2$

A 25mL round bottom flask was charged with Ru(II)(bpy)$_2$Cl$_2$ (100mg, 0.206mmol), ippz (48mg, 0.206mmol), and 95% ethanol (10mL). The mixture was stirred and heated to reflux for six hours, after which the solution was cooled, filtered, and diluted with water (5.0mL). To the filtrate was added ammonium hexafluorophosphate (1.0g), which resulted in the formation of a red precipitate. The precipitate was recovered by suction filtration, dried and chromatographed over alumina, eluting with acetonitrile. The deep orange band was collected and the solvent was evaporated to give [Ru(II)(bpy)$_2$(ippz)](PF6)2 (75 % yield). The extinction coefficient determined in water at 450nm was 1600 (ε_{450} = 16000).

Δ- [Ru(II)(bpy)$_2$(ippz)](PF$_6$)$_2$

A 25ml round bottom flask was charged with ippz (23mg, 0.100 mmol), Δ-Ru(II)(bpy)$_2$(py)$_2$]O,O'-dibenzoyl-(R,R)tartrate salt (111mg, 0.100 mmol), and (9/1) ethylene glycol/water (5L).The mixture was stirred and heated to reflux for six hours, after which the solution was cooled, filtered, and diluted with water (5.0mL). To the filtrate was added ammonium hexafluorophosphate (1.0g), which resulted in the formation of a red precipitate. The precipitate was recovered by suction filtration, dried and chromatographed over alumina, eluting with acetonitrile. The orange/red band was collected and the solvent evaporated to give Δ–[Ru(II)(bpy)$_2$(ippz)](PF$_6$)$_2$ (75% yield).

The extinction coefficients and NMR spectra were identical to that of the racemic complex.

Λ- [Ru(II)(bpy)$_2$(ippz)](PF$_6$)$_2$

A 25ml round bottom flask was charged with ippz (23 mg, 0.100 mmol), Λ-Ru(II)(bpy)$_2$(py)$_2$]O,O'-dibenzoyl-(S,S)tartrate salt (111mg, 0.100 mmol), and (9/1) ethylene glycol/water (5L).The mixture was stirred and heated to reflux for six hours, after which the solution was cooled, filtered, and diluted with water (5.0mL). To the filtrate was added ammonium hexafluorophosphate (1.0g), which resulted in the formation of a red precipitate. The precipitate was recovered by suction filtration, dried and chromatographed over alumina, eluting with acetonitrile. The orange/red band was collected and the solvent evaporated to give Λ–[Ru(II)(bpy)$_2$(ippz)](PF$_6$)$_2$ (75% yield). The extinction coefficients and NMR spectra were identical to that of the racemic complex.

Δ-[Ru(bpy)2(dpp)] [PF$_6$]$_2$ (Δ2) and Λ-[Ru(bpy)2(dpp)] [PF$_6$]$_2$ (Λ2)

In a round bottom flask, 2,3-bis(2-pyridyl)pyrazine (dpp), Δ-[Ru(bpy)$_2$(py)2]$^{2+}$, O,O'-dibenzoyl(R,R)-tartrate salt (resolution in chapter 17), and ethylene glycol-water was heated to reflux for six hours. The mixture was cooled, diluted with water, and pecipitated with ammonium hexafluorophosphate. The precipitate was recovered by suction filtration, dried and chromatographed over alumina, eluting with acetonitrile. The deep orange-yellow band was collected and the solvent was evaporated to give pure Δ-[Ru(bpy)2(dpp)] [PF$_6$]$_2$ (Δ2) This material exhibited a CD spectrum and a UV/VIS

spectrum corresponding to that previously reported for the stereoisomeric mixture. The ^{1}H and ^{13}C NMR spectra were measured in DMSO-d_6 solution. The ^{1}H spectrum exhibited a complex series of signals in the range δ 7.1-8.9. The ^{13}C spectrum exhibited 34 signals in accord with the number of unique carbon atoms in the proposed structure, eight of which were indicated by distortionless enhancement of polarisation transfer (DEPT) measurement to be devoid of attached hydrogen atoms. Correspondingly, pure Λ-[Ru(bpy)2(dpp)] $[PF_6]_2$ (**Λ2**) was prepared starting with Λ-$[Ru(bpy)_2(py)2]^{2+}$, O,O'-dibenzoyl(S,S)-tartrate salt, exhibiting identical UV/VIS and NMR spectra, and corresponding CD spectrum.

Δ-[Ru(bpy)2(ppz)] $[PF_6]_2$ (Δ3) and Λ-[Ru(bpy)2(ppz)] $[PF_6]_2$ (Λ3)

In a round bottom flask, pyrazino[2,3-f][4,7]phenanthroline (ppz), Δ-$[Ru(bpy)_2(py)_2]^{2+}$, O,O'-dibenzoyl(R,R)-tartrate salt, and ethylene glycol-water was heated to reflux for six hours. The mixture was cooled, diluted with water, and pecipitated with ammonium hexafluorophosphate. The precipitate was recovered by suction filtration, dried and chromatographed over alumina, eluting with acetonitrile. The deep orange-yellow band was collected and the solvent was evaporated to give pure Δ-$[Ru(bpy)_2(ppz)]$ $[PF_6]_2$ (**Δ3**). This material exhibited a CD spectrum and a UV/VIS spectrum corresponding to that previously reported for the stereoisomeric mixture.[2a] The ^{1}H and ^{13}C NMR spectra were measured in DMSO-d_6 solution. The ^{1}H spectrum exhibited a complex series of signals in the range δ 7.2-9.8. The ^{13}C spectrum exhibited 34 signals in accord with the number of unique carbon atoms in the proposed structure, ten of which were indicated by DEPT measurement to be devoid of attached hydrogen

hydrogen atoms. Correspondingly, pure Λ-$[Ru(bpy)_2(ppz)]$ $[PF_6]_2$ (Λ2) was prepared starting with Λ-$[Ru(bpy)_2(py)2]^{2+}$, O,O'-dibenzoyl(S,S)-tartrate salt, exhibiting identical UV/VIS and NMR spectra, and corresponding CD spectrum.

Preparation of $[RuL_3]^{2+}$ complexes

$Ru(pyoxazo)_3$ $(PF_6)_2$

A 25mL round bottom flask was charged with pyridyl-oxazoline (pyoxazo) (143mg, 0.966mmol), dichlorotetrakis (dimethyl sulfoxide) Ruthenium(II) [65] (100mg, 0.322mmol), and 95% ethanol (10mL). The mixture was stirred and heated to reflux for six hours, after which the solution was cooled, filtered, and diluted with water (5.0mL). To the filtrate was added ammonium hexafluorophosphate (1.0g), which resulted in the formation of a red precipitate. The precipitate was recovered by suction filtration, dried and chromatographed over alumina, eluting with acetonitrile/ethanol. The orange red band was colllected and evaporated to give $Ru(pyoxazo)_3$ $(PF_6)_2$ (70% yield). The extinction coefficients determined in water at 466nm was 12200 (ε_{466} = 12200).

$[Ru(dmpyoxazo)_3]$ $(PF_6)_2$

A 25mL round bottom flask was charged with dimethylpyridyl-oxazoline III (169mg, 0.966mmol), dichlorotetrakis(dimethyl sulfoxide)Ruthenium(II)[65] (100mg, 0.322mmol), and 95% ethanol (10ml). The mixture was stirred and heated to reflux for six hours, after which the solution was cooled, filtered, and diluted with water (5.0mL). To the filtrate was added ammonium hexafluorophosphate (1.0g), which resulted in the formation of a red precipitate. The precipitate was recovered by suction filtration, dried

and chromatographed over alumina, eluting with acetonitrile/ethanol. The orange red band was collected and evaporated to give $Ru(dmpyoxazo)_3 (PF_6)_2$ (72% yield). The extinction coefficients determined in water at 456nm was 10500 (ε_{456} = 10500).

$[Ru(bzp)_3] (PF_6)_2$

A 25mL round bottom flask was charged with benzo-1,10-phenanthroline (bzp) (222.18mg, 0.966mmol), dichlorotetrakis(dimethyl sulfoxide)Ruthenium(II)[65] (100mg, 0.322mmol), and 95% ethanol (10ml). The mixture was stirred and heated to reflux for six hours, after which the solution was cooled, filtered, and diluted with water (5.0mL). To the filtrate was added ammonium hexafluorophosphate (1.0g), which resulted in the formation of a orange-red precipitate. The precipitate was recovered by suction filtration, dried and chromatographed over alumina, eluting with acetonitrile/ethanol. The orange red band was collected and evaporated to give $Ru(bzp)_3 (PF_6)_2$ (70% yield). The extinction coefficient determined in water at 452nm was 18000 (ε_{452} = 18000).

Preparation of $[(bpy)_2Ru(L)Ru(bpy)_2]^{4+}$

ΔΔ-$[(bpy)_2Ru(dpp)Ru(bpy)_2][PF_6]_4$ (ΔΔ4) and ΛΛ-$[(bpy)_2Ru(dpp)Ru(bpy)_2][PF_6]_4$ (ΛΛ4)

In a round bottom flask, pyrazino[2,3-bis(2-pyridyl)pyrazine (dpp), Δ-$[Ru(bpy)_2(py)2]^{2+}$, O,O'-dibenzoyl(R,R)-tartrate salt, and ethylene glycol-water was heated to reflux for six hours. The mixture was cooled, diluted with water, and pecipitated with ammonium hexafluorophosphate. The precipitate was recovered by

suction filtration, dried and chromatographed over alumina, eluting with acetonitrile. The deep purple band was collected and the solvent was evaporated to give pure ΔΔ-$[(bpy)_2Ru(dpp)Ru(bpy)_2][PF_6]_4$ (ΔΔ4). This material exhibited a CD spectrum and a UV/VIS in accord with that observed[2a] previously for the stereoisomeric mixture. The ^1H and ^{13}C NMR spectra were measured in DMSO-d_6 solution. The ^1H spectrum exhibited a complex series of signals in the range δ 7.1-9.1. The ^{13}C spectrum exhibited 54 signals in accord with the number of unique carbon atoms in the proposed structure, twelve of which were indicated by DEPT measurement to be devoid of attached hydrogen atoms. Correspondingly, pure ΛΛ-$[(bpy)_2Ru(dpp)Ru(bpy)_2][PF_6]_4$ (ΛΛ4) was prepared starting with Λ-$[Ru(bpy)_2(py)2]^{2+}$, O,O'-dibenzoyl(S,S)-tartrate salt, exhibiting identical UV/VIS and NMR spectra, and corresponding CD spectrum.

ΔΛ-$[(bpy)_2Ru(dpp)Ru(bpy)_2][PF_6]_4$ (ΔΛ4)

In a round bottom flask, Δ-$[Ru(bpy)_2(dpp)][PF_6]_2$, Λ-$[Ru(bpy)_2(py)2]^{2-}$, O,O'-dibenzoyl(S,S)-tartrate salt, and ethylene glycol-water was heated to reflux for six hours. The mixture was cooled, diluted with water, and pecipitated with ammonium hexafluorophosphate. The precipitate was recovered by suction filtration, dried and chromatographed over alumina, eluting with acetonitrile. The deep purple-red band was collected and the solvent was evaporated to give pure ΔΛ-$[(bpy)_2Ru(dpp)Ru(bpy)_2][PF_6]_4$ (ΔΛ4). This material was inactive in the CD spectrum and exhibited a UV/VIS spectrum corresponding to that of the previously noted ΔΔ and ΛΛ isomers and in accord with that observed[2a] for the stereoisomeric mixture. The ^1H and ^{13}C NMR spectra were measured in DMSO-d_6 solution. The ^1H spectrum exhibited a complex series of signals in the range

δ 7.1-9.4. The ^{13}C spectrum exhibited 27 signals in accord with the number of unique carbon atoms in the proposed structure, six of which were indicated by DEPT measurement to be devoid of attached hydrogen atoms.

ΔΔ-[(bpy)$_2$Ru(ppz)Ru(bpy)$_2$][PF$_6$]$_4$ (ΔΔ5) and ΛΛ-[(bpy)$_2$Ru(ppz)Ru(bpy)$_2$][PF$_6$]$_4$ (ΛΛ5)

In a round bottom flask, pyrazino[2,3-f]-[4,7]phenanthroline (ppz), Δ-[Ru(bpy)$_2$(py)2]$^{2+}$, O,O'-dibenzoyl(R,R)-tartrate salt, and ethylene glycol-water was heated to reflux for six hours. The mixture was cooled, diluted with water, and pecipitated with ammonium hexafluorophosphate. The precipitate was recovered by suction filtration, dried and chromatographed over alumina, eluting with acetonitrile. The deep purple band was collected and the solvent was evaporated to give pure ΔΔ-[(bpy)$_2$Ru(ppz)Ru(bpy)$_2$][PF$_6$]$_4$ ΔΔ5. This material exhibited a CD spectrum and UV/VIS spectrum in accord with that observed[2c] for the stereoisomeric mixture. The ^1H and ^{13}C NMR spectra were measured in DMSO-d$_6$ solution. The ^1H spectrum exhibited a complex series of signals in the range δ 7.2-9.8. Although the structure of DD5 contains 54 unique carbon atoms, its ^{13}C spectrum exhibited only 29 completely resolved unique signals. We could not improve on the resolution to obtain fully separated signals for each unique carbon atom; it appears that in numerous instances the signals of several carbon atoms are clustered in a relatively broad unresolved band. Of the 29 signals observed, ix were indicated by DEPT measurement to be devoid of attached hydrogen atoms. Correspondingly, pure ΛΛ-[(bpy)$_2$Ru(ppz)Ru(bpy)$_2$][PF$_6$]$_4$ **ΛΛ5** was prepared starting with Λ-[Ru(bpy)$_2$(py)2]$^{2+}$, O,O'-dibenzoyl(S,S)-tartrate salt. This material exhibited

identical UV/VIS and NMR spectra, the latter consistent with the deficiency in number of unique carbon signals which were observed as (ΔΔ5), and a corresponding CD spectrum.

ΔΛ-[(bpy)$_2$Ru(ppz) Ru(bpy)$_2$][PF$_6$]$_4$ (ΔΛ5)

In a round bottom flask, Δ-[Ru(bpy)$_2$(ppz)][PF$_6$]$_2$, Λ-[Ru(bpy)$_2$(py)2]$^{2+}$, O,O'-dibenzoyl(S,S)-tartrate salt, and ethylene glycol-water was heated to reflux for six hours. The mixture was cooled, diluted with water, and pecipitated with ammonium hexafluorophosphate. The precipitate was recovered by suction filtration, dried and chromatographed over alumina, eluting with acetonitrile. The deep purple band was collected and the solvent was evaporated to give pure ΔΛ-[(bpy)$_2$Ru(ppz)Ru(bpy)$_2$][PF$_6$]$_4$ (ΔΛ5). This material was inactive in the CD spectrum and exhibited a UV/VIS spectrum corresponding to that of the previously noted ΔΔ and ΛΛ isomers, and in accord with that observed[2c] previously for the stereoisomeric mixture. The ^{1}H and ^{13}C NMR spectra were measured in DMSO-d$_6$ solution. The ^{1}H spectrum exhibited a complex series of signals in the range δ 7.2-9.8. The ^{13}C spectrum exhibited 27 signals, in accord with the number of unique carbon atoms in the proposed structure, seven of which were indicated by DEPT measurement to be devoid of attached hydrogen atoms.

Note:

The main purpose for synthesizing the Ru(II) metal complexes in this dissertation is to study their interactions with B-DNA. In order to do so these complexes should be fairly soluble in water. Therefore, the Ru(II) complexes were also precipitated as a BF_4 salt using sodium tetrafluoroborate instead of ammonium hexafluorophosphate since BF_4

salts are more soluble than PF_6 salts. The yield obtained using sodium tetrafluoroborate was found to be lower than that obtained from precipitation with ammonium hexafluorophosphate. Therefore, the PF_6 salt were used for percent yield calculations.

References

1. Colin, J.P.; Gavina, P.; Heitz, V.; Sauvage, J.P. Eur. J. Inorg. Chem.**1998**, 1-14.
2. Sauvage, J.P.; Collin, J.P.; Cambron, J.C.; Flamingni, L. Chem. Rev. **1994**, 94, 933.
3. Kalyanasundaram, K. Photochemistry of Polypyridine and Porphryin Complexes, Academic Press: San Diego, **1992**.
4. Meyer, G.J. J. Chem. Educ. **1997**, 74, 652-6.
5. Meyer, T.J. Acc. Chem. Res. **1989**, 22, 163-70.
6. Beer, P.D.; Szemes, F.; Balzani, V.; Sala, C.M.; Drew, M.G.B.; Dent, S.W.; Maestri, M. J. Am. Chem. Soc. **1997**, 119, 11864-75.
7. Beer, P.D. Acc. Chem. Res. **1998**, 31, 71-80.
8. Ziessel, R.F. J. Chem. Educ. **1997**, 74, 673-79.
9. Shen, Y.; Sullivan, B.P. J. Chem. Educ. **1997**, 74, 685-9.
10. Demas, J.N.; DeGraff, B.A. J. Chem. Educ. **1997**, 74, 690-5.
11. Yu, L.; Chan, W.K.; Peng, Z.; Gharavi, A. Acc. Chem. Res. **1996**, 29, 13-21.
12. Ghadiri, M.R.; Soares, C.; Choi, C. J. Am. Chem. Soc. **1992**, 114, 825-31, 4000-2.
13. Langen, R.; Chang, I.J.; Germanas, J.P.; Richards, J.H.; Winkler, J.R.; Gray, H.B. Science **1995**, 268, 1733-5.
14. Sardesai, N.; Lin, S.C.; Zimmermann, K.; Barton, J.K. Biconjugate Chem. **1995**, 6, 302-12.
15. Lincoln, P., Tuite, E., Norden, B. J. Am. Chem. Soc. **1997**, 119, 1454-5.

16. Arkin, M.R.; Stemp, E.D.A.; Holmlin, R.E.; Barton, J.K.; Hormann, A.; Olson, E.J.C.; Barbara, P.F. Science **1996**, 273, 475.

17. Meade, T.J.; Kayyem, J.F. Angew. Chem. Int. Ed. Engl. **1995**, 34, 352-4.

18. Barton, J.K.; Basile, L.A.; Danishefsky,A.; Alexandrescu, A. Proc. Natl. Acad. Sci. USA **1984**, 81,1961.

19. Barton, J.K.; Danishefsky, A.; Goldberg, J.M. J. Am. Chem. Soc. **1984**, 106, 2172.

20. Kumar, C.V.; Barton, J.K.; Turro, N.J. J. Am. Chem. Soc. **1985**, 107, 5518.

21. Barton, J.K.; Goldberg, J.M., Kumar, C.V.; Turro, N.J. J. Am. Chem. Soc. **1986**,108, 2081.

22. Kelly, J.M.; Tossi, A.B.; McConnell, D.J.; OhUigin, C. Nuc. Acid. Res. **1985**, 13, 6017.

23. Barton, J.K. Comm. Inorg. Chem. **1985**, 3, 21.

24. Pyle, A.M.; Barton, J.K. Inorg. Chem. **1987**, 26, 3820.

25. Kelly, J.M.; McConnell, D.J.; OhUigin, C.; Tossi, A.B.,Kirsch-De Mesmaeker, A.; Masschelein, A.; Nasielski, J. J. Chem. Soc. Chem. Commun. **1987**, 1821.

26. Kumar, C.V.; Barton, J.K.; Gould, I.R.; Turro, N.J.; Van, Houten, J. Inorg. Chem. **1988**, 27, 648.

27. Mei, H.; Barton, J.K. Proc. Natl. Acad. Sci. USA **1988**, 85, 1339.

28. Tossi, A.B.; Kelly, J.M. Photochem. and Photobiol. **1989**, 49, 545.

29. Pyle, A.M.; Rehmann, J.P.; Meshoyrer, R.; Kumar, C.V.; Turro, N.J.; Barton, J.K. J. Am. Chem. Soc. **1989**, 111, 3051.

30. Kirsch-De Mesmaeker, A.; Orellana, G.; Barton, J.K.; Turro, N.J. Photochem. And Photobiol. **1990**, 52, 461.

31. Hiort, C.; Norden, B.; Rodger, A. J. Am. Chem. Soc. **1990**, 112, 1971.

32. Pyle, A.M.; Chiang, M.Y.; Barton, J.K. Inorg. Chem. **1990**, 29, 4487.

33. Rehmann, J.P.; Barton, J.K. Biochemistry **1990**, 29, 1701, 1710.

34. Haworth, I.S.; Elcock, A.H.; Freeman, J.; Rodger, A.; Richards, W.G. J. Biomol. Struct.Dyn. **1991**, 9, 23.

35. Kirsch-De Mesmaeker, A.; Orellana, G.; Barton, J.K.; Turro, N.J. Photochem. And Photobiol. **1991**, 54, 499.

36. Morgan, R.J.; Chatterjee, S.; Baker, A.D.; Strekas, T.C. Inorg. Chem. **1991**, 30, 2687.

37. Eriksson, M.; Leijon, M.; Hiort, C.; Norden, B.; Graslund, A. J. Am. Chem. Soc. **1992**, 114, 4933.

38. Baker, A.D.; Morgan, R.J.; Strekas, T.C. J. Chem. Soc., Chem Comm. **1992**, 1099.

39. Friedman, A.E.; Chambron, J.; Sauvage, J.; Turro, N.J.; Barton, J.K. J. Am. Chem. Soc. **1990**, 112, 4960.

40. Jenkins, Y.; Friedman, A.E.; Kumar, C.V.; Turro, N.J.; Barton, J.K. Biochemistry **1992**, 31, 10809.

41. Friedman, A.E.; Kumar, C.V.; Turro, N.J.; Barton, J.K. Nuc. Acid, Res. **1991**, 19, 2595.

42. Hartshorn, R.M.; Barton, J.K. J. Am. Chem. Soc. **1987**, 109, 7548.

43. Bashkin, J.K.; Frolova, E.I.; Sampath, U. J. Am. Chem. Soc. **1994**, 116, 5981-82.

44. Sigman, D.S. Acc. Chem. Res. **1986**, 19, 180-186.

45. Chen, C.B.; Sigman, D.S. J. Am. Chem. Soc. **1988**, 110, 6570-6572.

46. Jennette, K.W.; Lippard, S.J.; Vassiliades, G.A.; Bauer, W.R. Proc. Nat. Acad. Sci. USA **1974**, 71, 3839-3843.

47. Holmlin, R.E.; Dandiker, P.J.; Barton, J.K. Angew. Chem. Int. Ed. Eng. **1997**, 36, 2714-2730.

48. Turro, C.; Bossmann, S.H.; Jenkins, Y.; Barton, J.K.; Turro, N.J. J.Am. Chem. Soc. **1995**, 117, 9026-9032.

49. Peyratout, C.S.; Aldridge, T.K.; Crites, D.K.; McMillin, D.R. Inorg. Chem. **1995**, 34, 4484-4489.

50. Liu, F.; Meadows, K.A.; McMillin, D.R. J. Am. Chem. Soc. **1993**, 115, 6699-6704.

51. Basile, L.A.; Barton, J.K. J. Am. Chem. Soc. **1992**, 114, 2303.

52. Kalsbeck, W.A.; Grover, N.; Thorp, H.H. Angew. Chem. **1999**, 104, 1523.

53. Kalsbeck, W.A.; Grover, N.; Thorp, H.H. Angew. Chem., Int. Ed. Eng. **1991**, 30, 1517.

54. Grover, N.; Thorp, H.H. J. Am. Chem. Soc. **1991**, 113, 7030.

55. Gupta, N.; Grover, N.; Neshart, G.A.; Liang, W.; Singh, P.; Thorp. H.H. Angew Chem. Int. Ed. Eng. **1992**, 31, No. 8, 1048.

56. Meyer, J.J. Pure Appl. Chem. **1990**, 62, 1003.

57. Fox, M.A.; Channon, M. Eds. Photoinduced Electron Transfer, Elsevier, Amsterdam, **1988**, p2.

58. Stilani, A.; Long, E.C.; Pyle, A.M.; Barton, J.K. J. Am. Chem. Soc. **1992**, 114, 2303.

59. Hartson, R.M.; Barton, J.K. J. Am. Chem. Soc. **1992**, 114, 5919.

60. Schafer, F.C.; Peters, L.G.A. JOC **1961**, 26, 412.

61. Dudwig Knorr ; Rosaler P. Deutsche Chemische **1903**, 36, 1278-1279.

62. Wenker, H. J. Amer. Chem. Soc. **1938**, 60, 2152-2153.

63. Bosnich, B.; Dwyer, F.P. Aust. J. Chem. **1996**, 19, 2231.

64. Hua, X.; Lappin, A.G. Inorg. Chem. **1995**, 34, 992.

65. Evans,I.P.; Spencer, A.; Wilkinson,G. J. Chem. Soc. , Dalton Trans. **1973**, 204

66. Barton, J.K. Science **1986**,233,727.

67. Lerman, L.S. J. Mol. Biol. **1961**, 3,18.

68. Blears, D.J.; Bangluk, S.S. Biopolymers **1967**, 5, 535.

69. Marky, L.A.; Blumenfield, S.; Breslauer, K.J. Nucl. Acid. Res. **1983**, 11, 2857.

70. Waring, M.J. J. Mol. Biol. **1965**, 13, 269.

71. Tysoe, S.A.; Morgan, R.J.; Baker, A.D.; Strekas, T.C. J. Phys. Chem. **1993**, 96, 1707-1711.

72. Bittman, R.J. Mol. Biol. **1969**, 46, 251.

73. Waring, M.J. J. Mol. Biol. **1970**, 54, 247.

74. Dougherty, G.; Pilbrow, J.R. Int. J. Biochem. **1984**, 16, 1179.

75. Bard, A.J.; Carter, M.J. Bioconjugate Chem. **1990**, 1, 257.

76. Cantor, C.R.; Schimmel, P.R. Biophysical Chemistry. W.H. Freeman and Company: San Francisico, **1980**.

77. Scatchard, G. Ann. N.Y. Acad. Sci. **1949**, 51, 660.

78. Mc Ghee, J.D.; Von Hippel, P.H. J. Mol. Biol. **1974**, 86, 469.

79. Tinoco, I. Molecular Biophysics Academic Press. N.Y., **1965**.

80. Chow, C.S.; Barton, J.K. Methods in Enzymology **1992**, 212, 219-242.

81. Hiort, C.; Lincoln, P.; Norden, B.J. Amer. Chem. Soc. **1993**, 115, 3448-3454.

82. Satyanarayana, S.; Dabrowiak, J.C.; Chaires, J.B. Biochemistry **1993**, 32, 2573-2584.

83. Naing, K.; Takahashi, M.; Taniguchi, M.;Yamagishi, A. Inorg. Chem. **1995**, 34, 350-356.

84. Eriksson, M.; Leijon, M.; Hiort, C.; Norden, B.J.; Graslund, A. Biochemistry **1994**, 33, 5031-5040.

85. Strekas, T.C.; Baker, A.D.; Zaltsman, L.; Wang, S. J. Coord. Chem. **1996**, 39, 281-291.

86. Lytle, F.E.; Hercules, D.M. J. Am. Chem. Soc. **1969**, 91, 253.

87. Mulazzani, Q.A.; Emmi, S.; Fuochi, P.G.; Venturi, M.; Hoffman, M.Z.; Simic, M.G. J. Phys. Chem. **1979**, 83, 1562.

88. Harriman, A.J. Photochem. **1978**, 8, 648.

89. Zuloaga, F.; Kasha, M. Photochem. Photobiol. **1968**, 7, 549.

90. Hanazaki, I.; Nagakura, S. Inorg. Chem. **1968**, 8, 648.

91. Crosby, G.A. Acc. Chem. Res. **1975**, 8, 231.

92. Crosby, G.A.; Perkins, W.G.; Klassen, D.M. J. Chem. Phys. **1965**, 43,1498.

93. Klassen, D.M.; Crosby, G.A. Chem. Phys. Lett. **1967**, 1, 127.

94. Klassen, D.M.; Crosby, G.A. J. Chem. Phys. **1968**, 48, 1853.

95. Demas, J.N.; Crosby, G.A. J. Mol. Spectrosc. **1968**, 26,72.

96. Demas, J.N.; Crosby, G.A. J. Am. Chem. Soc. **1970**, 92, 7262.

97. Demas, J.N.; Crosby, G.A. Chem. Soc. **1971**, 93, 2841.

98. Harrigan, R.W.; Crosby, G.A. J. Chem. Phys. **1973**, 59, 3468.

99. Harrigan, R.W.; Hager, G.D.; Crosby, G.A. Chem. Phys. Lett. **1973**, 21, 487.

100. Watts, R.J.; Crosby, G.A. J. Am. Chem. Soc. **1972**, 94, 2606.

101. Crosby, G.A.; Hipps, K.W.; Elfring, W.H. J. Am. Chem. Soc. **1974**, 96, 629.

102. Baker, D.C.; Crosby, G.A. Chem. Phys. **1974**, 4, 428.

103. Hager, G.D.; Crosby, G.A. J. Am. Chem. Soc. **1975**, 97, 7031.

104. Hager, G.D.; Watts, R.J.; Crosby, G.A. J. Am. Chem. Soc. **1975**, 97,7037.

105. Hipps, K.W.; Crosby, G.A. J. Am. Chem. Soc. **1975**, 97, 7042.

106. Elfring, W.H.; Crosby, G.A. J. Am. Chem. Soc. **1981**, 103, 2683.

107. Stone, M.L.; Crosby, G.A. Chem. Phys. Lett. **1981**, 81, 42.

108. Crosby, G.A.; Elfring, W.H. J. Phys. Chem. **1976**, 80, 2206.

109. Juris, A.; Balzani, V.; Barigelletti, F.; Campagna, S.;belser, P.; Von Zelewsky, A. Coord. Chem. Rev. **1988**, 84, 85.

110. Ferguson, J.; Herren, F. Chem. Phys. **1983**, 76, 45.

111. Dual, C.A.; Weber, J. Chem. Phys. Lett. **1981**, 81, 42.

112. Felix, F.; Ferguson, J.; Guedel, H.U.; Ludi, A. Chem. Phys. Lett. **1979**, 62, 153.

113. Carlin, C.M.; DeArmond, M.K.; Chem. Phys. Lett.**1982**, 89,297.

114. Dallinger, R.F.; Woodruff, W.H.J. Am. Chem. Soc. **1979**, 101, 4391.

115. Kober, E.M.; Sullivan, B.P.; Meyer, T.J. Inorg. Chem. **1984**, 23, 2098.

116. Bradley, P.C.; Kress, N.; Hornberger, B.A.; Dallinger, R.F.; Woodruff, W.H.; J. Am. Chem. Soc. **1981**, 103, 7441.

117. Braterman, P.S.; Heath, G.A.; Yellowlees, L.J. JCS, Dalton Trans. **1985**, 1081.

118. Kalyanasundaram, K. Coord. Chem. Rev. **1982**, 46, 159.

119. Kalyanasundaram, K. Photochemistry in Microheterogenous systems; Academic : New York, **1987**.

120. Metal-DNA Chemistry; Tullius, T.D. Ed.; ACS Symposium Series 401; American Chemical Society: Washington, DC, **1989**.

121. Macromolecular Complexes Dynamic Interactions and Electronic Processes; Tsuchida, E. Ed.;VCH: New York, **1991**.

122. Watts, R.J. J. Chem. Educ. **1983**, 60, 834.

123. Ford, P.C. Rev. Chem. Intermed. **1979**,2, 267.

124. Creutz, C.; Chou, M.; Netzel, T.L.; Okimura, M.; Sustin, N. J. Am. Chem. Soc. **1980**, 102, 1309.

125. Reitz, G. A.; Demas, J. N.; Stephens, E.; DeGraff, B. A. J. Am. Chem. Soc. **1988**, 110, 5051.

126. Sacksteder, L.; Demas, J. N.; DeGraff, B. A. Inorg. Chem. **1989**, 28, 1787.

127. Kraus, E.; Ferguson, F. Prog. Inorg. Chem. **1989**, 37, 293.

128. Erikkila, K.E.; Odom, D.T.; Barton,J. Chem. Rev. **1999**, 99, 2777-2795.

129. Barton,J.K.; Paranawitha, S.R. Biochemistry **1986**, 25, 2205-2211

130. Barton, J.K.; Lolis, E.J. J. Am. Chem. Soc. **1985**, 107, 708-709.

131. Barton, J.K.; Dannenberg, J.J.; Raphael, A.L. J. Am. Chem. Soc. **1982**, 104, 4967-4968.

132. Norden, B; Tjernfeid, F. FEBS Lett. **1976**, 67, 368-370.

133. Goldstein, B.M.; Barton, J.K.; Berman, H.M. Inorg. Chem. **1986**, 25, 842-847.

134. Holmlin, R.E.; Stemp, E.D.A.; Barton, J., Inorg. Chem. **1998**, 37, 29-34.

135. Schafer, F.C.; Peters, L.G.A. JOC **1961**, 26, 412.

136. Dudwig, Knorr ; Rosaler, P. Deutsche Chemische **1903**, 36, 1278-1279.

137. Wenker, H. J. Am. Chem. Soc. **1938**, 60, 2152-2153.

138. Morgan, O.; Wang, S.; Sung-A, B.; Morgan, R.J.; Baker, A.D.; Strekas, T.C.; Engel, R. J. Chem. Soc., Dalton Trans. **1997**, 3773-3776.

139. Engel, R. Adv. Dendritic Macromolecules **1995**, 2, 73.

140. Braunstein, C.H.; Baker, A.D.; Strekas, T.C.; Gafney, H.D. Inorg. Chem. **1984**, 23, 857.

141. Murphy, W.R.; Brewer, K.J.; Gettliffe, G.; Peterson, J.D. Inorg. Chem. **1989**, 28, 81.

142. Fuchs, Y.; Lofters, S.; Dieter, T.; Shi, W.; Morgan, R.J.; Strekas, T.C.; Gafney, H.D.; Baker, A.D. J. Am. Chem. Soc. **1987**, 109, 2691.

143. Campagna, S.; Denti, G.; Sabatino, L.; Serroni, S.; Ciano, M.; Balzani, V. J. Chem. Soc., Chem. Commun. **1989**, 1500.

144. DeCola, L.; Belser, P.; Ebmeyer, F.; Barigelletti, F.; Vogtle, F.; von Zeelewsky, A.; Balzani, V. Inorg. Chem. **1990**, 29, 495.

145. Denti, G.; Serroni, S.; Campagna, S.; Ricevuto, V.; Balzani, V. Coord. Chem. Rev. **1991**, 111, 227.

146. Denti, G.; Campagna, S.; Sabatino, L.; Serroni, S.; Ciano, M.; Balzani, V. Inorg. Chem. **1990**, 29, 4750.

147. Campagna, S.; Denti, G.; Serroni, S.; Ciano, M.; Balzani, V. Inorg. Chem. **1991**, 30, 3278.

148. Denti, G.; Serroni, S.; Campagna, S; Ricevuto, V.; Juris, A.; Ciano, M.; Balzani, V. Inorg. Chim. Acta. **1992**, 198-200, 507.

149. Serroni, S.; Denti, G.; Campagna, S.; Ciano, M.; Balzani, V., J.Chem. Soc. Chem. Commun. **1991**, 944.

150. Denti, G.; Campagna, S.; Serroni, S.; Ciano, M.; Balzani, V. J. Am. Chem. Soc. **1992**, 114, 2944.

151. Serroni, S.; Denti, G.; Campagna, S.; Juris, A.; Ciano, M.; Balzani, V. Angew. Chem., Int. Ed. Engl. **1992**, 31, 1493.

152. Nallas, G.N.A.; Jones, S.W.; Brewer, K.J. Inorg. Chem. **1996**, 35, 6974.

153. Hua, X.; von Zelewsky, A. Inorg. Chem. **1991**, 30, 3796.

154. Mac Donnell, F.M.; Bodige, S. Inorg. Chem. **1996**, 35, 5758.

155. Tzalis, D.; Tor, Y. J. Am. Chem. Soc. **1997**, 119, 852.

156. Crutchley, R.J.; Kress, N.; Lever, A.B.P. J. Am. Chem. Soc. **1983**, 105, 1170-1178.

157. Shinozaki, M.; Kaizu, Y.; Hirai, H.; Kobayashi, K. Inorg. Chem. **1989**, 28, 3675.

158. Hosek, W.; Tysoe, S.A.; Gafney, H.D.; Baker, A.D.; Strekas, T.C. Inorg. Chem. **1989**, 28, 1228-1231.

159. Waring, M.J. Annu. Rev. Biochem. 1981, 50, 159.

160. Neville, D.M.; Davis, D.R. J. Mol. Biol. **1966**, 17, 57.

161. Weill, G.; Calvin, M. Biopolymers **1963**, 1, 401.

162. Gardner, B.J.; Mason, S.F. Biopolymers **1967**, 5, 535.

163. Crothers, D. Biopolymers **1968**, 6, 575.

164. Peacocke, A.R.; Skerrett, J.N.H. J. Chem. Soc., Farad. Trans. **1956**, 52, 261.

165. Stone, A.L.; Bradley, D.F. J. Am. Chem. Soc. **1961**, 83, 3627.

166. Turro, N.J.; Barton, J.K.; Tomalia, D.A. Acc. Chem. Res. **1991**, 24, 332.

167. Marky, L.A.; Blumenfield, S.; Bresluer, K.J. Nucl. Acid. Res. **1983**, 11, 2857.

168. Berman, H.M.; Young, P.R. Ann. Rev. Biophys. Bioeng. **1981**, 10, 87.

169. Gale, E.F.; Cundliffe, E.; reynolds, P.E.; Richmond, M.H.; Waring, M. " The Molecular basis of Antibiotic Action," Wiley, **1972**. P173.

170. Neidle, S. Prog. Med. Chem. **1979**, 16, 151.

171. Espejo, R.T.; Lebowitz, J. Anal. Biochem. **1976**, 72, 95.

172. Wang, J.C. J. Mol. Biol. **1974**, 89, 783.

173. Lippard, S.J. Acc. Chem. Res. **1979**, 11, 211.

174. Bond, P.J.; Langridge, R.; Jennette, K.W.; Lipard, S.J. Ibid **1975**, 72, 4285.

175. Barton, J.K.; Lippard, S.J. Biochemistry **1979**, 18, 2661.

176. Howe-Grant, M.; Wu, K.C.; Bauer, W.R.; Llippard, S.J. Ibid **1976**, 15, 4339.

177. Wang, A.H.; Nathans, J.; Van der Marel, G.; Van Boom, J.H.; Rich, A. Nature (London) **1978**, 276, 471.

178. Wong, Y.S.; Lippard, S.J. J. Chem. Soc. Commun. **1977**, 824.

179. Hertzberg, R.P.; Dervan, P.B. J. Am. Chem. Soc. **1982**, 104, 313.

180. Van Dyke, M.W.; Hertzberg, R.P.; Dervan, P.B. Proc. Natl. Acad. Sci. U.S.A. **1982**, 72, 5470.

181. Van Dyke, M.W.; Dervan, P.B. Biochemistry **1983**, 22, 2373.

182. Cartwright, I.I.; Elgin, S.C.R. Nucleic Acids Res. **1982**, 10, 5835.

183. Barton, J.K.; Dannenberg, J.J.; Raphael, A.L. J. Am. Chem. Soc. **1982**, 104, 4967.

184. Barton, J.K.; Raphael, A.L. J. Am. Chem. Soc. **1984**, 106, 2466.

185. Barton, J.K.; Raphael, A.L. Proc. Natl. Acad. Sci. U.S.A. **1985**, 82, 6460.

186. Fleisher, M.B.; Waterman, K.C; Turro, N.J.; Barton, J.K. Inorg. Chem. **1986**, 25, 3549.

187. Krishenbaum, M.R.; Tribolet, R.; Barton, J.K. Nuc. Acid Res. **1988**, 16, 7943.

188. Barton, J.K.; Dannenberg, J.J.; Raphael, A.L. J. Am. Chem. Soc. **1982**, 104, 4967.

189. Barton, J.K. J. Biomol. Struct. Dyn. **1983**, 1, 621-632.

190. Collins, J.G.; Sleeman, A.D.; Aldrich-Wright, J.R.; Greguric, I.; Hambley, T.W. Inorg. Chem. **1988**, 37, 3133-3141.

191. Watson, R.T.; Desai, N.; Wildsmith, J.; Wheeler, J.J.; Knae-Maguire, N.A.P. Inorg. Chem. **1999**, 38, 4486-4497.

192. Coggan, D.Z.M.; Haworth, I.S.; Bates, P.J.; Robinson, A.; Rodger. A. Inorg. Chem. **1999**, 38, 4486-4497.

193. Hayoz, P.; Von Zelewsky, A.; Stoeckli-Evans, H. J. Am. Chem. Soc. **1993**, 115, 5111-5114.

194. Erikkila, K.E.; Odom, D.T.; Barton, J.K. Chem. Rev. **1999**, 99, 2777-2795.

195. Homlin, R.E.; Stemp, E.D.A.; Barton, J.K. Inorg. Chem. **1998**, 37, 29-34.

196. Lippard, S.J.; Bond, P.J.; Wu, K.C.; Bauer, W.R. Science (Washington, D.C.) **1976**, 194, 726.

197. Barton, J.K. J. Biomol. Struct. Dyn.1 **1983**, 621-632.

198. Watts, R.J.; Crosby, G.A. J. Am. Chem. Soc. **1971**, 93, 3184-3188.

199. Lin, C.T.; Bottcher, W.; Chou, M.; Creutz, C.; Sutin, N. J. Am. Chem. Soc. **1976**, 98, 6536-6544.

200. Santella, R.M.; Grunberger, D.; Weinstein, E.B.; Rich, A. Proc. Natl. Acad. Sci. U.S.A. **1981**, 78, 1451-1455.

201. Schmechel, D.E.V.; Crothers, D.M. Biopolymers **1971**, 10, 465-480.

202. Wolfe, A.; Shimer Jr., G.H.; Meehan, T. Biochemistry **1987**, 26, 6392-6396.

203. Goss, D.J.; Carbery, S.E.; Dever, T.E.; Merrick, W.C.; Rhoades, R.E. Biochemistry **1990**, 29, 5008-5012.

204. Record, M.T.; Anderson, C.F.; Lohman, T. Quart. Rev. Biophys. **1978**, 11, 103-178.

205. Howe-Grant, M.; Lippard, S.J. Biochem. **1979**, 5762.

206. Kumar, C.V.; Barton, J.K.; Turro, N.J. J. Am. Chem. Soc. **1985**, 107, 5518-5523.

207. Barton, J.K.; Goldberg, J.M.; Kumar, C.V.; Turro, N.J. J. Am. Chem. Soc. **1986**, 108, 2081-2088.

208. Pyle, A.M.; Barton, J.K. Progress in Inorganic Chemistry: Bioinorganic Chemistry, Lippard, S.J., Ed.: John Wiley and Sons: New York, **1990**, vol. 38.